Experimental Studies on Geocells and Mat Systems for Stabilization of Unpaved Shoulders and Temporary Roads

By

Jun Guo

Submitted to the graduate degree program in Civil, Environmental, and Architectural Engineering and the Graduate Faculty of the University of Kansas in partial fulfillment of the requirements for the degree of Master of Science.

_____

Dr. Jie Han, Chairperson

_____

Dr. Robert L. Parsons

_____

Dr. Steven D. Schrock

Date Defended: 12/02/2014

The Thesis Committee for Jun Guo

certifies that this is the approved version of the following thesis:

Experimental Studies on Geocells and Mat Systems for Stabilization of Unpaved Shoulders and Temporary Roads

_____

Dr. Jie Han, Chairperson

_____

Dr. Robert L. Parsons

_____

Dr. Steven D. Schrock

Date approved: 12/02/2014

Abstract

Geosynthetics have been used to improve the performance of geomaterials, especially when weak soil exists in roadway applications. In this study, two types of geosynthetic materials, geocell and a mat system, were studied for their applications for unpaved roads and shoulders. The study of geocell was focused on its application for unpaved shoulders. The ability of geocell to improve different geomaterials over intermediate strength subgrade and its possible effect on vegetation were investigated. The study of the mat system was focused on investigating the performance of the mat system over soft and intermediate subgrade with different strengths under cyclic loading to simulate temporary roadway conditions.

In the study of geocell for the application for unpaved shoulders, six large scale plate loading tests were conducted on a single type of geocell on target 5% CBR subgrade to investigate the benefits of geocell reinforcement on different base course and topsoil combinations. Different base course and topsoil combinations were investigated including: 200-mm thick unreinforced aggregate, 200-mm thick soil-aggregate mixture (50% aggregate and 50% top soil) with and without geocell reinforcement, 200-mm thick geocell-reinforced topsoil, 50-mm thick aggregate over 150-mm soil-aggregate mixture (50% aggregate and 50% top soil), and 50-mm thick top soil over 150-mm thick geocell-reinforced soil-aggregate mixture (50% aggregate and 50% top soil). Earth pressure cells were install at the interface between subgrade and base course to monitor the load distribution. The cyclic plate loading tests showed

that geocell effectively reduced the permanent deformation and the geocell-reinforced soil-aggregate mixture slightly outperformed the unreinforced aggregate at the same thickness. The plate loading tests also suggested the topsoil cover resulted in large permanent deformations.

A one-year long outdoor field vegetation test was conducted on base courses with different combinations of aggregate and topsoil including: 200-mm thick unreinforced topsoil, 200-mm thick soil-aggregate mixture (50% aggregate and 50% topsoil), 50-mm thick aggregate over 150-mm soil-aggregate mixture (50% aggregate and 50% topsoil), and 50-mm thick topsoil over 150-mm reinforced soil-aggregate mixture (50% aggregate and 50% topsoil) to investigate the possible effect of geocell on shoulder vegetation established mainly by tall fescue grass and perennial ryegrass. One control (unreinforced) section and one geocell-reinforced section were prepared for each base course combination with a surface area of 1.5 m by 1.5 m. During the one-year test period, soil moisture temperature and volumetric moisture content were monitored. Weather data, such as precipitation and air temperature, were obtain from the nearby weather station at the Lawrence airport. Vegetation growth was evaluated by grass leaf blade length, root length, and grass density. Vegetation biomass was obtained at the end of the test. The test results showed no definite evidence of geocell influencing the vegetation in unpaved shoulders.

In the study of the mat system, six large-scale cyclic plate loading tests were conducted on a single type of polyethylene mat system with anchorage to study its performance over soft and intermediate subgrade with the CBR ranging from 1% to 4%.

For the comparison purposes, test sections with and without the mat system were prepared and evaluated. For the test section with 1% CBR subgrade, an aggregate base course was used for the test section without the mat system to enable the cyclic plate loading test. The size of the mat system under the investigation was 1.92 m by 1.92 m. A cyclic load at the magnitude of 40 kN was applied through a 300 mm diameter loading plate with a thin rubber pad to simulate a vehicle tire. Earth pressure cells were installed at the interface between the mat system and the subgrade to monitor the load distribution. Loading plate displacements were measured by the displacement transducer inside the actuator. Test results concluded that the mat system was more effective over the intermediate subgrade than the soft subgrade and when large permanent deformations were allowed.

Dedication

The author dedicates this work to his parents,
Dr. Jie Guo and Mrs. Liying Liu

Acknowledgement

First of all, I would like to express my most sincere gratitude to Prof. Jie Han, my advisor and mentor, for providing me the opportunity to continue my study at the University of Kansas. His guidance extended beyond the field of academic. The knowledge and skills he imparted not only guaranteed the completion of the projects but will benefit me for the rest of my career. I also owe my thanks to Prof. Steven D. Schrock and Prof. Robert L. Parsons for their valuable advice and assistance without which I would never be able to finish my study at KU. I am grateful for the opportunity to study under such excellent professors.

The geocell-reinforced unpaved shoulder study was funded by the Kansas Department of Transportation while the matting system study was funded by the Presto Geosystems. The geocell material and the matting system used in this study were provided by the Presto Geosystems. I would also like to express my gratitude for the financial support provided by the Kansas Department of Transportation and the Presto Geosystem. The University of Kansas Facility Services provided the area for my vegetation study. I would also like to extend my gratitude to Prof. Thomas E. Mulinazzi, Prof. Bryan Young, Mr. Jonathan P. Marburger, and Mr. Scott Shields for their advice.

I am indebted to the members of KUGS (Kansas University Geotechnical Society)

especially Xiaohui Sun and Fei Wang who provided their help and support. The laboratory coordinator, Matthew Maksimowicz; technologists, David Woody and Eric Nicholson; financial managers, Cathy Johnson and Mickie Gillispie from the Kansas University Transportation Research Institute provided the strong logistic support. The undergraduate research assistance, Byron Whitted, Brandon Basgall, Lee Crippen, Zach Brady, Felipe Brandao, and David Rivero, who worked tirelessly throughout the projects.

Table of Contents

List of Tables

List of Figures

Chapter One

Introduction

1.1 Problem Statements

Geosynthetics, factory-manufactured plastic materials, have been increasingly used in civil engineering projects to solve geotechnical problems (for example, roadway construction over soft subgrade) since the 1970s. Although the application of geosynthetics for unpaved roads has been much studied, not much has been done on the use of geosynthetics for unpaved shoulders.

Unpaved shoulders, including aggregate and turf shoulders, are often constructed along rural two-lane highways for a design traffic volume of 0 to 874 Annual Average Daily Traffic (AADT) according to the Kansas Department of Transportation. Typically aggregate shoulders have a uniform thickness of 150 mm. Turf shoulders are constructed by bringing the grade up to the pavement edge. Unpaved shoulders are often constructed on compacted natural soil of a CBR value at 3 to 4% or higher. Many two-lane highways featured aggregate or turf shoulders required maintenance on a recurring basis. Rutting and edge drop-offs are the most common performance problems associated with granular shoulders as shown in Figure 1.1 (Mekkawy et al. 2010). The maintenance of an unpaved shoulder is typically done by placing more material and compacting it. This practice is considered temporary and does not address the cause of the problem; therefore, the problem often recurs. There have been a few successful projects using geosynthetics for unpaved shoulder construction

to improve shoulder performance (for example, Gantenbein, 2006). To provide a good condition for vegetation and maintain sufficient load carrying capacity, Gantenbein (2006) used a soil-aggregate mixture for the unpaved shoulder construction. However, the possible effect of geosynthetics on the soil ecological environment and the effect of soil-aggregate mixture and base course-cover combination on the structural performance of unpaved shoulders are not well studied.

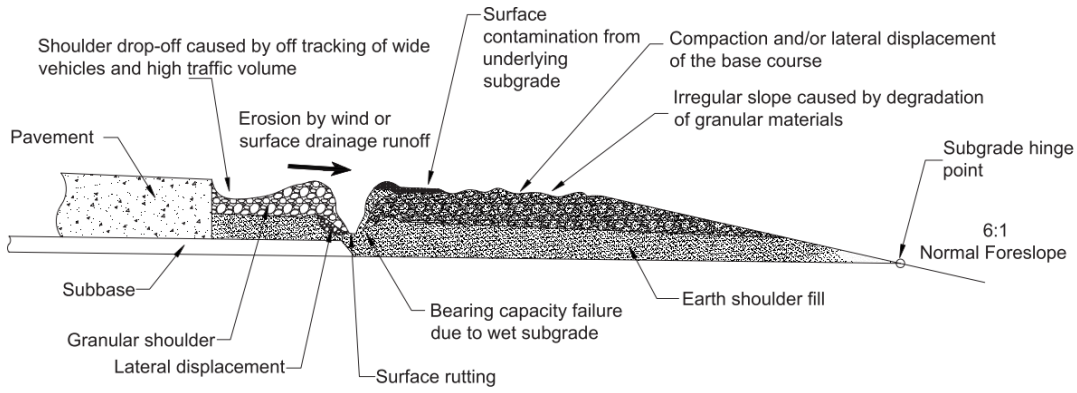

Figure 1.1 Typical granular shoulder performance problems (Mekkawy et al. 2010)

Mat systems have been developed for temporary support of vehicles or construction equipment on access roads, oil drilling platforms, construction platforms, vessel ducking facility, and other roads or areas. Mat systems are often deployed over area where weak subgrade is present and the treatment for the weak subgrade is unfeasible. Shoofly detours are temporary roadways that allow traffic bypass construction zone where mat systems are applicable. Despite the use of mat systems in the practice, limited studies have been done so far. Past research showed the

performance of mat systems depended on the subgrade condition. However, most mat systems investigated in the past did not have an anchorage system. The anchorage system available in the new mat system is expected to provide additional benefits and deserves further research.

1.2 Research Objectives

This study investigated two geosynthetic materials, the geocell and the mat system, which were used to stabilize unpaved shoulders and unpaved temporary roads. The effect of geocell reinforcement on unpaved shoulders over intermediate subgrade (5% CBR) was studied by conducting large scale cyclic plate loading tests on the following test sections:

1. 200-mm thick unreinforced aggregate.
2. 200-mm thick unreinforced soil-aggregate mixture.
3. 200-mm geocell-reinforced soil-aggregate mixture.
4. 50-mm thick topsoil over 150-mm thick geocell-reinforced soil-aggregate mixture.
5. 50-mm thick aggregate over 150-mm thick geocell-reinforced soil-aggregate mixture.
6. 200-mm thick geocell-reinforced topsoil.

Furthermore, the possible effect of geocell on soil ecological environment was investigated by an outdoor field vegetation test. One control (unreinforced) section and one geocell-reinforced section were constructed in the size of 1.5 m by 1.5 m each

with the following soil and aggregate compositions:

1. 200-mm thick topsoil.
2. 200-mm thick unreinforced soil-aggregate mixture.
3. 50-mm thick topsoil over 150-mm thick soil-aggregate mixture.
4. 50-mm thick aggregate over 150-mm thick soil-aggregate mixture.

In the study of the mat system, cyclic plate loading tests were conducted on subgrade of 1%, 2%, and 4% CBR with and without a mat system to investigate the effectiveness of the mat system. An aggregate base course was constructed on one test section with 1% CBR subgrade to enable the plate loading test for a comparison purpose.

1.3 Organization of Chapters

This thesis includes five chapters. Chapter 1 – Introduction presents a brief introduction to this study. Chapter 2 – Literature review provides a review of past studies related to this study. Chapter 3 – Geocell reinforced unpaved shoulders presents the setup and results of tests conducted on geocell-reinforced shoulder, which include the cyclic plate loading tests and the vegetation test. Chapter 4 – Mat systems for unpaved temporary roads presents the setup and results of tests conducted on mat systems over soft and intermediate subgrade. Chapter 5 – Conclusion and recommendation concludes the test results and presents the recommendation for future studies.

Chapter Two

Literature Review

Geosynthetics are factory-manufactured plastic materials used for geotechnical applications. The history of applying geosynthetic-like materials in civil engineering projects can be traced back to 200 B.C. when straws were used as reinforcements in the construction of the Great Wall in the ancient China. Various modern geosynthetic materials, that aim to meet different challenges in soil stabilization, were introduced in the past 50 years. Geosynthetics have many types and used for different functions. Reinforcement is one of the common functions for geosynthetics. Common geosynthetics used for reinforcement include woven geotextile, geogrid, and geocell. Geocell is also referred to geoweb. Mat systems, also made of plastics, have been increasingly used to support vehicles on construction sites with weak ground. In this study, geocell and a mat system were investigated for the stabilization of unpaved shoulders and weak subgrade. This chapter presents a literature review of past studies and projects on geocells and mat systems for roadway applications.

2.1 Geocell

2.1.1 Early Development

Between 1975 and 1976, the U.S. Army Corp conducted research aimed to develop the construction techniques for tactical bridge approach roads across weak ground. This research developed a sand-confinement system for base courses over weak

subgrade. Tests showed that "both large-volume confinement system and small-volume system outperformed the crushed stone control item by a substantial margin" (Webster, 1977). The sand-confinement system, which is considered as the prototype of geocell, was constructed by fastening 300-mm-long sections of 150-mm diameter corrugated plastic drainage pipes together in a honeycomb arrangement as shown in Figure 2.1 (Webster and Watkins 1977). The following studies in the late 1970s and early 1980s investigated geocells constructed with different materials, such as aluminum sheet and Kraft paper (Rea and Mitchell 1978; Webster 1979; Webster 1981). Nowadays, geocells are usually manufactured by ultrasonically or heat melt bonded high density polyethylene strips. They have been used in different applications in civil engineering, including erosion control and soil stabilization on steep slopes, revetment and flexible channel lining systems, roadway load support and stabilization, and earth retention structures (State of California Department of Transportation 2006; Yuu et al. 2008).

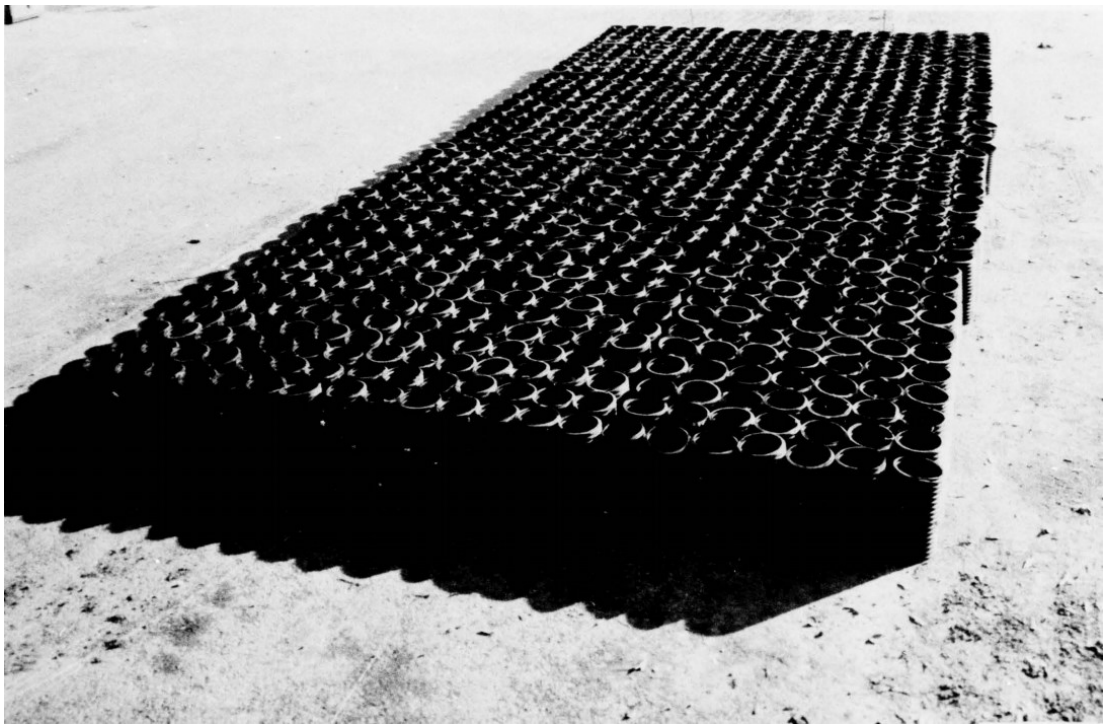

a) Sand-confinement system

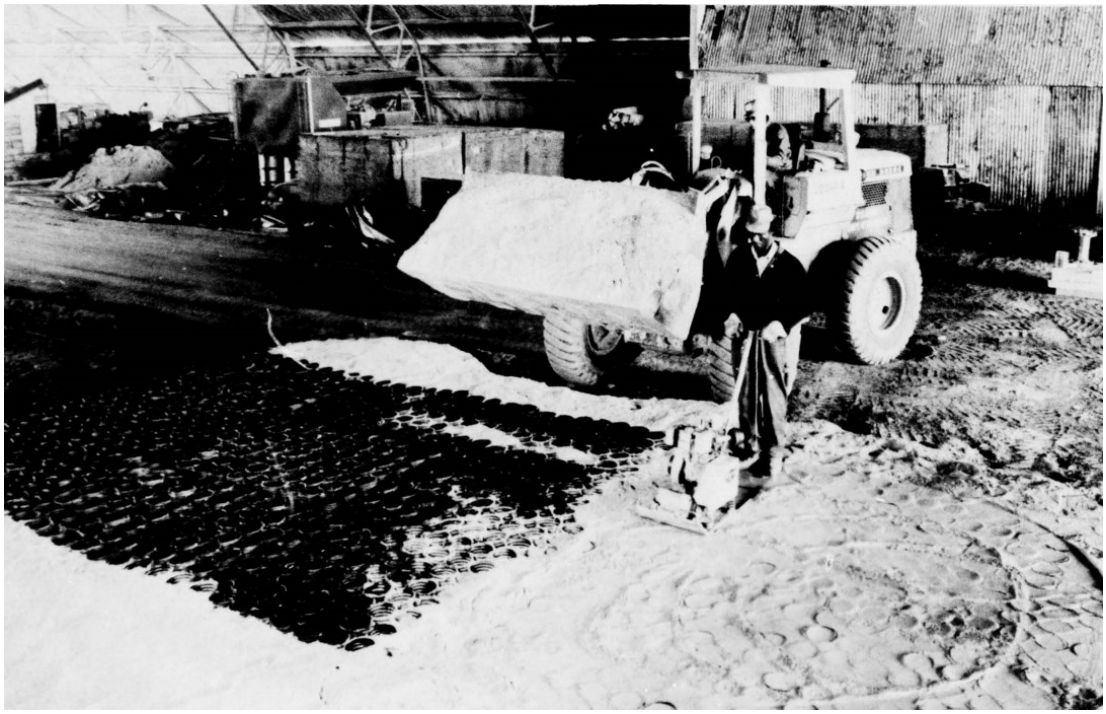

b) Installing and compacting sand in plastic tubing

Figure 2.1 Prototype of geocell (Webster and Watkins 1977)

2.1.2 Reinforcement Mechanisms

Early studies in the late 1970s investigated the effects of following factors: (1) geocell geometry, (2) subgrade stiffness, and (3) loading position as well as identified possible failure modes of geocell (Mitchell et al. 1979; Rea and Mitchell 1978). These studies concluded the optimum ratios of h/d (height to equivalent opening diameter of geocell) was 1.42 to 2.13, and w/d (diameter of loading plate to equivalent opening diameter of geocell) was 1.42. Seven possible failure modes identified in these studies are: (1) geocell penetration into subgrade, (2) cell bursting due to excessive stress from infill material, (3) cell wall buckling due to lacking of lateral constrain, (4) bearing capacity failure in subgrade, (5) bending failure in the soil-geocell composite layer, (6) durability failure due to geocell exposure to environment, and (7) excessive rutting.

As demonstrated by Pokharel et al. (2010) in Figure 2.2, geocells provide confinement in two ways: (1) the friction between cell wall and soil, and (2) the restraint of the infill soil upwards and lateral movement under loading.

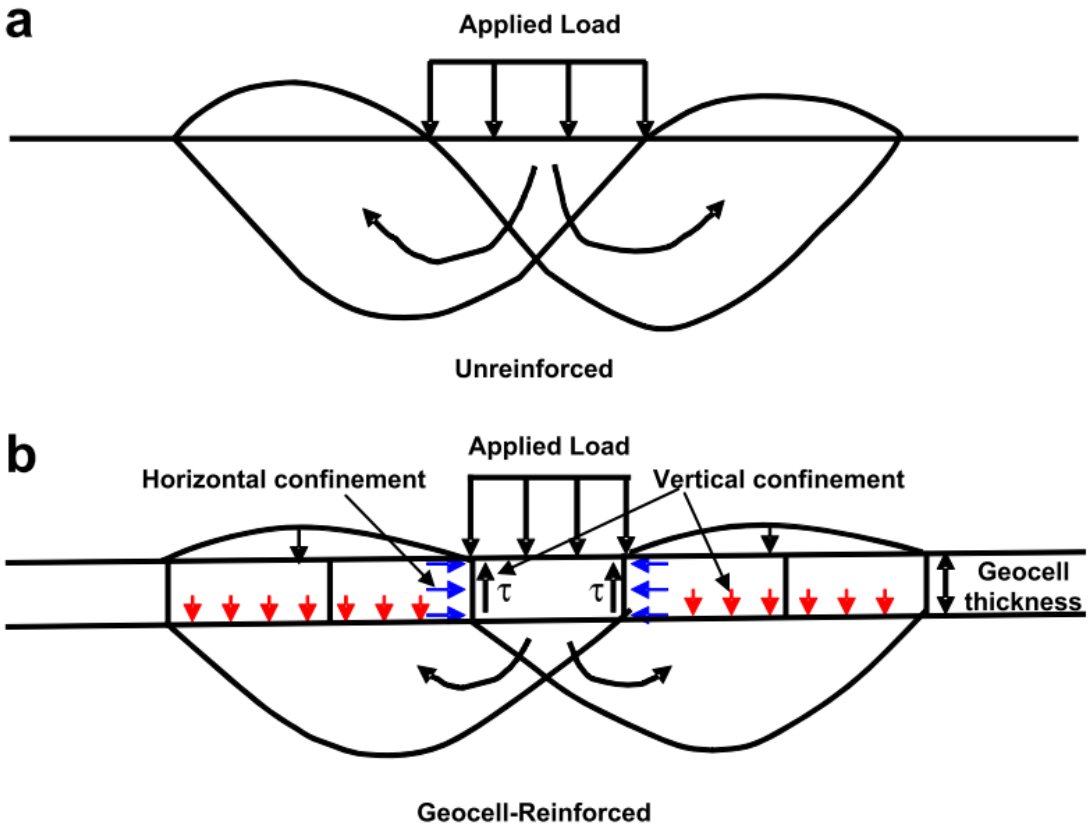

Figure 2.2 Unreinforced and geocell-reinforced soil behavior (Pokharel et al. 2010)

Bathurst and Karpurapu (1993) conducted a series of large scale triaxial compression tests and numerical analysis. Their study proposed the enhancement of the soil strength from the confinement effect could be expressed in the terms of equivalent cohesion c_r using Equation 2.1 and Figure 2.3. The study by Madhavi Latha et al. (2006) verified the equation of the equivalent cohesion.

$$c_r = \frac{\Delta\sigma_3}{2}\tan\left(\frac{\pi}{4}+\frac{\varphi}{2}\right) \qquad \textbf{Equation 2.1}$$

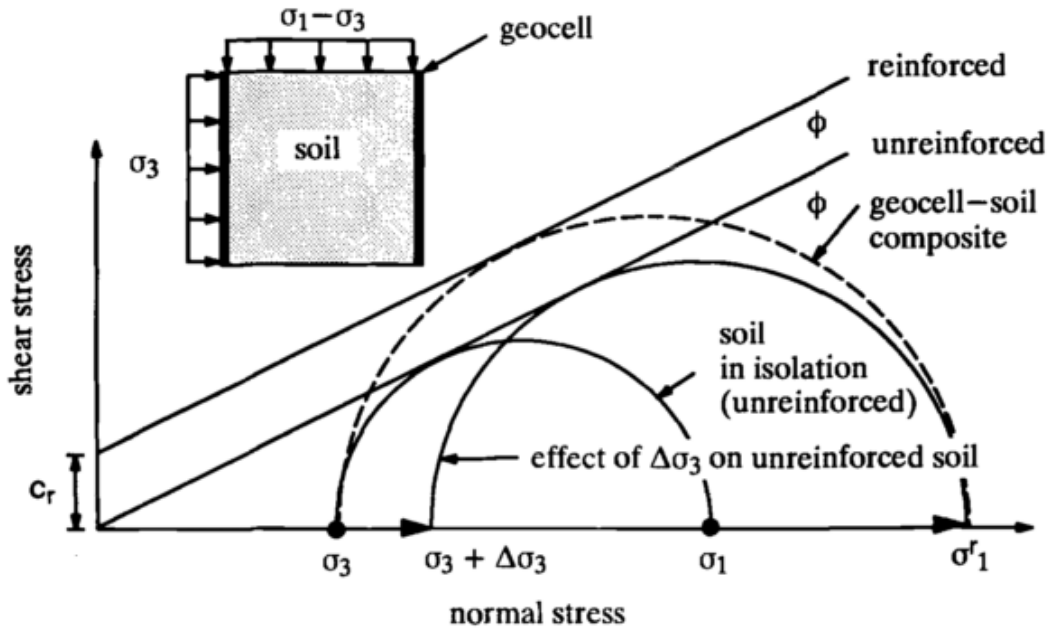

Figure 2.3 Mohr circle construction for calculation of equivalent cohesion for geocell-soil composites (Bathurst and Karpurapu 1993)

2.1.3 Applications with various infill materials

The experimental and numerical studies done by Yang et al. (2008) showed a 65% increase in the bearing capacity of the sand up to 1.25 mm deformation by geocell reinforcement. Pokharel et al. (2011) showed a 170-mm thick geocell-reinforced crushed-stone section outperformed a 300-mm thick crushed-stone section in the accelerated moving-wheel tests. Another accelerated moving-wheel loading tests indicated that the inclusion of geocell reinforcement in the 70-mm thick aggregate (AB-3) base yielded 48 mm rut depth under an 80 kN axle load at 5000 passes while the unreinforced base at the same thickness could not support one pass (Yang et al. 2012). The experimental studies on the application of geocell with recycled asphalt pavement (RAP) material indicated that the inclusion of geocell significantly increased the

strength and stiffness of the RAP base, distributed the load to a wider area, and reduced the permanent deformation under cyclic loading (Jitendra K. Thakur 2013; Thakur et al. 2012).

2.1.4 Design of geosynthetic-reinforced unpaved roads

Giroud and Noiray (1981) developed a design method considering the tensioned membrane effect of a geotextile based on both empirical formula and theoretical analysis. Two beneficial effects identified in the study are: (1) confinement of the subgrade soil between and beyond the wheels areas and (2) reduction of the pressure applied by the wheels on the subgrade soil.

Giroud and Han developed a design method for geogrid-reinforced unpaved roads (Giroud and Han 2004 a and b). In their design method, the thickness of the geogrid-reinforced base course h is given in Equation 2.2:

$$h = \frac{1+k\log N}{tan\alpha_0[1+0.204(R_E-1)]} \times \left\{ \sqrt{\frac{P}{\pi r^2\left(\frac{s}{f_s}\right)\left\{1-\xi \exp\left[-\omega\left(\frac{r}{h}\right)^n\right]\right\}N_c c_u}} - 1 \right\} r \qquad \textbf{Equation 2.2}$$

where

k = constant depending on base course thickness and reinforcement

N = number passes

α_0 = reference stress distribution angle in degree

R_E = modulus ratio of base course to subgrade

r = radius of tire contact area in meter

s = allowable rut depth in millimeter

f_s = failure rut depth (typically 75 mm)

P = wheel load in kN

N_c = bearing capacity factor

c_u = undrained shear strength of subgrade soil in kPa

ξ, ω, and n are constants.

This equation considers the following parameters: traffic loading patterns, geometry of unpaved road structure, rut depth, properties of base course and subgrade, properties of geogrid and serviceability.

Pokharel (2010) calibrated the constant k in Equation 2.2 for geocell-reinforced unpaved roads using laboratory large-scale cyclic plate loading tests and accelerated moving-wheel test data.

2.1.5 Unpaved shoulders

The above review was focused on the use of geocell for unpaved roads. The research results and design methods for geosynthetic-reinforced unpaved roads should be applicable to unpaved shoulders in terms of their structural aspects. Geocells have been proven to reduce rutting on unpaved shoulders effectively in limited tests and projects (for example, Gantenbein, 2006). However, no study has been reported on the geosynthetics impact on vegetation. Many studies showed that vegetation can effectively reduce the wind speed on the ground surface thus shoulder vegetation presents two main benefits: (1) reduction of dust emission, and (2) erosion control (Udo, 2007; Zhou, 2006; Munson, 2011).

Chow et al. (1992) pointed out agricultural vehicle movements along unpaved roads and along unpaved shoulders are believed to be one of the main contributors to PM_{10} (particles with a diameter of 10 micrometer or less suspended in air). Moosmüller et al. (1998) concluded that large turbulence events resulted in significant dust entrainment. Such events were caused by vehicles with a large size or poor aerodynamics traveling at high speeds (80 to 104 km/hr). Van de Ven et al. (1989) conducted wind tunnel simulation and found even sparsely standing vegetation can significantly reduce soil loss. Udo and Takewaka (2007) found the complex interaction among the turbulence, the mean wind velocity field, and the vibration of the leaves reduce the sand-transport rate considerably. Munson et al. (2011) conducted a long-term monitoring of climate and vegetation in national parks. Their study indicated a decline in the dominant vegetation cover due to increased temperature leads to exponential increased in wind erosion. Leenders et al. (2007) showed that shrubs have the ability to reduce the wind speed and its low hanging branches can trap sediment.

2.2 Mat System

Mat systems, also known as “modular systems”, “road mats”, or “temporary road systems”, usually consist of inter-lockable panels and anchorages (for some systems). Such systems have been developed and used for temporary support for vehicles, airplanes, and construction equipment over weak ground. Major applications of mat systems include: access roads, haul roads, oil-drilling platforms, construction platforms, sandy or muddy stream or beach crossings, helicopter landing pads, and airfield

runways. The major advantages of mat systems when compared to conventional road construction methods are rapid deployment, relatively low cost, and recyclable. Depending on the mat system, the panels can have a shape of interconnected roll, rectangle, or hexagon. Mat systems are also made from a large varieties of materials. The US Army Corps conducted tests on temporary road systems made from following materials (Anderton and Gartrell 2005; Rushing and Howard 2011; Rushing et al. 2009; Santoni 2003; Santoni et al. 2001; Webster and Tingle 1998): (1) fiberglass-reinforced polyester composite, (2) reinforced plastic, (3) unreinforced plastic, (4) aluminum, (5) steel, (6) wood, (7) nucleated copolymer polypropylene, (8) recycled HDPE, and (9) fiberglass.

Mason and Greenfield (1995) suggested the following required characteristics for portable crossing products (such as mat systems) over weak soil areas and streams:

1. able to handle anticipated traffic loads
2. easy relocation with available labor and equipment
3. durable enough to withstand relocation
4. adequate traction for perform well while immersed in water or mud
5. cost effective and readily available

Mak (2013) proposed three performance requirements for a mat system. First, it should have adequate structural capacity to resist the vertical load expressed in equivalent single axle load of 18 kip (80 kN). However, mat systems have also be designed for larger loads with higher pressure and wider contact area, such as aircraft landing gears (Doyle et al. 2012; Gartrell 2007; Gonzalez and Rushing 2010). Second,

it should have adequate structural capacity to resist horizontal loads such as breaking and centrifugal force from vehicles. The breaking force varies with the type of vehicle and the friction coefficient between tire and pavement surface. The centrifugal force can be calculated with vehicle mass, velocity, and turning radius. Third, it should have adequate skid resistance of the road plate surface. Other than the performance requirements, Mak (2013) also suggested that the cost and durability of the mat system should be taken into consideration.

2.2.1 Past studies

Due to the fast deployment nature, mat systems present great military values thus the US Army Corps of Engineers conducted extensive studies on different products. The studies were focused on (1) the application in airfield, which required the mat system to sustain higher gross loads and tire pressures than regular traffic and (2) the application for expedient roads for military vehicles, which have a similar loading pattern as civilian vehicles.

Webster and Watkins (1977) observed a 50 to 87.5 mm subgrade deformation of the M8A1 steel landing mat over 1%-CBR subgrade after 39,100 passes (ESAL). All panels sustained without any damage at 15,000 passes. The loading was achieved by a 5-ton, tandem-axle, military dump truck.

Webster and Tingle (1998) conducted comparison tests on five different mat systems over 0.9-m thick concrete sand subgrade with a 6 by 6 military truck of a gross vehicle weight of 21 ton. The test result is presented in Table 2.1. The control section without any mat system yielded a 200-mm rut depth after the 25th truck pass.

Table 2.1 Rut depth summary (reproduced from Webster and Tingle, 1998)

Mat	Rut Depth, mm, at Truck Passes				
	20	700	2500	3500	5000
Fiberglass-reinforced mat	15	25	27.5	27.5	27.5
Plastic Hexagonal mat	17.5	47.5	62.5	62.5	70
Aluminum hexagonal mat	17.5	37.5	45	45	45
plastic mesh mat(unreinforced)	55	-	-	-	-
Plastic mesh mat reinforced with glass fiber/polyester	82.5	-	-	-	-

Santoni et al. (2001) investigated the application of mat systems over soft soil: lane 1 with 0.1 – 0.5% CBR subgrade and lane 2 with 0.1 – 0.7 CBR using the same loading truck as (Webster and Tingle 1998). Due to the extreme soft soil, geotextile and geogrid had to be placed prior to the test to enable personnel to walk on the soil and install mat systems. The permanent deformations after 2,000 passes in both subgrade conditions indicated one type of plastic mat system and one type of wood mat system performed similarly to a 375-mm thick geogrid-reinforced limestone layer placed over a 525-mm thick wood chip layer and an 875-mm thick geogrid-reinforced crushed limestone layer.

Santoni (2003) investigated two mat systems and one fiber reinforcement to enhance the load carrying capacity of sand: hexagonal mat (plastic and aluminum), fiberglass-reinforced polyester composite mat, and 50-mm long geofiber (0.8 percent by dry weight of sand), under both straight-line and turning traffic loading generated

with the same 5-ton military truck used in Webster and Tingle (1998) study. The plastic hexagonal mat, which was placed over 4.3% CBR sand, reached 62.5 mm permanent deformation after 165 passes and the aluminum hexagonal mat reached 77.5 mm permanent deformation after 600 passes. The fiberglass-reinforced mat system, which was placed over 2.9% CBR sand, yielded 32 mm and 33 mm deformations after 600 passes in a straight line and 16.7 m turning radius respectively. The fiber-reinforced sand yielded 48 mm and 51 mm deformations after 600 passes in a straight line and 16.7 m turning radius respectively.

Rushing et al. (2009) conducted tests on one type of mat system over different subgrade strength and temperature. Table 2.2 presents the summary of their test results. This study suggested the subgrade CBR and the connection between panels have a significant impact on the performance of the mat systems.

Table 2.2 Summary of Supa-Trac test results (reproduced from Rushing et al., 2009)

CBR ,%	Temperature,℃	Scenario	Passes at failure		Notes
			20% breakage	75-mm rut	
15	29.5	Beach	3500+	3500	
1-3	29.5	Mudflat	1	1	
5	29.5	Mudflat	10	10	
5	18	Mudflat	100	100	Staggered Joints
7	12.7	Mudflat	2000+	2000+	Staggered Joints
5	-3.8	Partially frozen	100	70	Staggered Joints
80	-9.4	Completely frozen	2000+	2000+	CBR 1 when unfrozen; staggered joints

The effect of subgrade CBR on the mat system performance was also confirmed by Rushing and Howard (2011) and Gartrell et al. (2009). Their studies showed the mat system reduced the accumulation rate of rutting more effectively and sustained more loading cycles without breakage over the subgrade with a higher CBR.

2.2.2 Design methods

The early design method for airfield mat systems, dating back to 1950s, was an empirical equation based on the CBR design equation for flexible pavements (Foster and Burns 1952; Gonzalez and Rushing 2010):

$$t = (0.23\log C + 0.15)\sqrt{\frac{P}{8.1CBR} - \frac{A}{\pi}} \qquad \textbf{Equation 2.3}$$

where t = total thickness of flexible pavement above the subgrade in inches

C = number of aircraft passes

P = single or equivalent single-wheel load in pounds

CBR = subgrade CBR

A = tire contact area in square inches.

Gonzalez and Rushing (2010) proposed a new design method for airfield mat systems based on the beta method for flexible pavements, considering the following factors: (1) the load of aircraft, (2) aircraft tire pressure, (3) mat panel flexural rigidity, (4) mat panel modulus elasticity, (5) mat thickness, (6) Poisson's ratio of mat panel, and (7) pass-to-coverage ratios. The pass-to-coverage ratio is the inverse of the sum of

probabilities that the aircraft tire will cross a given point on the pavement during one pass. Based on the properties of the mat system and aircraft characteristics, a relationship between deviatoric stress and depth can be established and the maximum deviatoric stress can be used in following equation to calculate β.

$$\beta = \frac{\sigma_f \cdot \pi}{CBR} \qquad \textbf{Equation 2.4}$$

Based on the past tests on mat systems, a correlation between β and coverage-to-failure was established. The design chart for one mat system to support a designated type of aircraft is presented in the form of required design passes, subgrade CBR, and required thickness under the mat system, as shown in Figure 2.4.

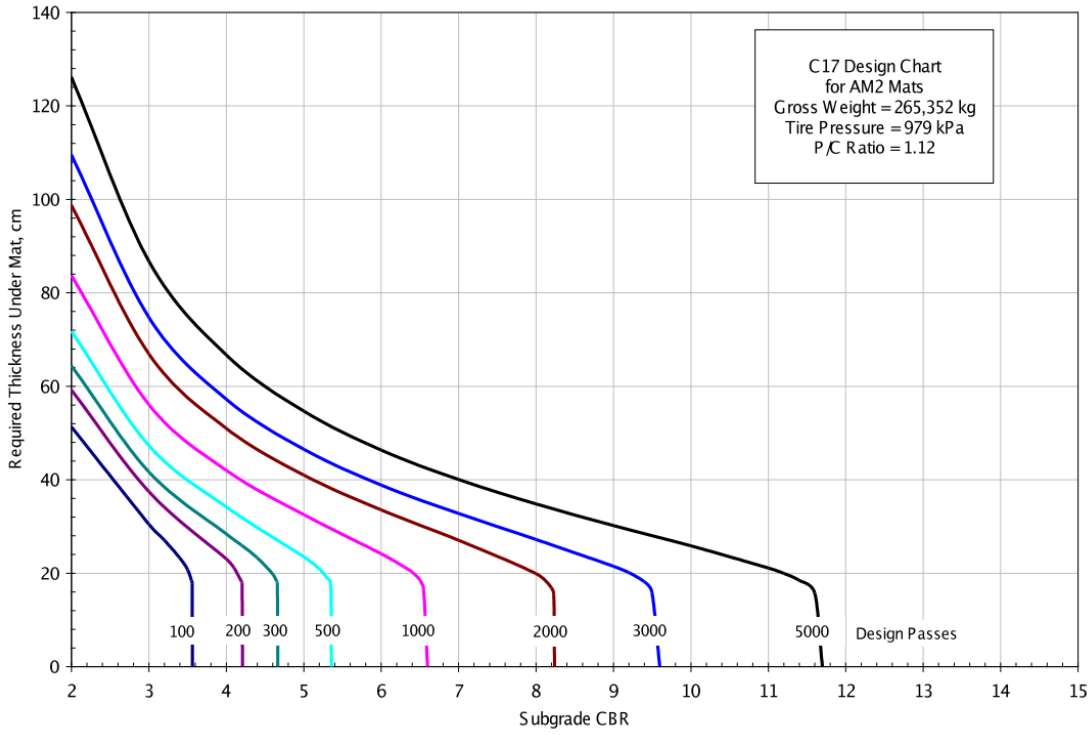

Figure 2.4 AM2 mat design chart for the C-17 aircraft loaded at a gross weight of 265,352*kg* (Gonzalez and Rushing 2010)

2.3 Summary of literature review

The following can be summarized from the literature review:

1. Geocells provide confinement, tension membrane effect and widen distribution of an applied stress, which lead to an increase in bearing capacity and stiffness, and a reduction in permanent deformation of a base course over a weak subgrade.
2. Geocell reinforcement is applicable to various geomaterials for improving the performance of the material.
3. Vegetation is an important component of an unpaved shoulder
4. Mat systems are effective as a temporary roadway support system.
5. Subgrade conditions have a significant effect on the performance of a mat system.
6. There are a large variety of mat systems and their effectiveness varies.

Chapter Three

Geocell-Reinforced Unpaved Shoulders

3.1 Introduction

This chapter presents the materials, equipment, procedures, and results of the following two tests performed to investigate the performance of geocell-reinforced unpaved shoulders: (1) plate loading test and (2) outdoor vegetation test.

3.2 Materials

3.2.1 AB-3 Aggregate

AB-3 aggregate is commonly used in Kansas as a course material in road construction. The grain size distribution is shown in Figure 3.1. The compaction curve was obtained based on the modified Proctor tests (ASTM standard D1557) as shown in Figure 3.2. The well-graded aggregate contained approximately 10% fine. The optimum moisture content of this aggregate was approximately 11.5% and its corresponding maximum dry density was 2050 kg/m^3.

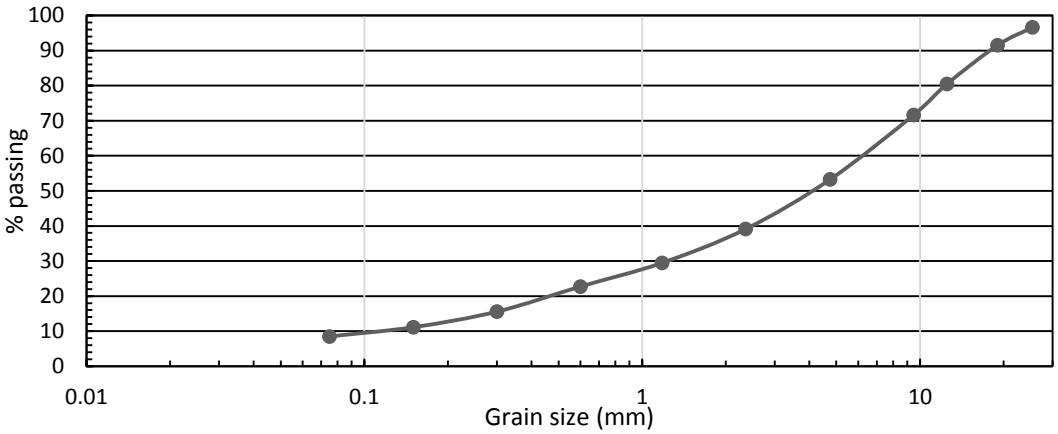

Figure 3.1 Grain size distribution of the AB3 aggregate

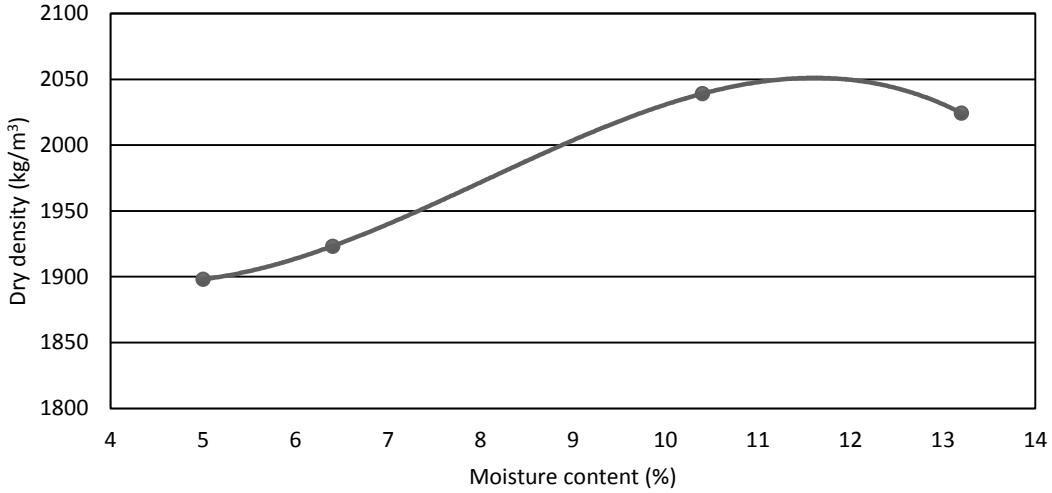

Figure 3.2 Modified Proctor compaction curve of the AB3 Aggregate

3.2.2 Topsoil

The topsoil was obtained from the outdoor vegetation test area on the University of Kansas west campus. The native grass was removed prior to the excavation to avoid contamination as shown in Figure 3.3

Figure 3.3 Topsoil source area

The topsoil is classified as organic silt, which appears black in color with traces of light brown. The plastic limit of the topsoil is 33.7 and the plastic index is 14.6. The organic content of soil is 19% following ASTM D2974. The modified Proctor compaction curve of the topsoil is shown in Figure 3.4. The compaction curve indicates the optimum moisture content of the topsoil is approximately 21% and the maximum dry density is approximately 1570 kg/m^3.

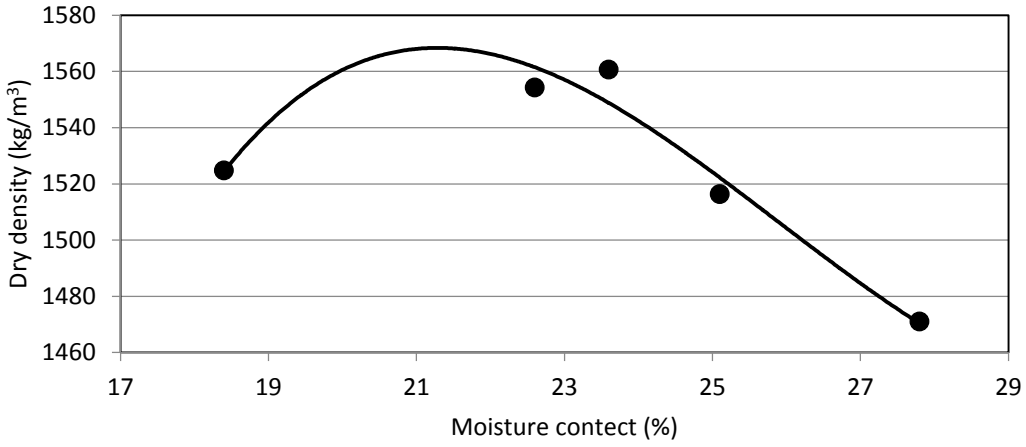

Figure 3.4 Modified Proctor compaction curve of top soil

3.2.3 Soil-aggregate mixture

The soil-aggregate mixture consisted of 50% AB-3 aggregate and 50% topsoil by dry weight. This material is referred to as the mixture in the current and following chapters. The modified Proctor compaction curves of the mixture is shown in Figure 3.5. The compaction curve indicates the optimum moisture content is approximately 15% and the maximum dry density is approximately 1830 kg/m^3.

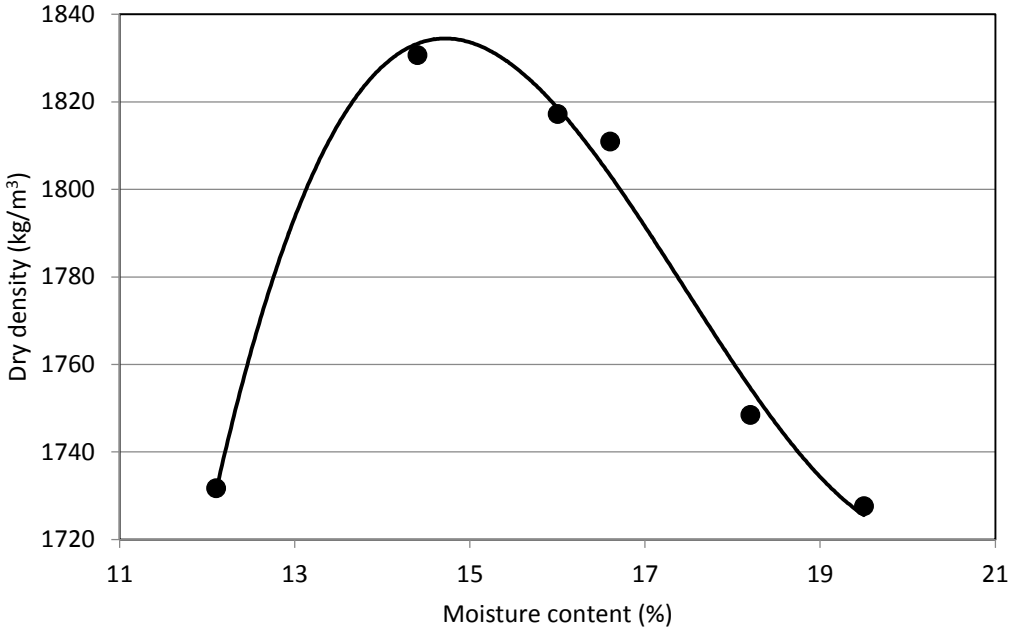

Figure 3.5 Modified Proctor compaction curve of soil-aggregate mixture

3.2.4 Subgrade

The subgrade material for the plate loading tests was a mixture of 25% kaolin and 75% Kansas River sand (by dry weight). Previous tests by Pokharel (2010) on this subgrade material showed that the maximum dry density was 2010 kg/m^3 at 10.8% moisture content by the standard Proctor method. In the field vegetation test, the topsoil was used as the subgrade.

3.2.5 Geocell

The Presto Geosystem supplied the geocells used for this study. The geocell is made of polyethylene with a density of 0.935-0.965 g/cm^3. The height of the cell is 150 mm. Figure 3.6 presents the detailed schematic of the geocell including holes on the cell wall.

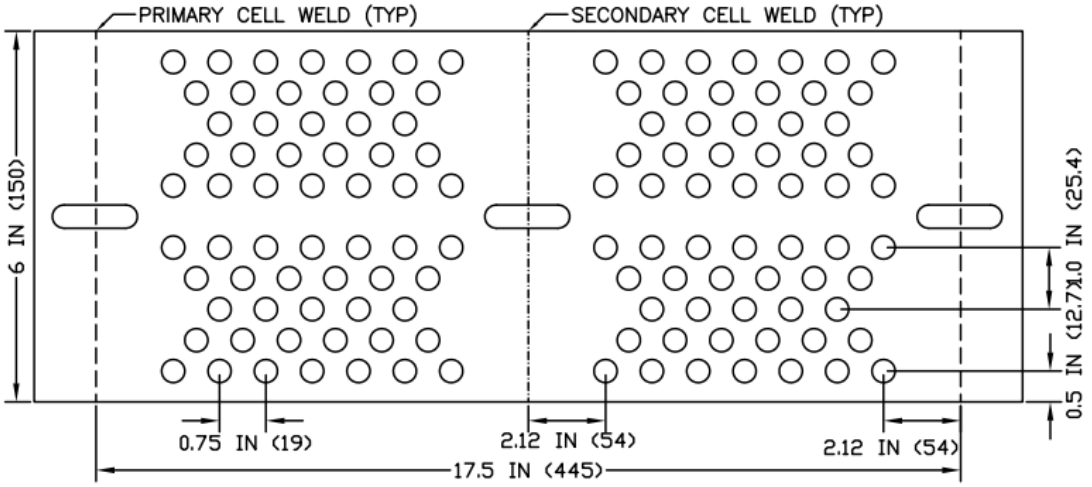

Figure 3.6 Geocell dimension and hole pattern (Presto 2011)

3.2.6 Seeds

The seed mixture for the vegetation test followed the standard by the Kansas Department of Transportation (KDOT 2013) as shown in Table 3.1.

Table 3.1 Seed mixture

Species Name	Amount
	g/m^2
Fertilizer (12-12-12)	**23.15**
Blue Grama Grass Seed (Lovington)	**0.04**
Buffalograss Seed (Treated)	**0.53**
Perennial Ryegrass	**5.2**
Prairie Junegrass	**0.31**
Side Oats Grama Grass Seed (El Reno)	**0.71**
Tall Fescue (Endophyte Free)	**5.2**
Western Wheatgrass Seed (Barton)	**0.71**

As Table 3.1 demonstrates, two primary species are perennial ryegrass and tall fescue. According to the USDA, perennial ryegrass cannot survive severe weather, such as heat and dry in the summer and low temperature in the winter (USDA 2002). Tall fescue is more robust than perennial ryegrass and can survive for a long time period under different weather conditions. Tall fescue's roots can reach deeper depths as compared with perennial ryegrass. Tall fescue grass also tends to grow on

soil surfaces with large clumps (Newman 2001). Grime et al (1998) indicated that tall fescue often becomes a locally dominant species. For decades, Kentucky-31 type of tall fescue has been planted widely for forage and erosion control due to its easy establishment and long life cycle under harsh conditions and tolerance to mistreatment (Henson 2001). Raeside et al. (2012) concluded that tall fescue is more tolerable to heat and more responsive to precipitation in the summer and has deeper roots than perennial ryegrass.

For both species, the seeding rates (weight of seed per m^2) recommended by the KDOT for permanent seed mixes are significantly higher than those recommended by the USDA (2002).

3.3 Large-scale cyclic plate loading tests

3.3.1 Equipment and test setup

A total of six cyclic plate loading tests were conducted with the large-scale geotechnical testing box. The box dimension is 2.2 m × 2 m × 2 m (L × B × H). The loading system produces cyclic loading in a trapezoidal wave form as shown in Figure 3.7. The maximum load is 40 kN and the minimum load is 0.5 kN. The loading is transferred to a test section via a 304-mm diameter steel loading plate with a 12.5 mm-thick rubber base. At the peak load of 40 kN, the loading plate generates a contact pressure of 552 kPa or 80 psi.

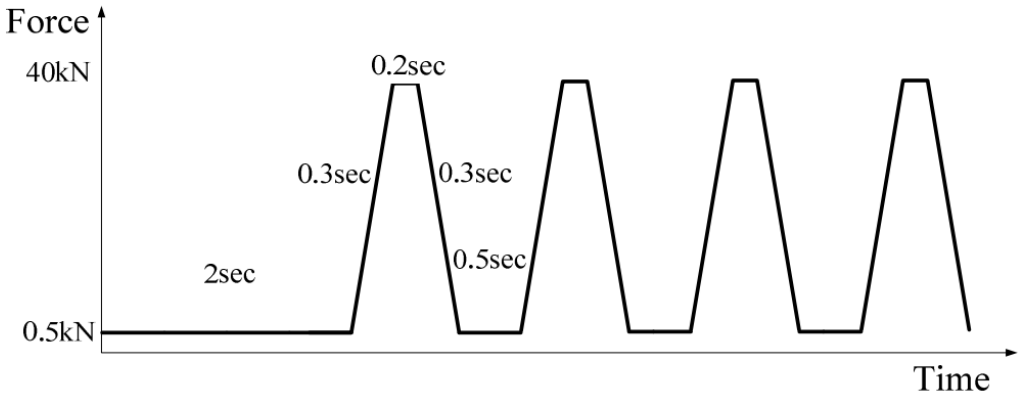

Figure 3.7 Cyclic loading wave form (Pokharel 2010)

The box was filled up to one meter with the subgrade material (the Kansas River sand and kaolin mixture), which was prepared at a target CBR value of 5%. Four earth pressure cells were installed at the interface between subgrade and base course at the center of loading plate, and at the distances of 150 mm, 300 mm, and 600 mm from the center with the sensitive side of the pressure cell towards the subgrade. After the construction of the base course, three displacement transducers, which were suspended from a reference beam across the top of the box, were positioned at 300 mm, 450 mm, and 600 mm away from the center of the loading plate measuring the base surface deformations. Both the data acquisition system was set at 10 Hz frequency to record the data from the earth pressure cells and displacement transducers. An overall schematic drawing of the test setup is presented in Figure 3.8.

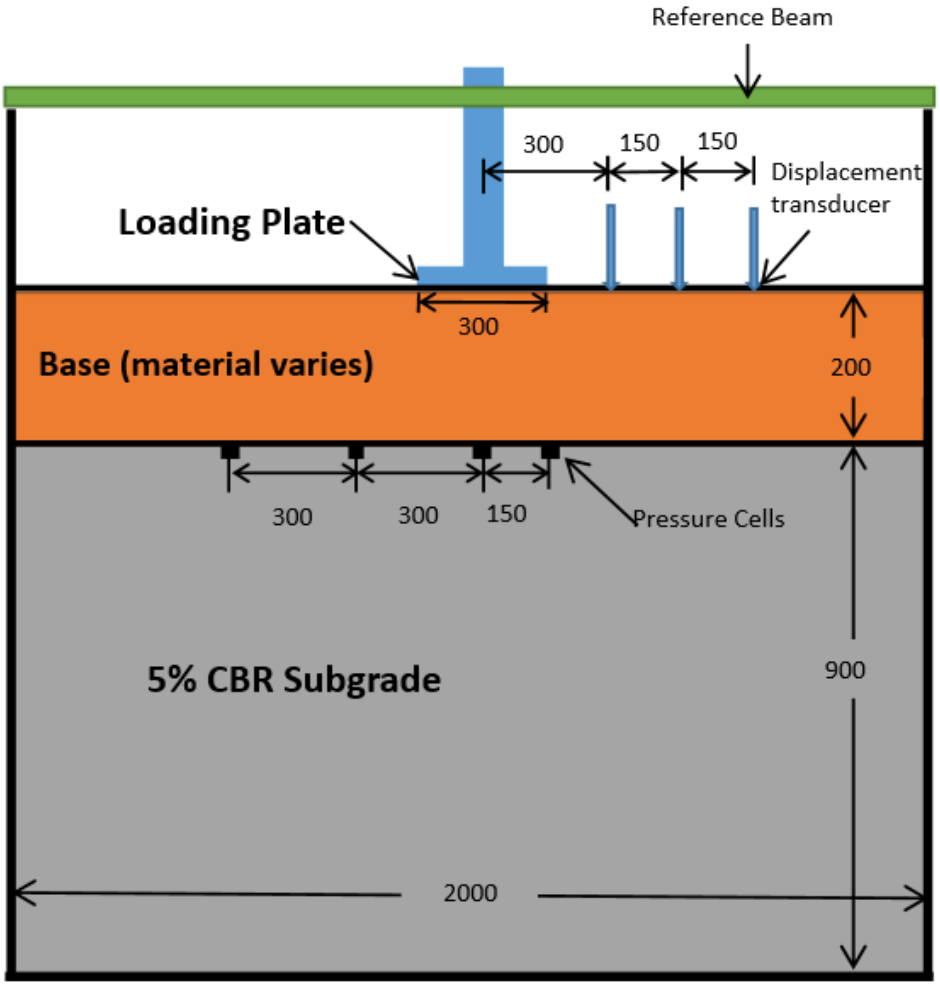

Figure 3.8 Schematic drawing of the test setup (not to scale, all units in mm)

3.3.2 Test preparation

The subgrade was filled in the box in 150-mm lifts. The subgrade material was placed in the box, leveled, and then compacted with an electrical vibratory compactor as shown in Figure 3.9. Five vane shear tests were conducted after the compaction of the subgrade each lift with a hand held vane shear machine at the depth of 100 mm,

175 mm, and 250 mm. The subgrade CBR and undrain shear strength correlation was developed by Khatri (2014) shown in Equation 3.1.

$$\text{CBR}(\%) = \frac{c_u}{25.95} \qquad \textbf{Equation 3.1}$$

where c_u = measured undrained shear strength in kPa.

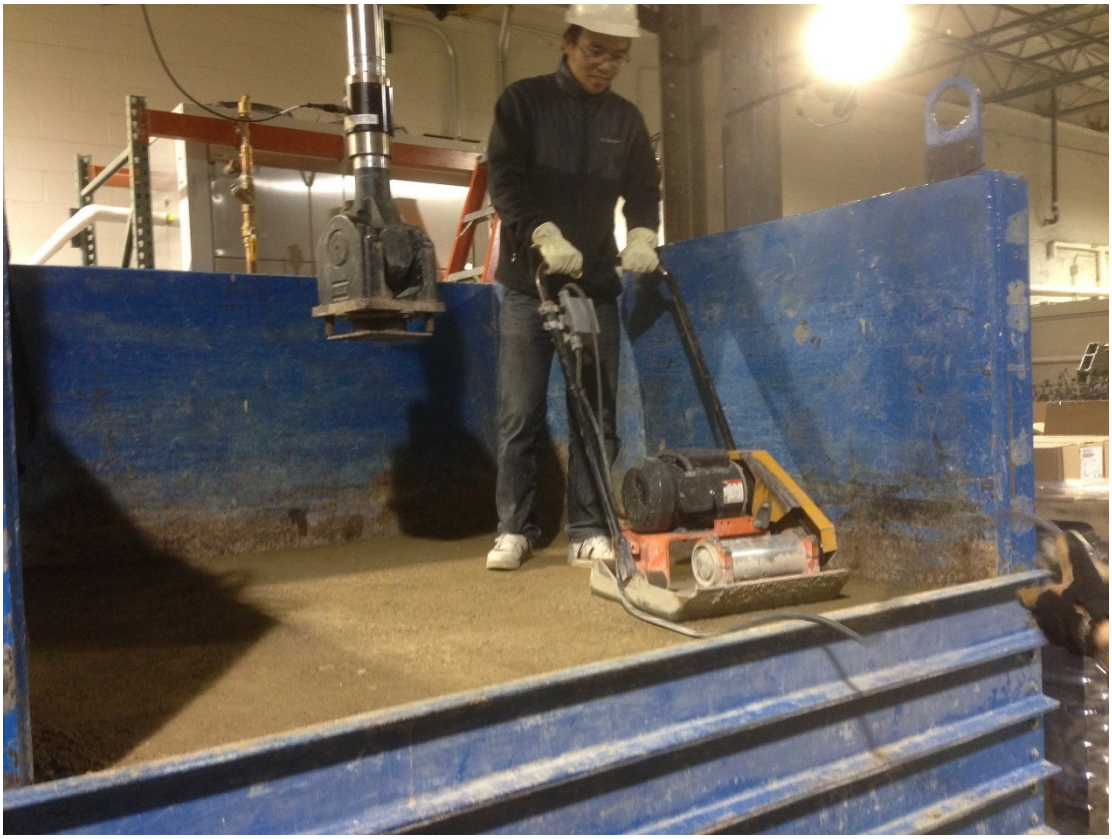

Figure 3.9 Compaction with the electric vibratory compactor

After the box was filled to the target height with the subgrade material, earth pressure cells were installed. To protect earth pressure cells during the compaction and testing, trenches were dug for pressure cells and wires. A level was used to adjust the position of pressure cells as shown in Figure 3.10.

Figure 3.10 Installation of earth pressure cell

The quality of the base course was controlled via adjusting the moisture content to the optimum moisture content. The 200-mm thick base courses were constructed

in 2 or 3 lifts. The reinforced base consisted of a 150-mm thick geocell-reinforced layer and a 50-mm thick cover layer. The vibratory compactor was used for the unreinforced sections. For the geocell-reinforced bases, the geocell was first placed over the subgrade with each edge fixed with rebar as shown in Figure 3.11. The rebar also provided lateral constraint of the geocell under cyclic loading. The first lift was compacted in each cell individually with an air-driving compactor operating at 550 kPa (80 psi), shown in Figure 3.12. The air compactor has a 130-mm diameter plate. The second lift was compacted with the vibration compactor when the cover layer consisted of the same geomaterial as the first lift. Under the circumstance of the cover layer with different geomaterial, the second lift was also compacted with the air compactor and the cover layer was compacted with the vibratory compactor.

Figure 3.11 Placement of geocell

Figure 3.12 Air-driving compacter

The prepared section was left over night (approximately 20 hours) prior to the cyclic loading test.

Three LWD (light weight deflectormeter) tests and four DCP (dynamic cone

penetrometer) tests were conducted prior to the plate loading test. The CBR value of the geomaterial was calculated from the DCP tests based on Equation 3.2 from the ASTM D6951.

$$\mathrm{CBR}(\%) = \frac{292}{DCP^{1.12}} \qquad \textbf{Equation 3.2}$$

where DCP = measured in mm/blow.

3.3.3 Test results

Six test sections under cyclic plate loading tests were evaluated in this study. Table 3.2 presents a summary of these tests with different base combinations.

Table 3.2 Test sections

Test/section No.	**Base Course**	
	Cover layer (50 mm)	Sub layer (150 mm)
1*	AB3	AB3
2*	Mixture	Mixture
3	Mixture	Geocell-reinforced mixture
4	AB3	Geocell-reinforced mixture
5	Topsoil	Geocell-reinforced mixture
6	Topsoil	Geocell-reinforced topsoil

* Control test without geocell reinforcement

Test 1 - 200-mm aggregate base

The control test consisted of a 200-mm thick AB3 aggregate base over 5% CBR subgrade. The subgrade strength was at 4.1% CBR based on the vane shear correlation, while the DCP data indicated a subgrade strength of 6.1% CBR. The base course CBR was 11% based on DCP.

Figure 3.13 presents the surface permanent and rebound deformations of the loading plate with the number of cycles. Figure 3.14 presents the interface pressures at different pressure cell locations. Surface permanent deformations at 300 and 450 mm from the center of the plate are presented in Figure 3.15, in which the positive value indicates settlement.

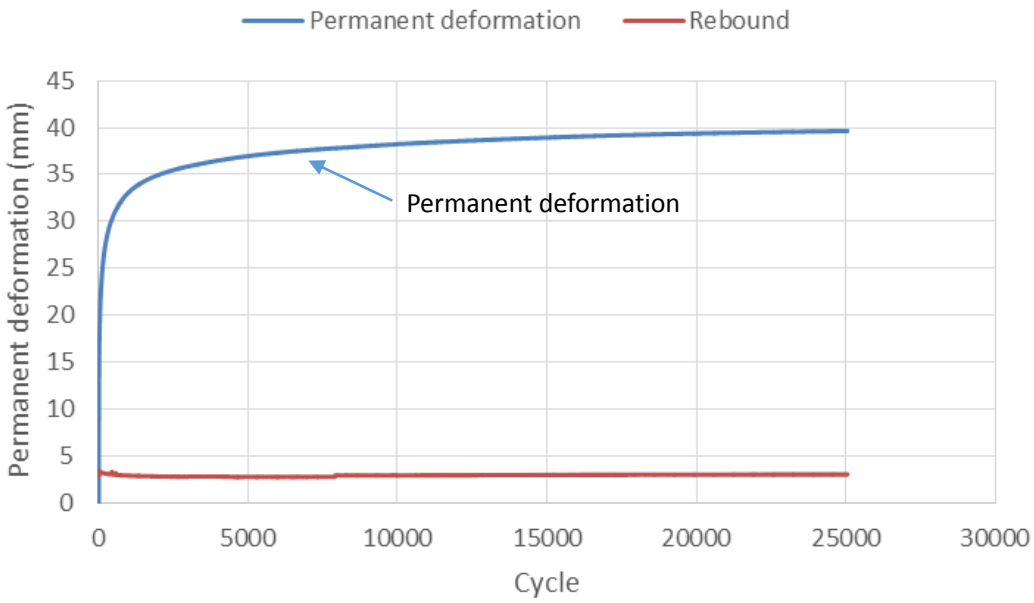

Figure 3.13 Permanent and elastic rebound deformations of the loading plate in Test 1

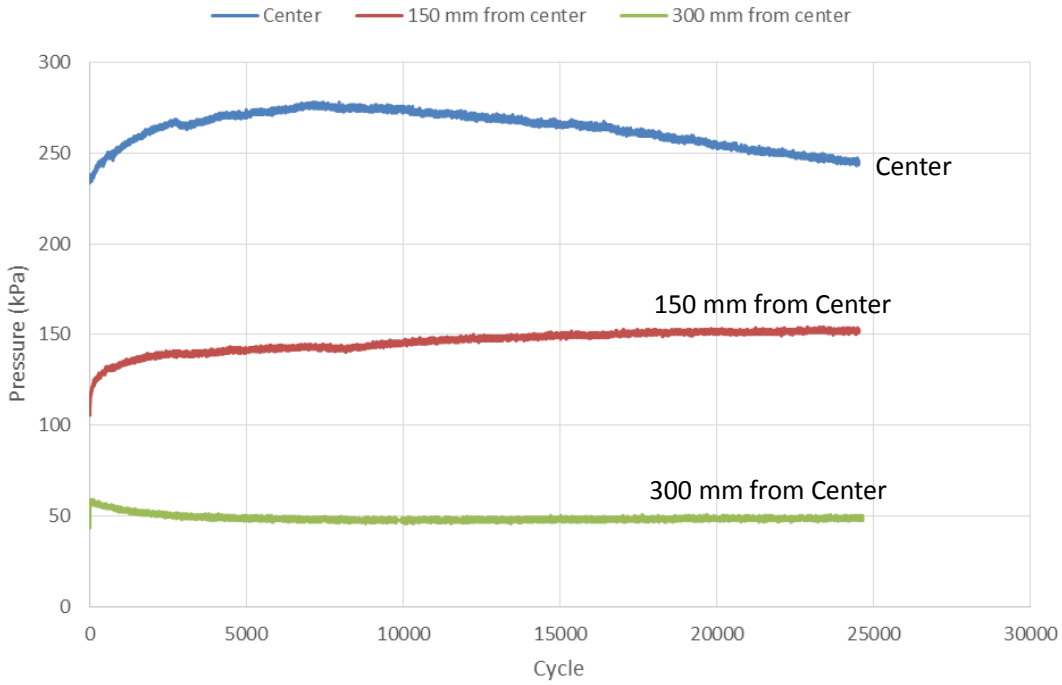

Figure 3.14 Interface pressures at various locations in Test 1

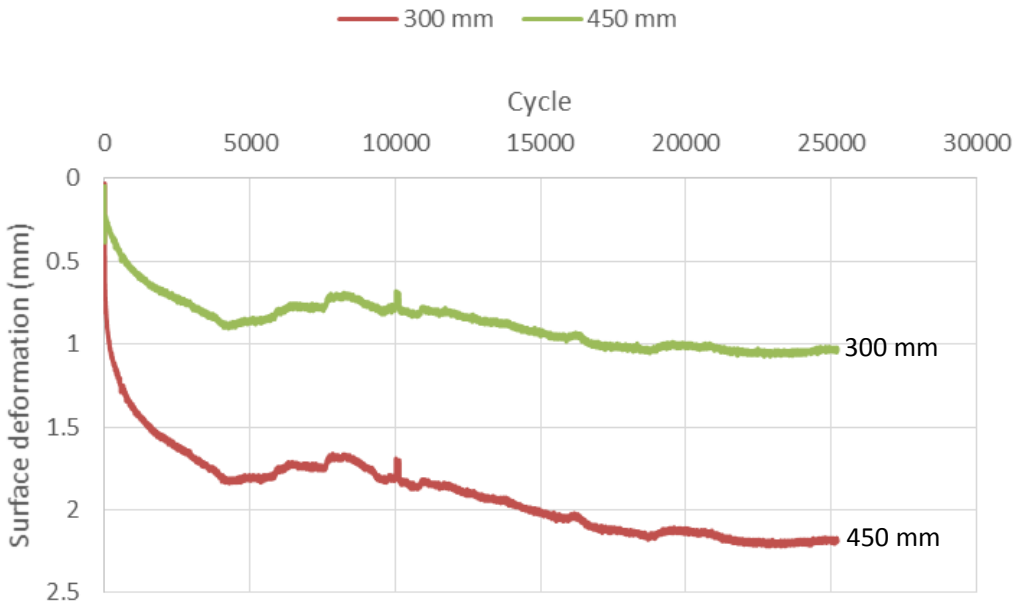

Figure 3.15 Surface permanent deformations at distances from the center in Test 1

The test was interrupted several times due to the overheating of the oil pump. The test was terminated at the pre-set maximum number of cycles (i.e., 25,000 cycles) before reaching the failure criterion of 75 mm. The permanent deformation at 25,000 cycles was approximately 39.6 mm. The average elastic rebound deformation was 2.9 mm. The interface pressure at the center of the loading plate first increased then decreased. The highest pressure recorded on the center pressure cell was 278 kPa. The interface pressure at 150 mm from the center of the loading plate increased rapidly in the first 100 cycles from 105 kPa to 121 kPa. Then the pressure continued increased at a slower rate, and at 25,000 cycle, the pressure was at 154 kPa. The interface pressure at 300 mm from the center gradually decreased from 57 kPa to 49 kPa. The earth pressure cell at 600 mm from the center did not record any pressure significant enough to be distinguished from the noise thus was not presented. Figure 3.15 shows that the surface permanent deformations away from the plate were small.

Test 2 – 200-mm soil-aggregate mixture base

The vane shear test data indicated the subgrade had a CBR of 5.1%. The DCP test indicated a 4.9% CBR of the base and 7.5% CBR of the subgrade. The LWD test showed an average elastic modulus of the base course at 29.1 MPa. The lower CBR value of the base course as compared with that in Test 1 was because of the existence of the topsoil and the higher moisture content in the preparation.

Figure 3.16 presents the permanent and rebound deformations of the loading plate with the number of cycles. Figure 3.17 presents the interface pressure at different pressure cell locations. Surface permanent deformations at the distances of 300, 450, and 600 mm from the center of the plate are presented in Figure 3.18, in which the positive value indicates settlement and the negative value indicates heave.

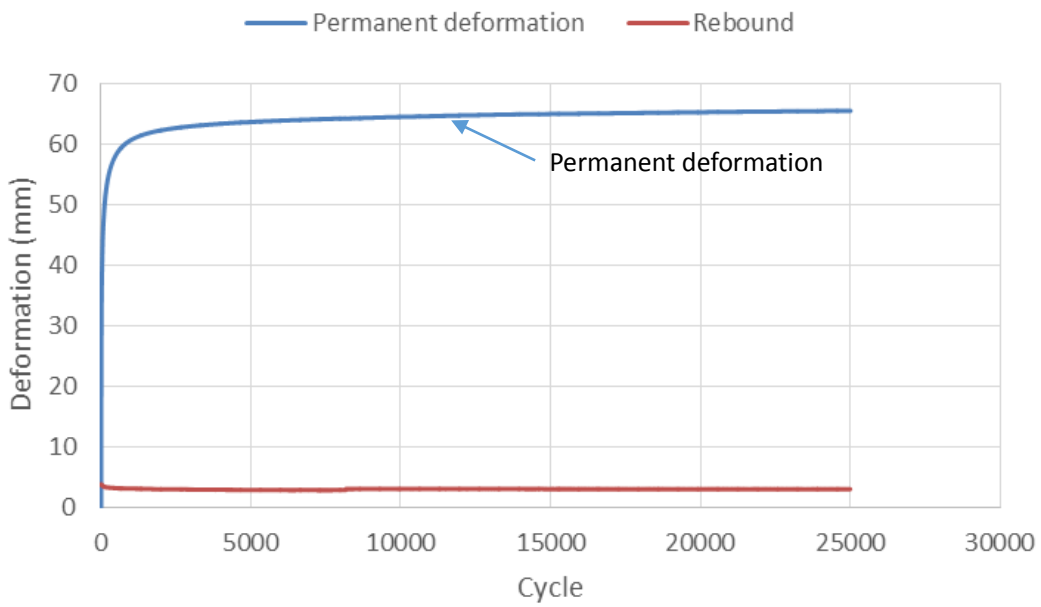

Figure 3.16 Permanent and elastic rebound deformations of the loading plate in Test 2

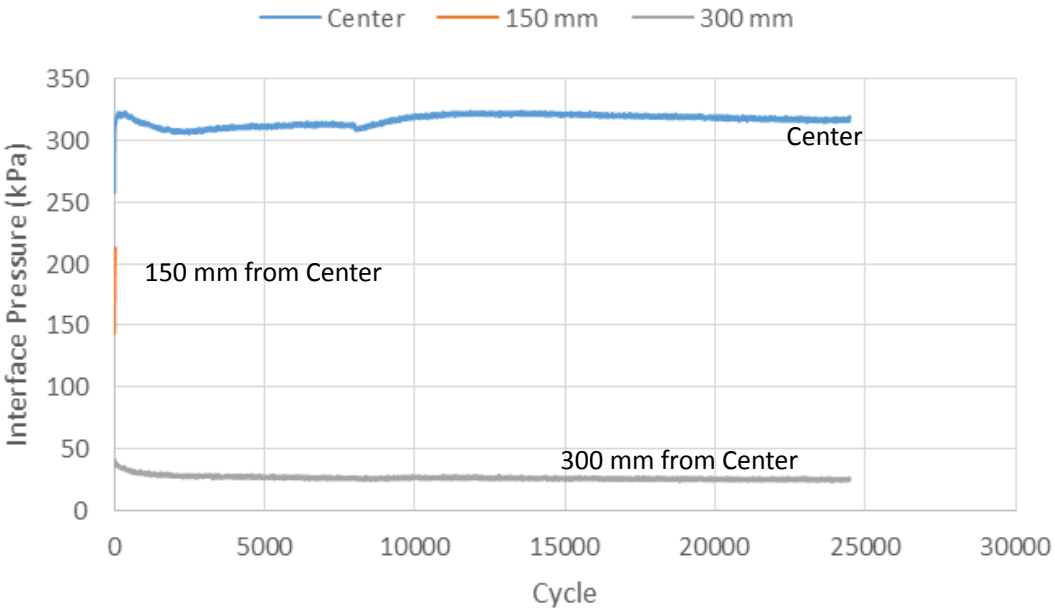

Figure 3.17 Interface pressures at various locations in Test 2

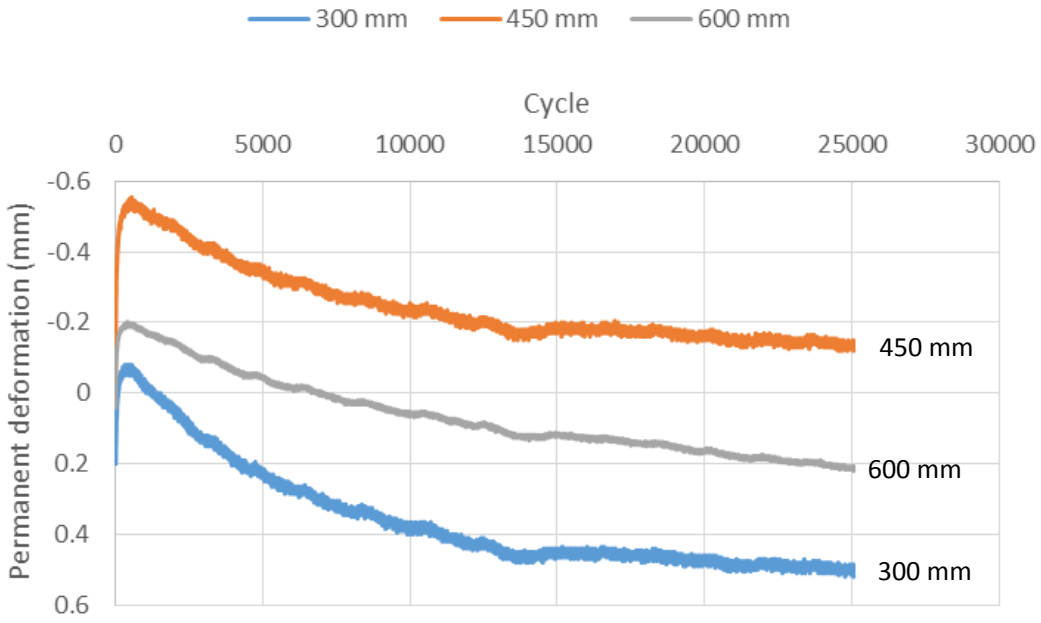

Figure 3.18 Surface permanent deformations at distances from the center in Test 2

The 200-mm thick soil-aggregate mixture base did not reach the 75 mm

permanent deformation failure criterion thus the test was terminated at 25,000 cycles. The final permanent deformation under the loading plate was approximately 65 mm. The average elastic deformation under the loading plate was 2.9 mm. Figure 3.18 indicates that the surface around the loading plate first heaved then settled. The surface permanent deformations indicated the settlements (but less than 0.6 mm) at 300 mm and 600 mm and heave at 450 mm from the center. The earth pressure cell at 150 mm from the center was damaged at the 26th loading cycle. Within the first 26 cycles, the interface pressure at 150 mm increased from 143 kPa to 212 kPa rapidly. The interface pressure at the center increased from 257 kPa at the first loading cycle to a peak 323 kPa at approximately 300 cycles then remained relatively constant. The interface pressure at 300 mm from the center decreased from 40 kPa to 27 kPa within the first 5000 cycles and then remained constant. The earth pressure cell at 600 mm from the center did not record any pressure significant enough to be distinguished from the noise thus was not presented.

Test 3 – 200-mm geocell-reinforced soil-aggregate mixture base

The vane shear tests indicated a 4.7% CBR for the subgrade. The DCP tests showed 8% CBR for the base course and 6.1% CBR for the subgrade. The LWD test indicated the elastic modulus of the base course was 34.2 MPa.

Figure 3.19 presents the permanent and elastic rebound deformations with the number of cycles. Figure 3.20 presents the interface pressures at different pressure

cell locations. The surface permanent deformations at distances of 300, 450, and 600 mm are presented in Figure 3.21.

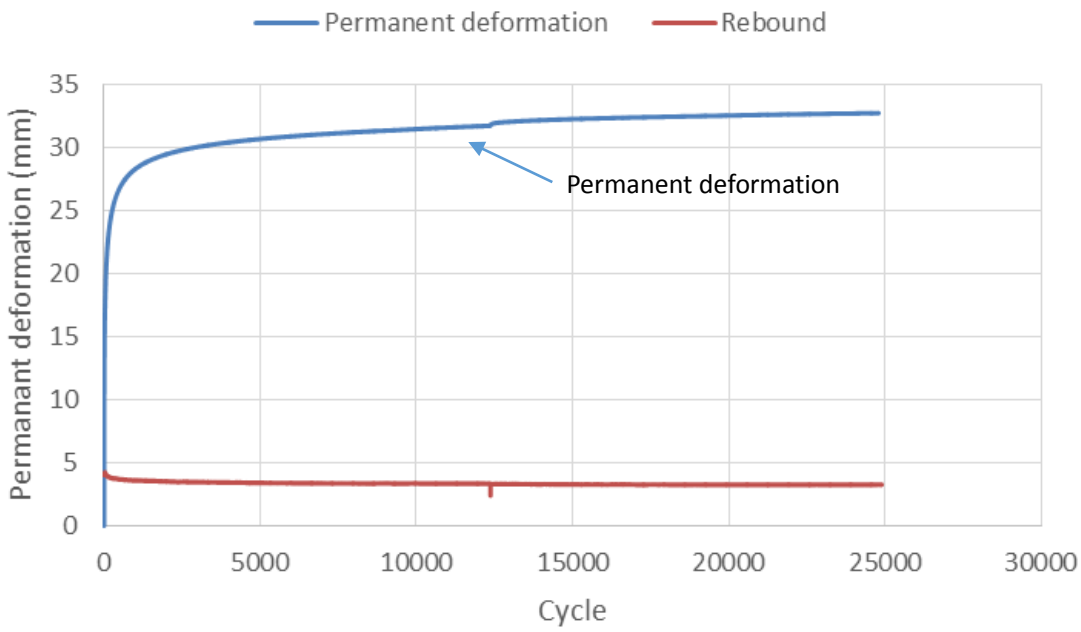

Figure 3.19 Permanent and elastic rebound deformations of the loading plate in Test 3

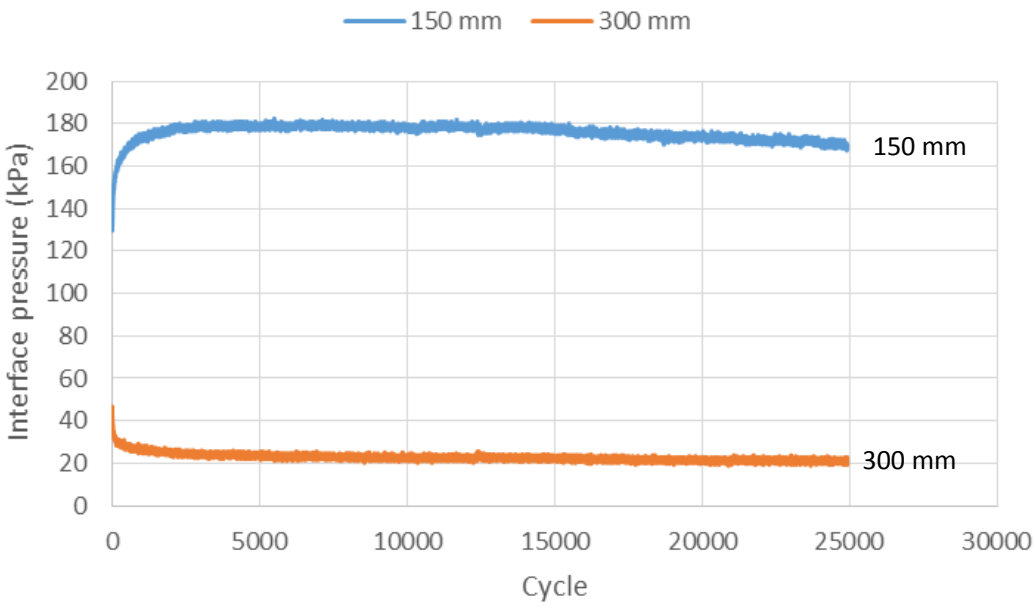

Figure 3.20 Interface pressures at various locations in Test 3

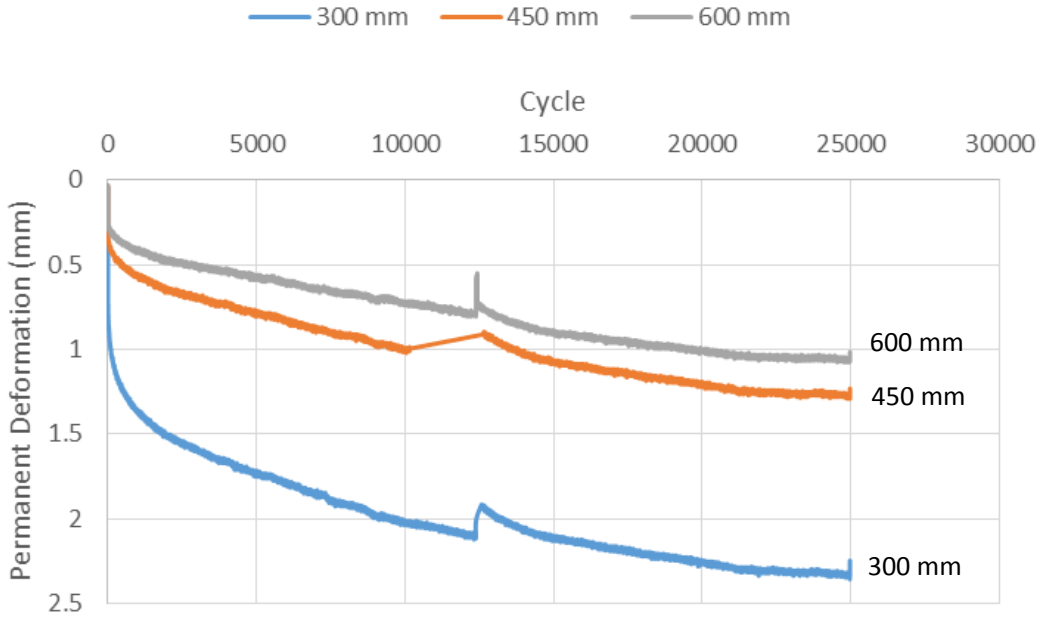

Figure 3.21 Surface permanent deformations at distances from the center in Test 3

Test 3 was paused at around 12,000 cycles due to the overheating of the oil pump. The test was terminated at 25,000 cycle and the final permanent deformation was 32.7 mm. The average elastic deformation under the loading plate was 3.4 mm. The pressure cell at the center was damaged during installation. The interface pressure at 150 mm from the center increased rapidly from 130 kPa to 180 kPa in the first 2,500 cycles and then decreased slightly after the 15,000 cycles. The interface pressure at 300 mm from the center decreased from 40 kPa to approximately 20 kPa. The earth pressure cell at 600 mm from the center did not record any pressure significant enough to be distinguished from the noise thus was not presented. The surface of the test section settled over the process of the test at all three measured locations. At 300 mm from the center, the final permanent deformation was 2.4 mm.

Test 4 –50-mm thick AB3 over 150-mm geocell-reinforced soil-aggregate mixture

The vane shear tests showed a 4.4% CBR subgrade. The DCP tests indicated the base course CBR at 8.2% and the subgrade CBR at 6.0%. The LWD tests indicated the base elastic modulus was 34.3 MPa.

Figure 3.22 presents the permanent and elastic rebound deformations of the loading plate. Figure 3.23 presents the interface pressures at different pressure cell locations. The surface permanent deformations at distances of 300, 450, and 600 mm are presented in Figure 3.24.

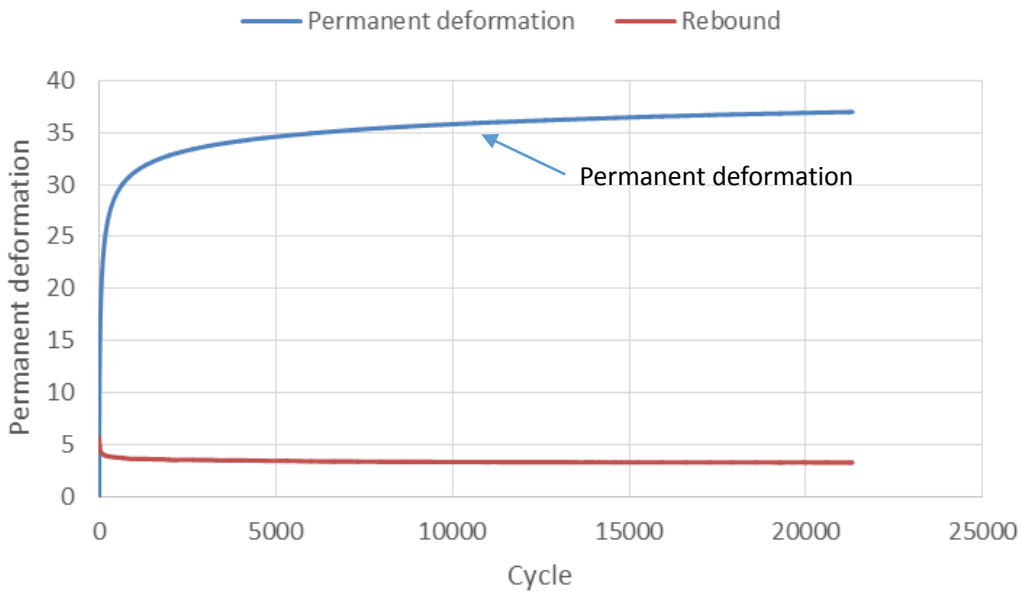

Figure 3.22 Permanent and elastic rebound deformations of the loading plate in Test 4

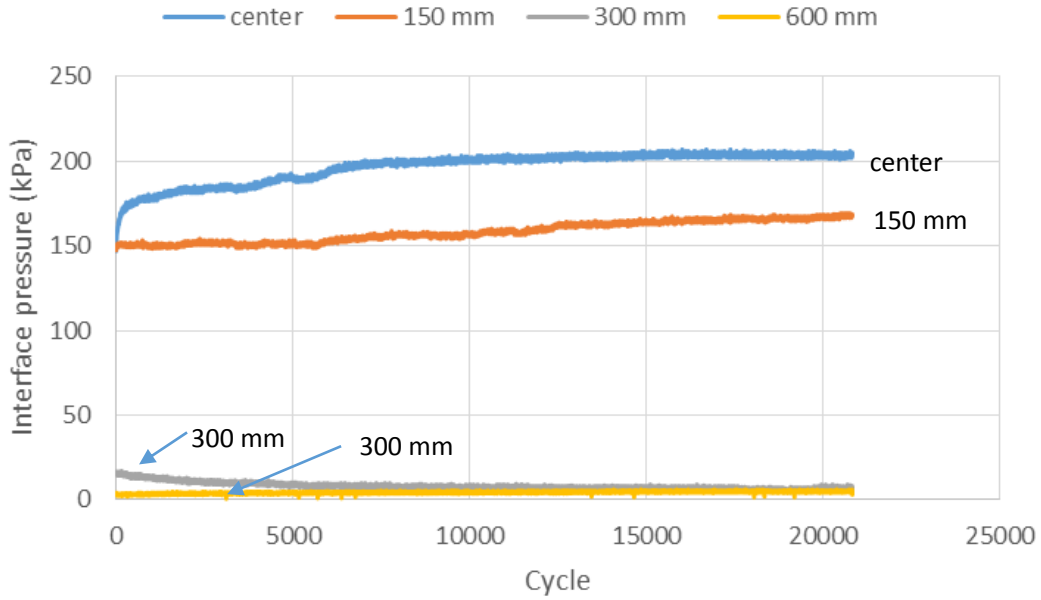

Figure 3.23 Interface pressures at various locations in Test 4

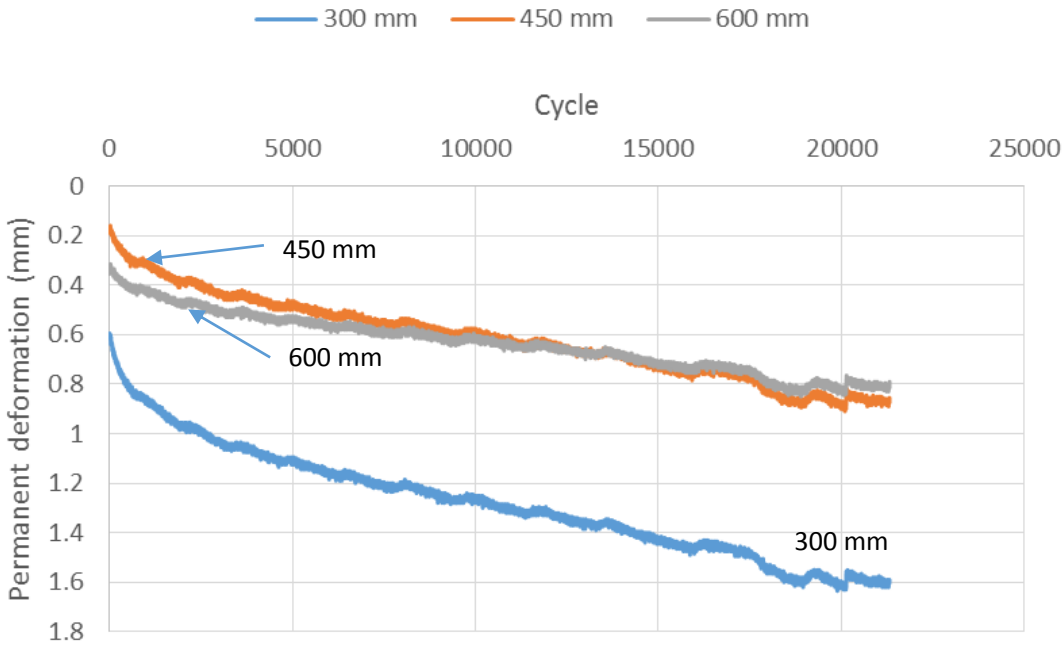

Figure 3.24 Surface permanent deformations at distances from the center in Test 4

The test was terminated at 22,000 cycles. The test section had a final

permanent deformation of 37 mm. The average elastic deformation was 3.4 mm. The center interface pressure increased from 150 kPa to 200 kPa within the first 7,500 cycles and increased slightly in the rest of the test. The Interface pressure at 150 mm from the center remained constant in the first 5,500 cycles and then started to increase and reached a maximum value of 170 kPa. The interface pressure at 300 mm from the center decreased from 16 kPa to 7 kPa gradually over the test period. The interface pressure at 600 mm from the center started from 3 kPa and reached 5 kPa at the end of the test. The surface of the test section settled as the progress of the test. At 300 mm from the center, the surface settled 1.6 mm at the end of the test while the surfaces at 450 mm and 600 mm from the center settled around 0.8 mm.

Test 5 –50-mm thick topsoil over 150-mm geocell-reinforced soil-aggregate mixture

The vane shear tests showed a 4.5% CBR subgrade. The DCP tests indicated the base course CBR at 5% and the subgrade CBR at 7%. The LWD tests indicated the base elastic modulus was 15.7 MPa.

Figure 3.25 presents the permanent and elastic rebound deformations of the loading plate. Figure 3.26 presents the interface pressures at different pressure cell locations. The surface deformations at distances of 300, 450, and 600 mm from the center are presented in figure 3.27.

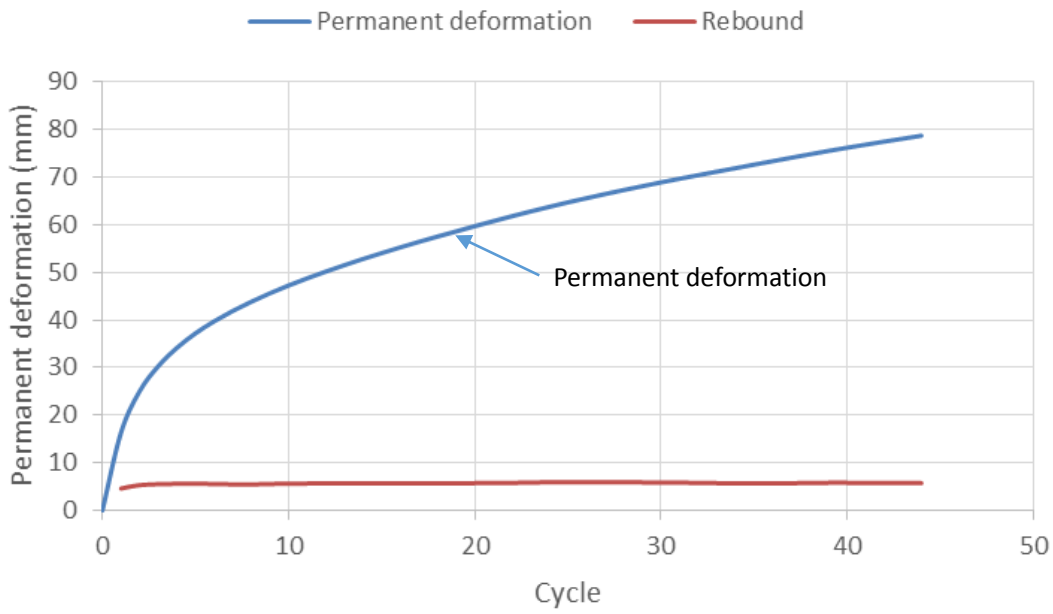

Figure 3.25 Permanent and elastic rebound deformations of the loading plate in Test 5

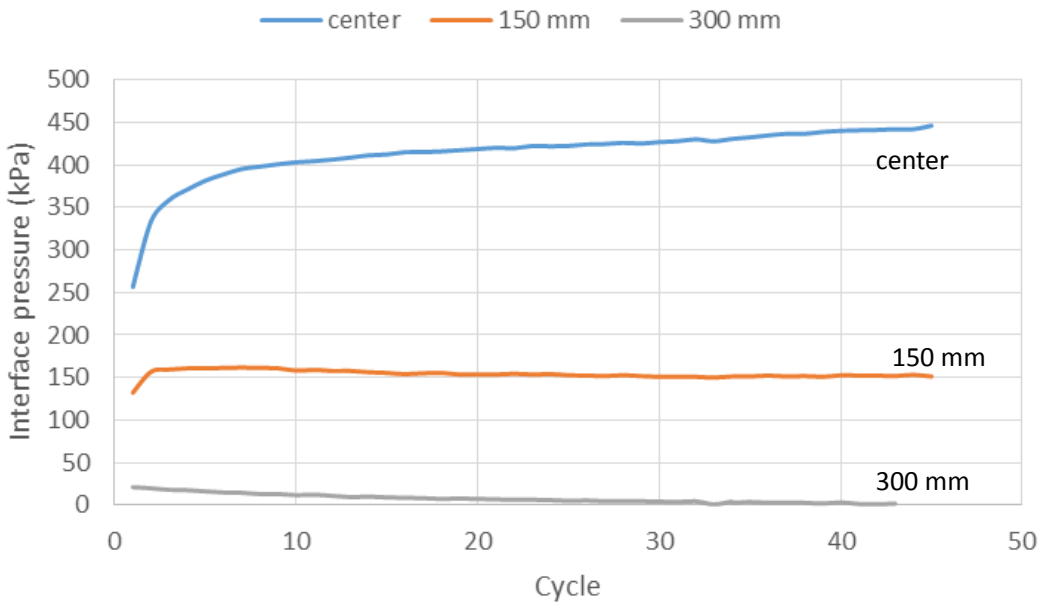

Figure 3.26 Interface pressures at various locations in Test 5

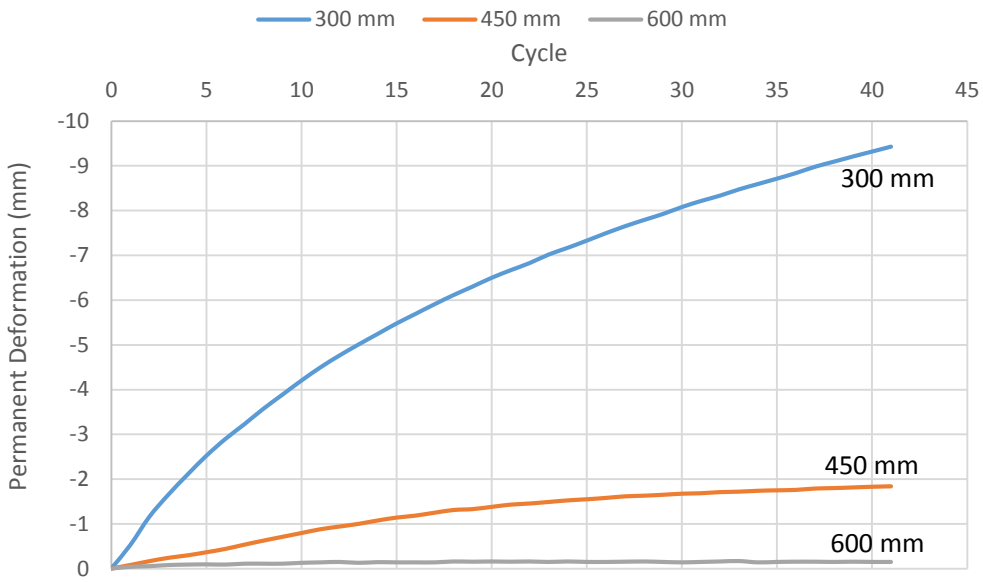

Figure 3.27 Surface permanent deformations at distances from the center in Test 5

Test 5 only lasted 39 cycles before reaching 75 mm permanent deformation. After failure, the test was continued to 44 cycles. The average elastic deformation was 5.7 mm. Both the earth pressure cells at the center and 150 mm from the center showed an increase in the pressure within the first 4 cycles. The center interface pressure continued increasing to 450 kPa while the interface pressure at 150 mm from the center slightly decreased after the first 4 cycles and maintained at 150 kPa. The interface pressure at 300 mm from the center decreased from 21 kPa initially to 1 kPa at the 40th cycle. The surface of the test section showed relatively large heave at the distances of 300 mm and 450 mm from the center while the surface at a distance of 600 mm from the center remained unchanged. At the distance of 300 mm from the center, the surface heaved up approximately 9 mm while at 450 mm from the center,

the surface heaved approximately 2 mm at the end of the test. These heaves indicated the failure of the soil cover.

Test 6 – 200-mm thick geocell-reinforced topsoil

The vane shear tests showed a 4.5% CBR subgrade. The DCP tests indicated the base course CBR at 2.3% and the subgrade CBR at 4.4%. LWD tests indicated the base elastic modulus was 10.9 MPa.

Figure 3.28 presents the permanent and elastic rebound deformations of the loading plate with the number of cycles. Figure 3.29 presents the interface pressures at different pressure cell locations. The surface deformations at the distances of 300, 450, and 600 mm are presented in Figure 3.30.

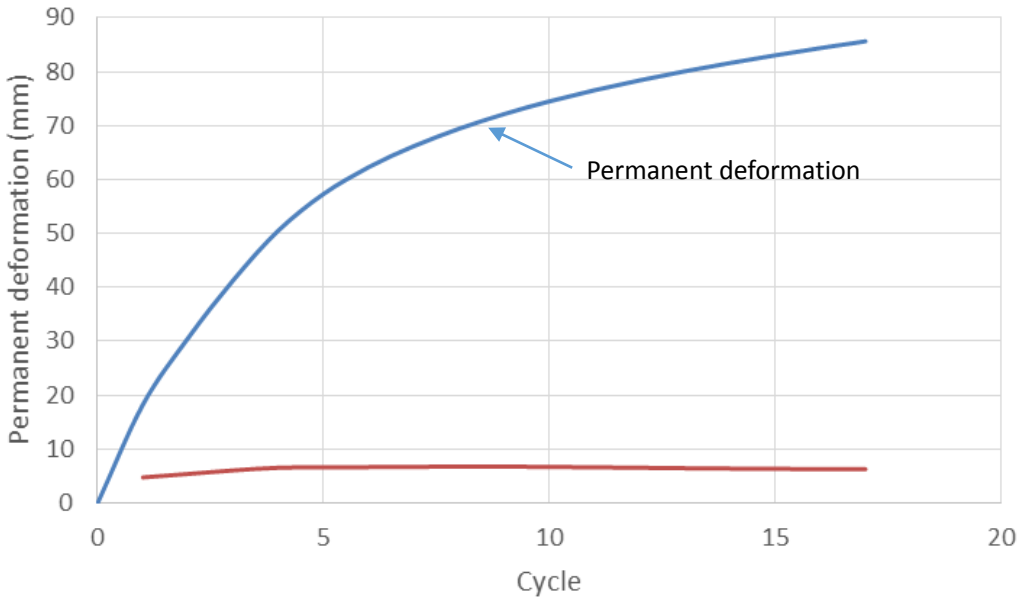

Figure 3.28 Permanent and elastic rebound deformations of the loading plate in Test 6

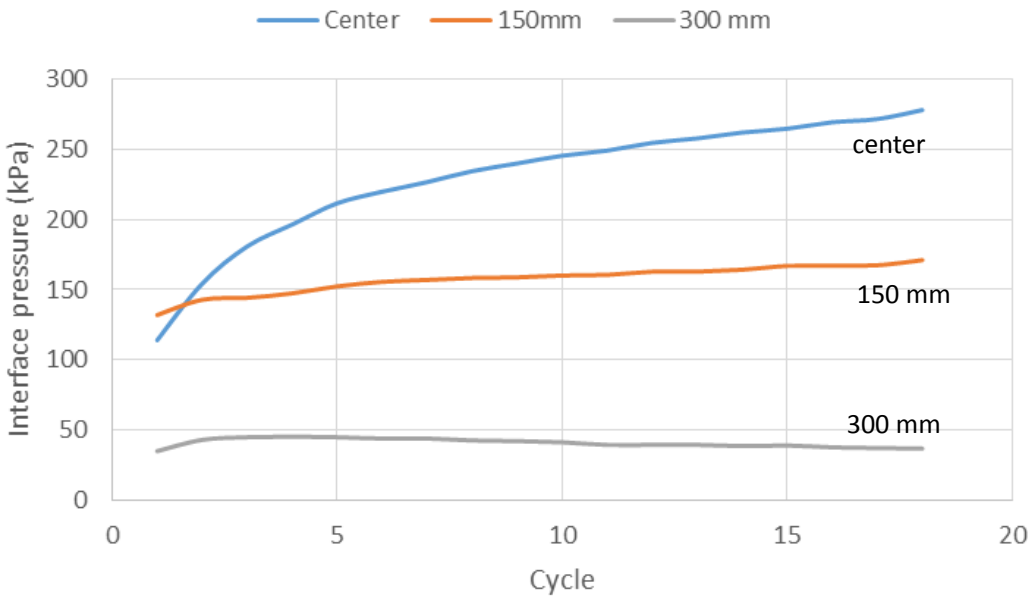

Figure 3.29 Interface pressures at various locations in Test 6

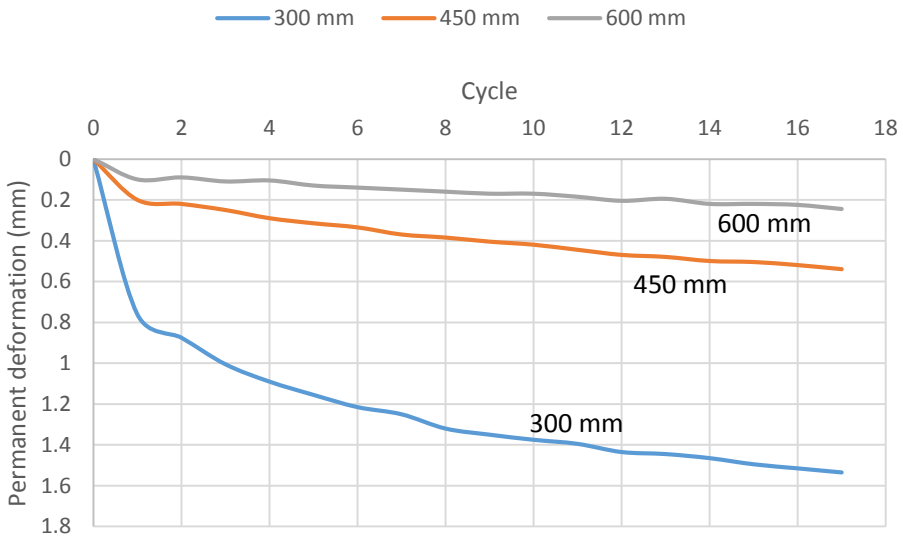

Figure 3.30 Surface permanent deformations at distances from the center in Test 6

In Test 6, the test section reached the 75 mm failure criterion at the 11th cycle. The test was then terminated at the 18th cycle. The average elastic deformation was

6.3 mm. The interface pressures at both the center and the distance of 150 mm from the center increased with the number of cycles. The interface pressure at the center increased from 114 kPa to 278 kPa at the 18th cycle and showed no sign of stabilization. The interface pressure at the distance of 150 mm from the center increased more gradually as compared with that at the center, for example, 132 kPa at the 1st cycle and 171 kPa at the 18th cycle. The interface pressure at the distance of 300 mm increased from 35 kPa to 45 kPa in the first 5 cycles and then decreased to 37 kPa at the end of the test. The surface deformations indicated the surface of the test section settled slightly at the end of the test.

3.3.4 Summary and discussion

The permanent deformation and elastic deformation under the loading plate as well as the subgrade and base course strengths from each test are listed in Table 3.3. In this table, the DCP test data are used to calculate the subgrade and base CBR values.

The only two test sections in Tests 5 and 6 failed due to the excessive deformation, both of which contained a topsoil cover layer. The topsoil was compacted at the moisture content of 21% to produce the maximum dry density. As compared with the aggregate cover and the soil-aggregate mixture cover, the topsoil cover was much softer and weaker thus yielding lower elastic moduli and higher elastic deformations.

Test sections 2 and 3 both consisted of a 200-thick mixture base course.

However, at 20,000 cycles, the reinforced section (i.e., Test 3) outperformed the unreinforced section (i.e., Test 2) by a large margin. The plate permanent deformation of the reinforced section at 20,000 cycles was less than half of that of the unreinforced section despite the subgrade in the unreinforced section was stronger. In addition, the elastic modulus of Test section 3 was 17.5% higher than that of Test section 2, which might result from the combined effect of the different compaction method and the geocell reinforcement.

Table 3.3 Summary of deformation under loading plate

Section No.	Subgrade CBR	Base CBR	Base elastic modulus	Plate permanent deformation at 20000 cycle	Average plate elastic deformation
	%	%	MPa	mm	mm
1	6.1	11	-	39	2.9
2	7.5	4.9	29.1	65	2.9
3	6.1	8	34.2	32	3.4
4	6	8.2	34.3	37	3.4
5	7	5	15.7	?	5.7
6	4.4	2.3	10.9	?	6.3

? Test terminated prior to 20,000 cycles due to the excessive deformation.

Test sections 3 and 4 performed similarly. Both sections had the LWD elastic modulus of 34 MPa and the elastic deformation of 3.4 mm. Test section 3 had a slightly less permanent deformation at 20,000 cycles than Test section 4. The 50-mm AB3 aggregate cover layer showed no improvement than the 50-mm soil-aggregate mixture cover layer. Both Test sections 3 and 4 performed slightly better than Test section 1 despite Test section 1 consisted of the base course with a higher CBR value.

All test sections except Test section 5 had less than 2.5 mm surface settlement throughout the test based on the displacement measurements. In Test 5, the surface heaved at all three measured locations because of the failure of the topsoil cover.

Figure 3.31 presents the comparison of the interface pressures at the 15^{th} cycle. The center interface pressure of Section 3 is estimated based on Section 4. Section 3 and Section 4 showed significantly lower center interface pressure, which indicted the geocell-reinforced base effectively reduced the pressure on subgrade directly blow the loading plate. Section 5 showed the greatest center pressure partially due to the base consisting of a low strength cover layer and a strong reinforced layer. The weak cover layer reduced the effective depth of the base.

Figure 3.32 presents the comparison of interface pressure at the $20{,}000^{th}$ cycle for all six test sections. The interface pressure at the distance of 300 mm in Test section 2 and the interface pressure at the center in Test section 3 were estimated based on the applied load and the pressures measured by functional pressure cells. The interface pressures at the center at the $20{,}000^{th}$ cycle were higher than those at the 15^{th} cycle. The interface pressures at the center in Test sections 3 and 4 were lower than those in Test sections 1 and 2.

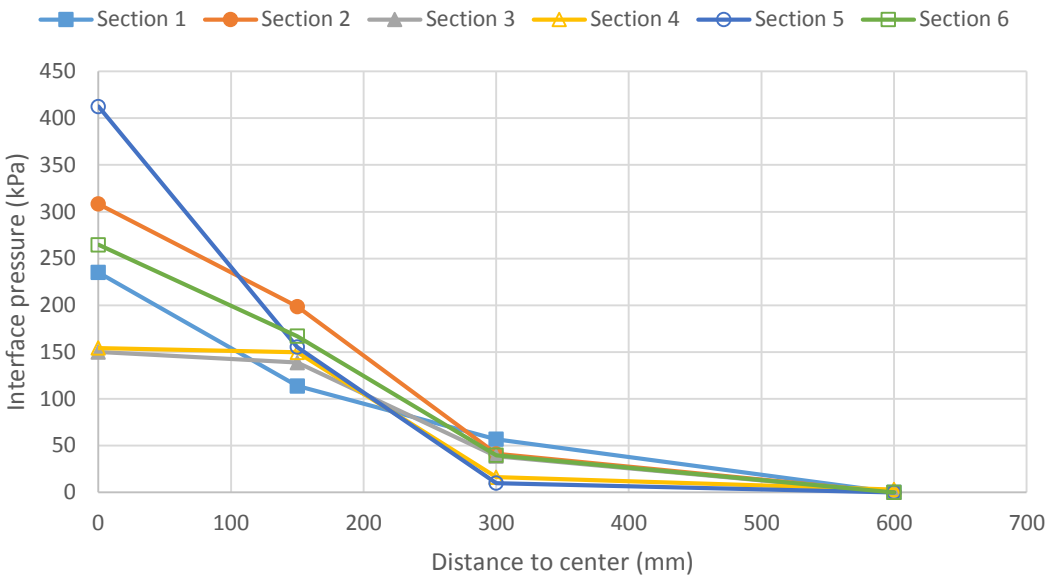

Figure 3.31 Interface pressure distributions for all test sections at the 15th cycle

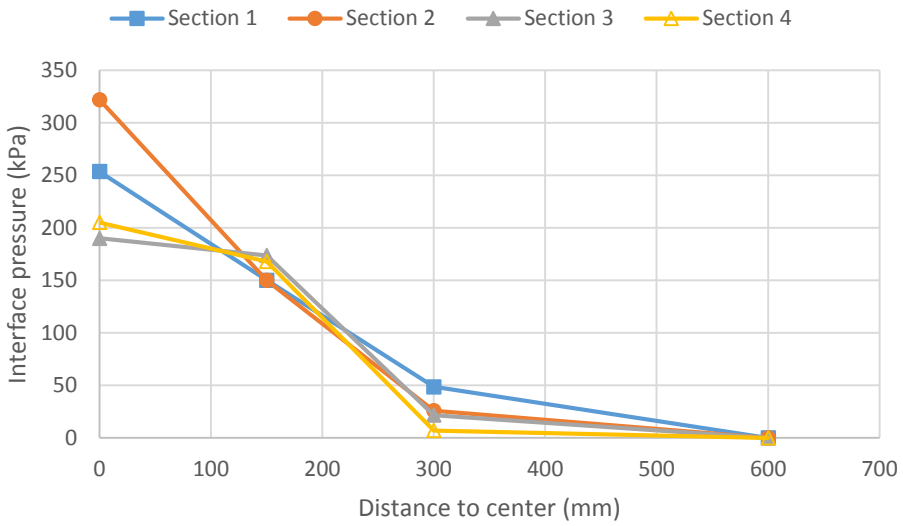

Figure 3.32 Interface pressure distributions for Test sections 1 to 4 at the 20,000th cycle

3.4 Vegetation Tests

The goal of the outdoor field vegetation tests was to investigate the possible effect of the following factors on vegetation growth: (1) base course composition and (2) geocell reinforcement. The test was continued for a period of 13 months. To eliminate uncertain factors, human activities were restricted as much as possible and the nearby trees were taken down. The sections were not mowed over the test period. The grass leaf blade length, root length, and vegetation density were measured as the indicators of vegetation growth. Biomasses were collected at the end of the test.

3.4.1 Test setup and preparation

The outdoor vegetation test was conducted on the University of Kansas West Campus. The location of the test site is noted with white box in Figure 3.33.

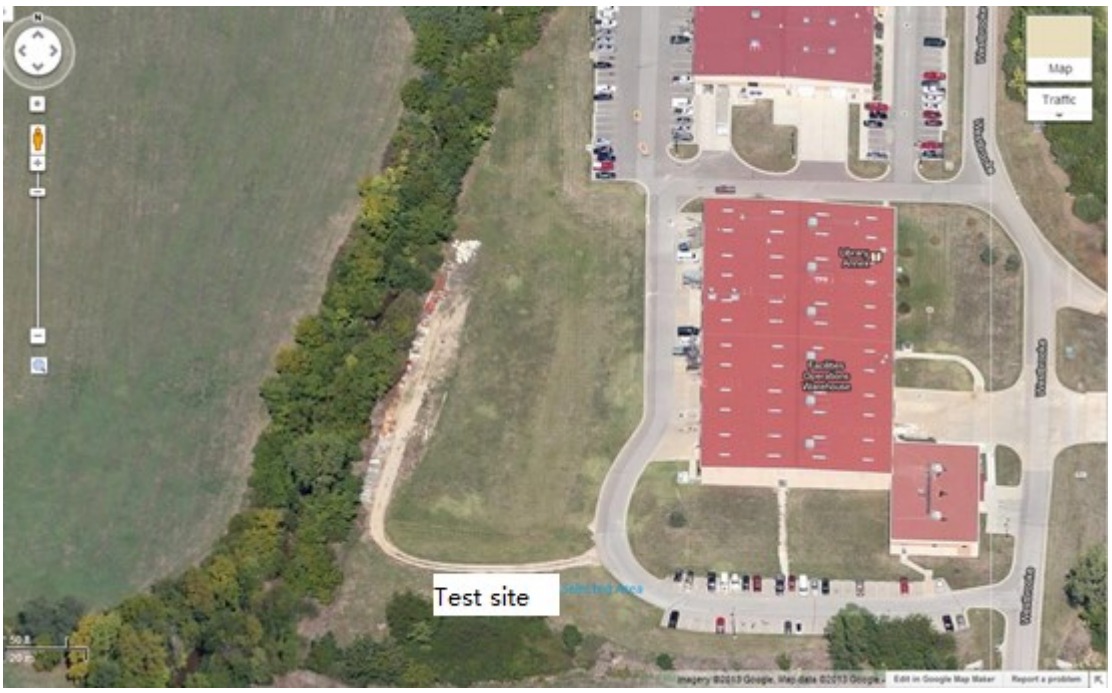

Figure 3.33 Location of the test site (Google 2013)

Eight test sections were constructed in this study, which are divided into four groups (numbered from one to four). Each test section was in the size of 1.5 m × 1.5 m. Two sections in each group were constructed with identical base course and soil cover materials at identical thickness and received the same amount of seeds. Each group consisted of a control (unreinforced) section (noted with C followed by the group number), in which no geocell reinforcement was installed, and a reinforced section (noted with R followed by the group number) was installed with the geocell. All the groups were arranged in a line with all control sections placed on the north side and the reinforced sections on the south side. Each test section was constructed with a transverse slope to simulate the slope of the shoulder. According to the

KDOT Road Design Manual, a 1.6% slope was used for both the subgrade and the base course and a 4.2% slope was used for the top surface. A longitudinal slope along the centerline of the groups was created in place to provide drainage of each section. The group arrangement and the cross section of each group are shown in Figure 3.34.

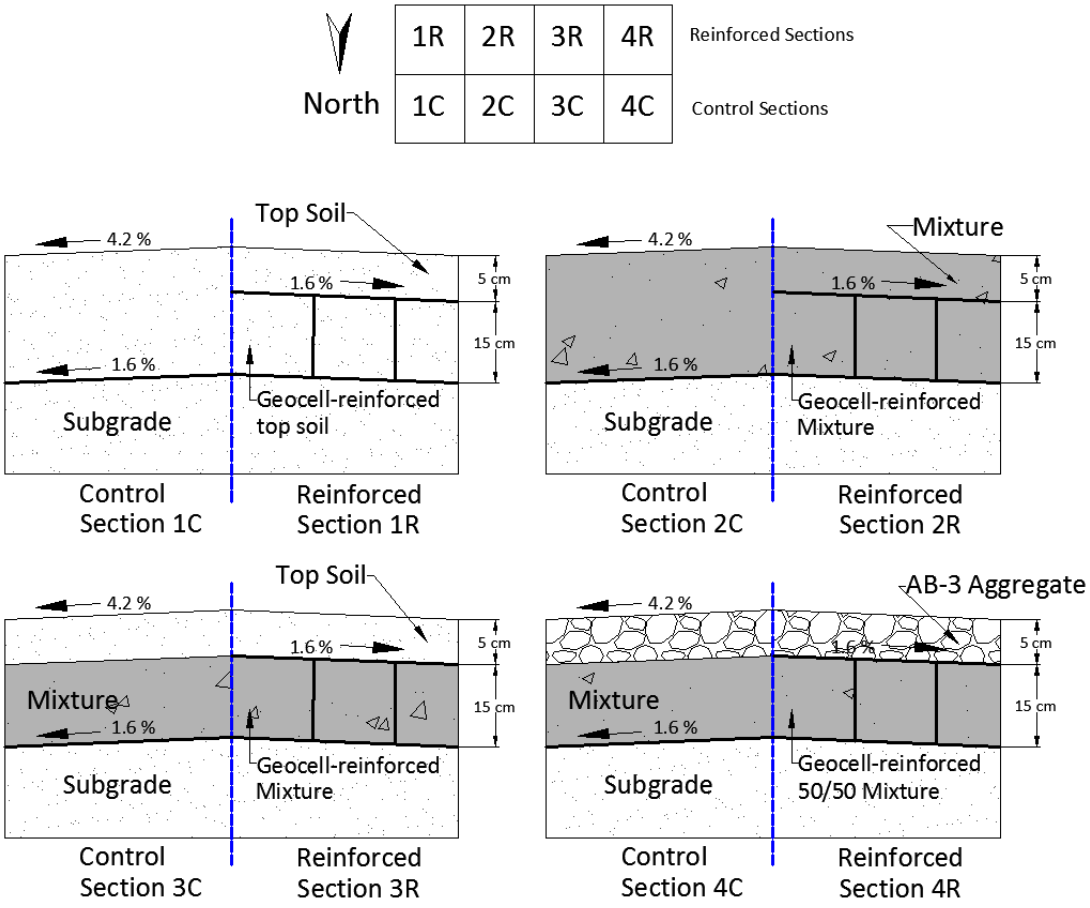

Figure 3.34 Test section arrangement and cross sections

Native grass was trimmed off in a 4 m × 10 m area. Then a 3.5 m × 10 m test area was excavated to a depth of 170 mm, as shown in Figure 3.35.

Figure 3.35 Area for the vegetation test

After the excavation, leveling equipment and a compactor were brought in to create the desirable depth and slope of the subgrade. In order to maintain the desired size and depth of each section and minimize the influence by adjacent sections, plywood frames were assembled on the site. Instead of setting the plywood frames directly on the subgrade, they were elevated with small pieces of wood block leaving a gap of approximately 50 mm between the frames and the subgrade to allow the drainage of water and prevent excessive water trapped in each test section. According to the Kansas Department of Transportation Road Design Manual, a 1.6% slope was constructed on the native soil shown in Figure 3.36.

To provide a drainage condition similar to that for actual unpaved shoulders, a 20-mm-thick layer of geotextile-wrapped ballast (not shown in figure) was placed between the fill material and the plywood board along each side allowing water flow to the drainage trench. The drainage trench then led water to a water storing hole (not shown) at the far end in Figure 3.37.

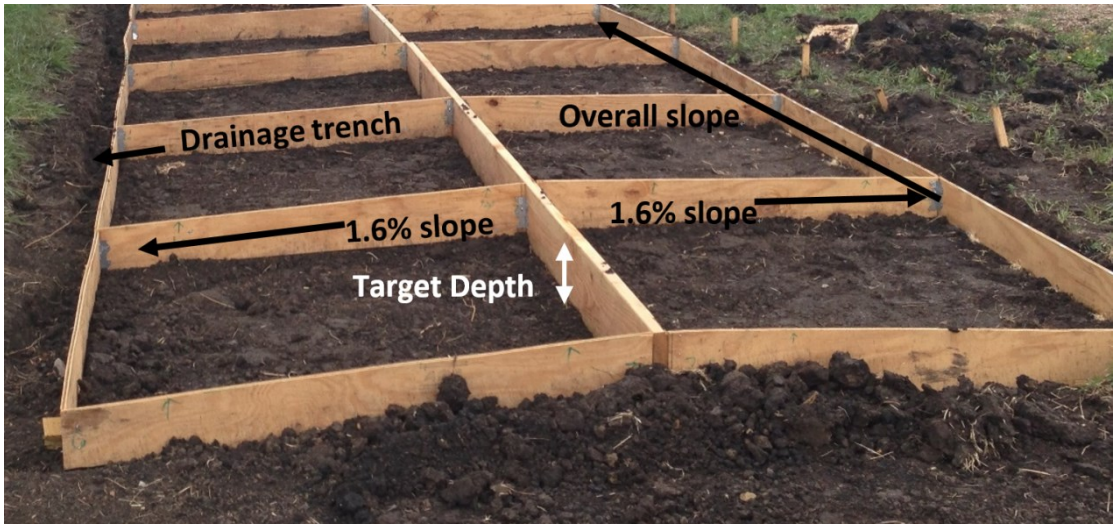

Figure 3.36 Plywood frame

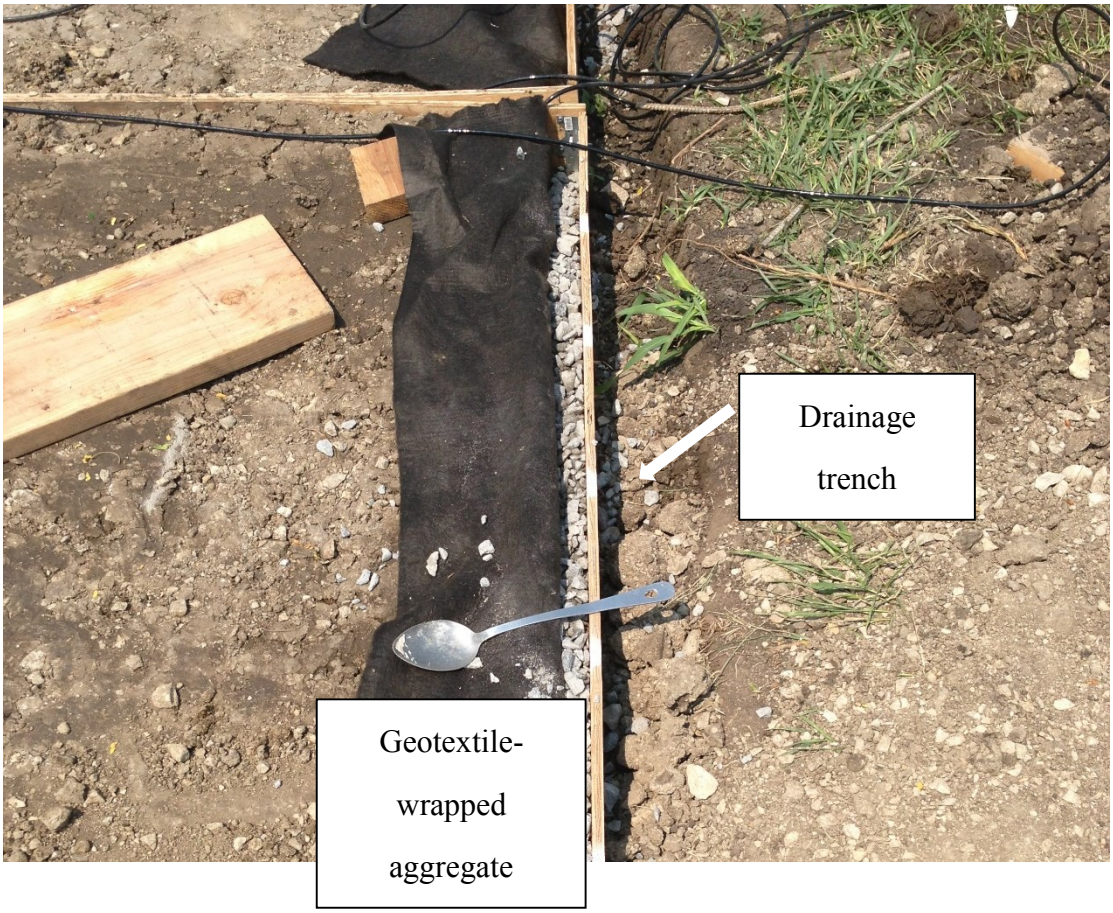

Figure 3.37 Drainage system

During the backfill, a diesel vibratory compactor was used to compact the soil to approximately 90% relative compaction based on the maximum dry density determined by the modified Proctor method. To achieve 90% compaction, the materials were compacted in three to four layers. The degree of compaction in each section was verified with sane cone tests. Sand cone tests showed the degrees of relative compaction for all sections ranged from 87.2% to 90.5%. Figure 3.38 (a) shows the placement of geocell and Figure 3.38 (b) shows the compacting with a vibratory compactor.

(a)

(b)

Figure 3.38 (1) Placement of geocell and (b) compaction of geocell-reinforced section.

Preparation for seeding started after all sections were filled and compacted to the desired thickness. For each section to receive an equal amount of seeds of each species, seeds were pre-mixed for each section separately. The test sections were watered for the equal amount of time prior to spreading seeds to provide the water that the seeds needed in the planting process. The surface of each section was gently loosened so that the seeds would not be directly exposed to sunlight. Then seeds were spread evenly on each section by hand. At the end, a thin layer of red mulch was placed over all the sections to further protect the seeds from overheating and to maintain moisture. Figure 3.39 shows the section after sowing.

Figure 3.39 Sections after sowing.

Two types of moisture sensors produced by the Campbell Scientific, CS-655 and CS-616L, were installed horizontally at a depth of 75 mm below the surface in the center of each test section. The CS-655 sensors had a rod length of 120 mm and was capable of measuring both temperature and volumetric water content. The CS-655 sensors were installed in sections 1C, 1R, 2R, and 4R. The CS-616L sensors had a rod length of 300 mm and could only measure water content. The CS-616L sensors were installed in sections 2C, 3C, 3R, and 4C. The volumetric moisture sensors could only detect water in a liquid form thus the data collected in the dormancy period was not representative. The CS-616L sensor installed in section 3C could not fit in a single geocell pocket. The sensor was placed in two pockets with rods through the opening of the geocell wall.

3.4.2 Results and discussions

Based on the field observations and recorded data the vegetation growth can be divided into three periods or stages. The first period started from the initial establishment in the fall of 2013 and ranged from day 0 (i.e., the sowing day) to day 89 (i.e., mostly during the fall season). During this period, the average daily temperature gradually decreased with the highest time of 20℃ and lowest temperature of 6℃ while a few major rainfalls were recorded. The average temperature during this period was 13.3℃ and the accumulated precipitation was 295.5 mm according to the National Climatic Data Center record. The second period was the dormancy stage, ranging from day 90 to day 220 (i.e., mostly during

the winter season). During this period, a portion of the vegetation died and vegetation growth was seized. Temperature fluctuated largely during this period with the highest temperature of 18℃ and the lowest temperature of -18℃. The average temperature in this period was 0 ℃ and 83 mm precipitation was accumulated in the forms of rainfall and snow. The third time period was mostly within the spring and summer seasons of 2014, i.e., from day 221 to day 360. During this period, the temperature increased with an average temperature of 16℃ and the vegetation recovered and grew again. Some heavy rainfalls were recorded between day 300 to day 330 and the accumulated precipitation during this period was 431 mm. The weather data record obtained from the National Climatic Data Center between day 0 to day 400 are plotted in Figure 3.40, in which the average daily temperature is presented.

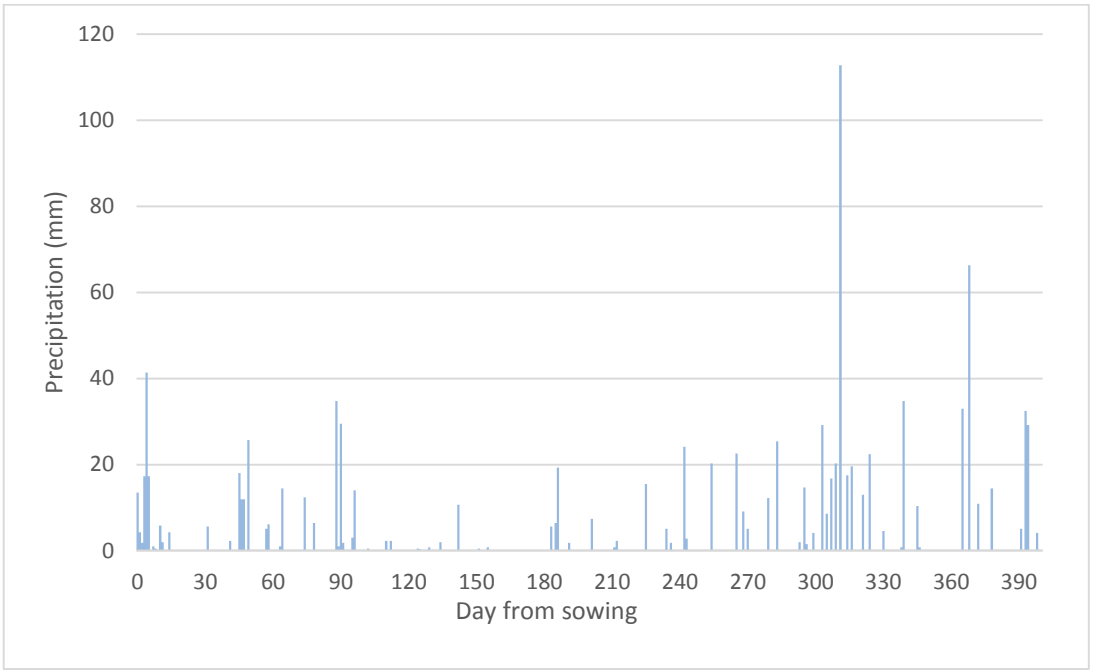

(a)

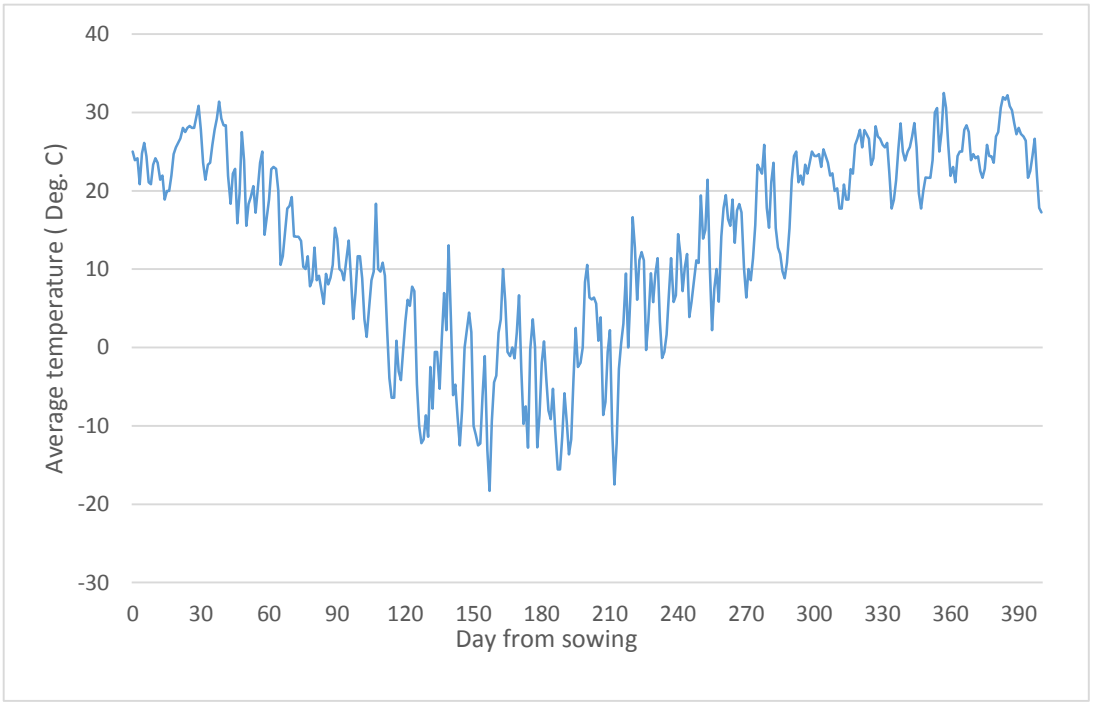

(b)

Figure 3.40 Daily weather record of: (a) precipitation and (b) average daily temperature

Soil volumetric water contents and temperatures were measured with sensors. The volumetric water content depends on not only the amount of water but also the soil density. The soil degree of compaction near the geocell wall might be different from the soil in the pocket center which may induce error in the measurement. The soil volumetric water content and temperature fluctuated with time thus the data collected at the chosen time in each day was presented in Figure 3.41. Figures 3.41 (a) to (d) presents the volumetric water contents of each section. The soil temperatures at 5:00 and 15:00 from four CS655 sensors were averaged and compared with air temperature in Figure 3.41 (e).

Water contents of group 1 were close to each other throughout the entire test period. In group 2, the control section presented significantly higher water content than the reinforced section at the beginning. The difference in the water content gradually decreased in the first 90 days. Between day 250 and day 400, the control section showed approximately 5% more volumetric water content than the reinforced section. In group 3, the reinforced section showed higher water content than the control section throughout the entire test. The difference between two sections gradually decreased. The difference between control and reinforced sections was most likely caused by the placement of the water content sensor in section 3C. In group 4, the control section showed higher water content in the first 50 days than the reinforced section. Both sections showed the similar amount of water content in the period between day 220 and day 400. The measured volumetric water contents in

all the sections showed a similar trend with precipitation. The volumetric water content decreased in dry days and increased sharply after heavy rain. For example, the peaks of water contents were recorded on day 339 and day 369. High precipitations were recorded on both days based on the weather data. The soil temperature showed a similar overall trend as the air temperature but the soil temperatures fluctuated less than the air temperature. In the winter, the soil temperatures were kept around 0℃. In the spring, the summer, and the fall, the soil temperatures at 15:00 were higher than those at 5:00.

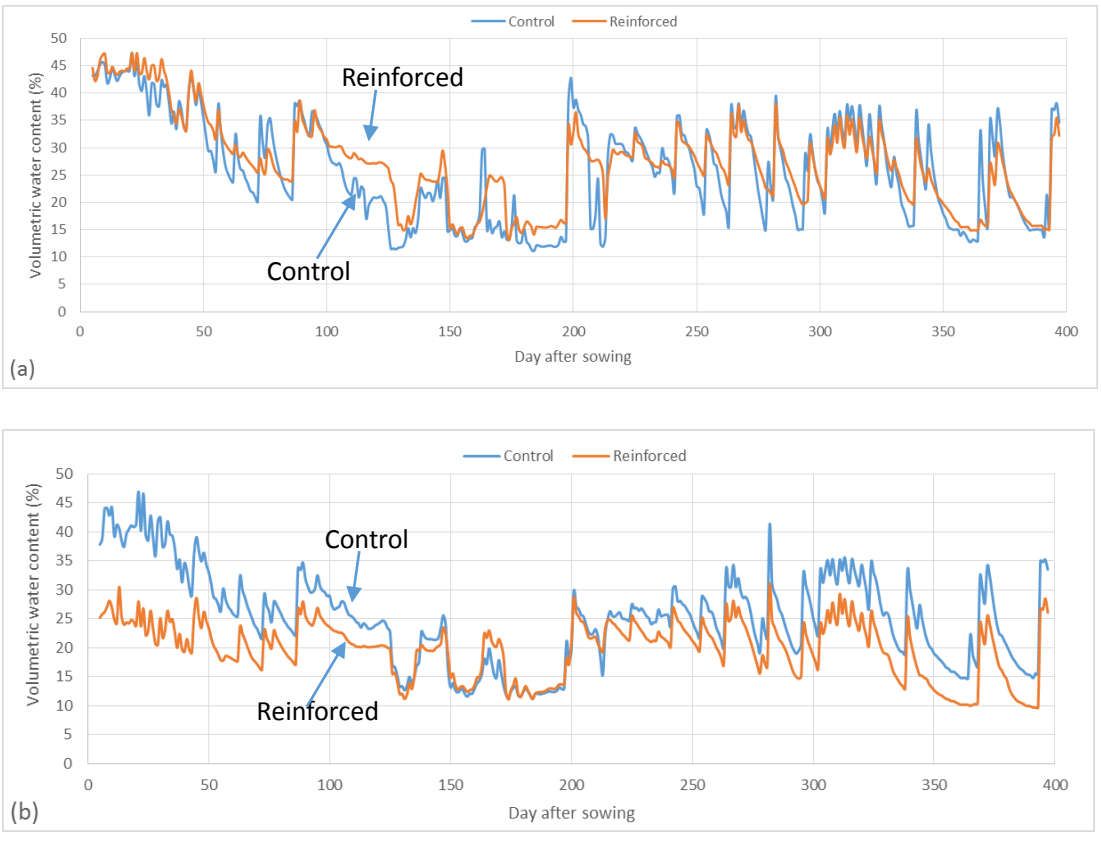

Figure 3.41 Soil volumetric water content of: (a) group 1; (b) group 2; (c) group 3; (d) group 4; and (e) soil and air temperatures.

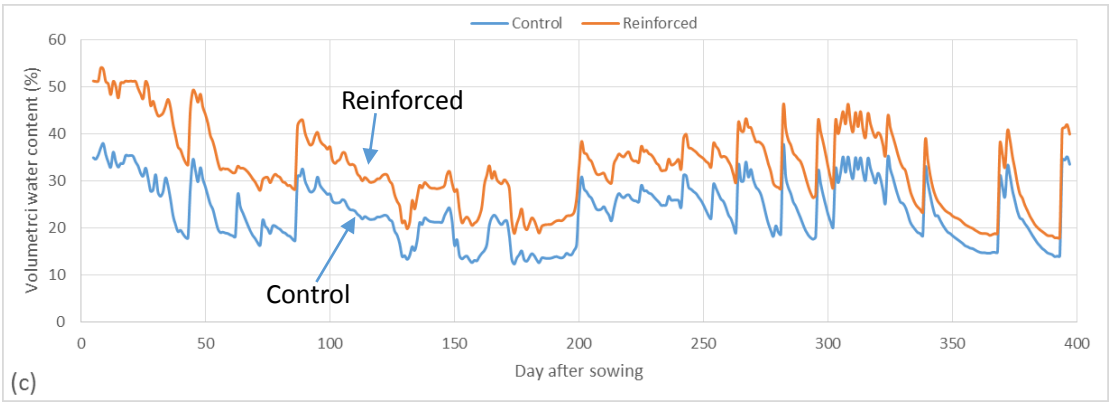

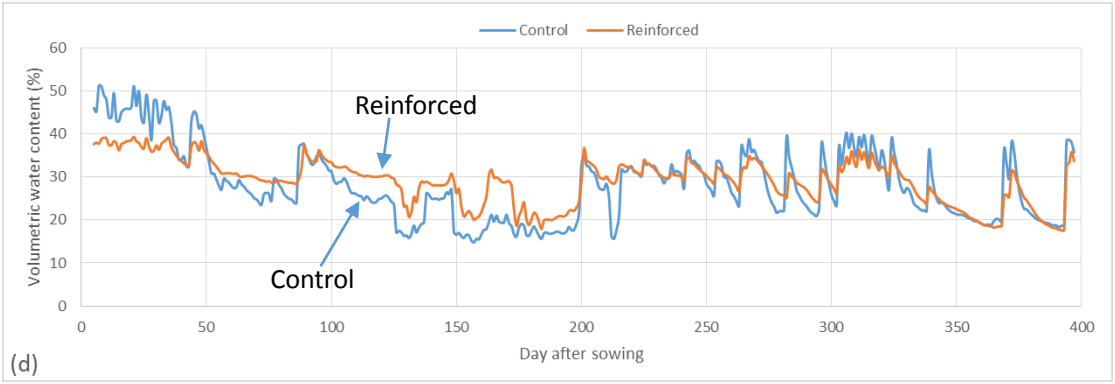

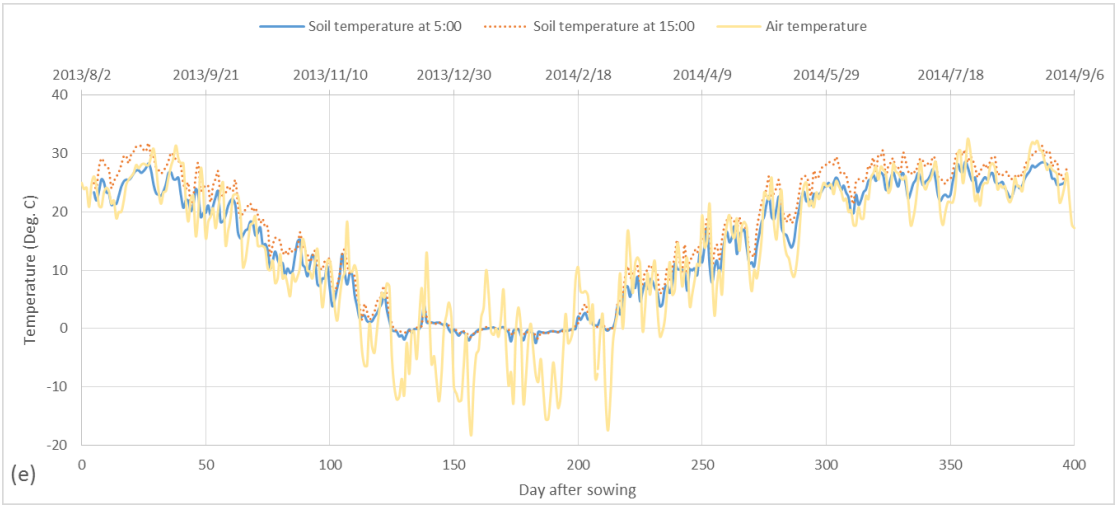

Figure 3.41 Soil volumetric water content of: (a) group 1; (b) group 2; (c) group 3; (d) group 4; and (e) soil and air temperatures (continued).

Grass leaf blade length

Five to eight individual plants, regardless of the species, were chosen randomly from each section as the sample of population. The limited number of plants were sampled considering the total number of plants available in each section at that time. The longest green leaf on each individual plant was measured and the average length was used to represent the blade length of the section. Figure 3.42 presents a picture taken during the blade length measurement.

Figure 3.42 Measuring blade length

The first buds appeared on day 2 in all sections. Due to the large blade length in the establishment stage differed significantly from the later stages, the results of the blade lengths for all test sections are presented separately in Figures 3.43 and 3.44.

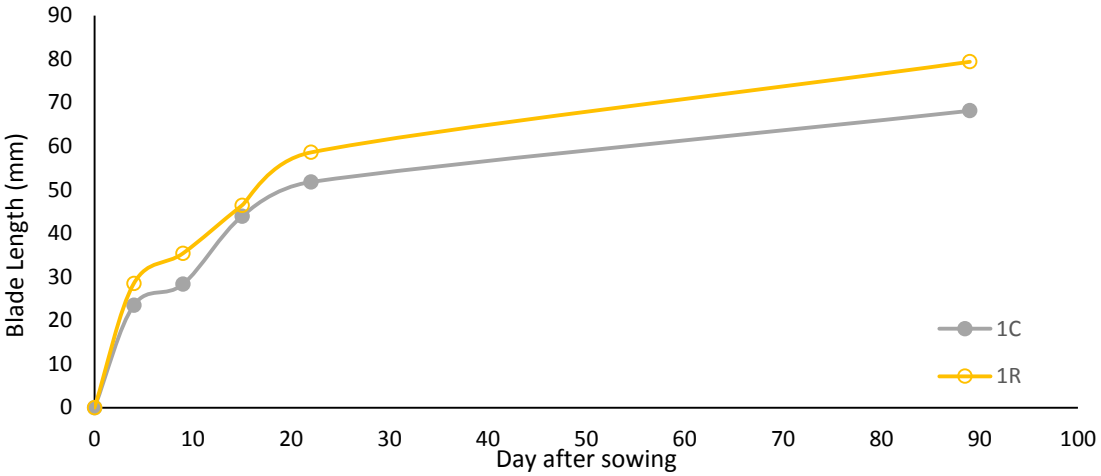

(a)

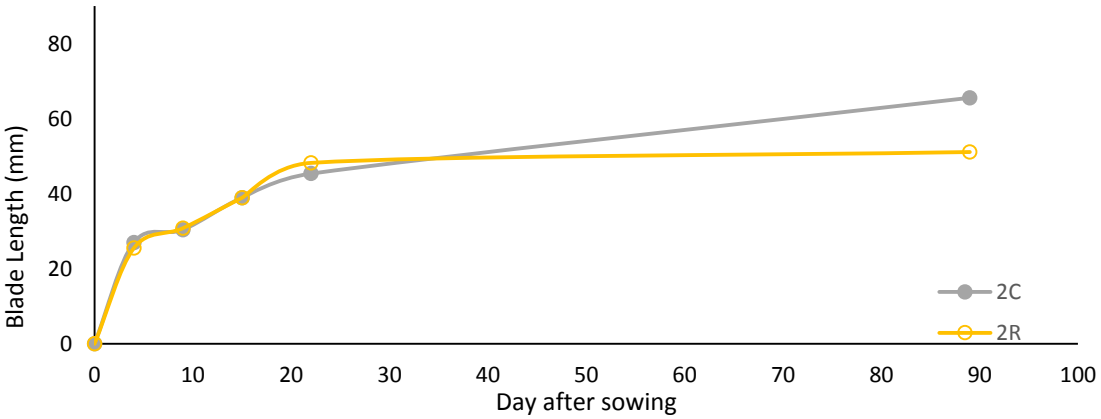

(b)

Fig. 3.43 Average blade length from day 0 to day 89 for: (a) group 1 section comparison; (b) group 2 section comparison; (c) group 3 section comparison; (d) group 4 section comparison; (e) all groups with the average value for each group.

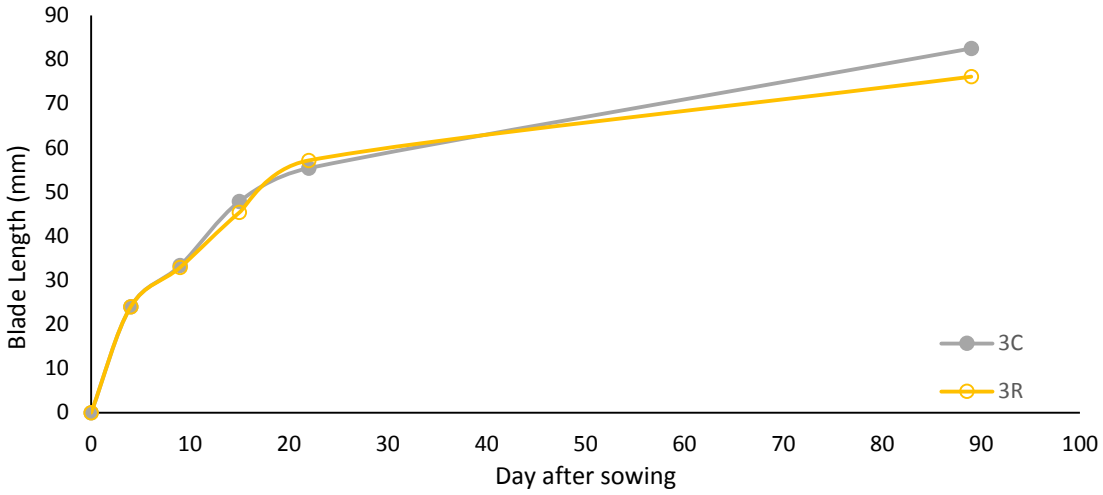

(c)

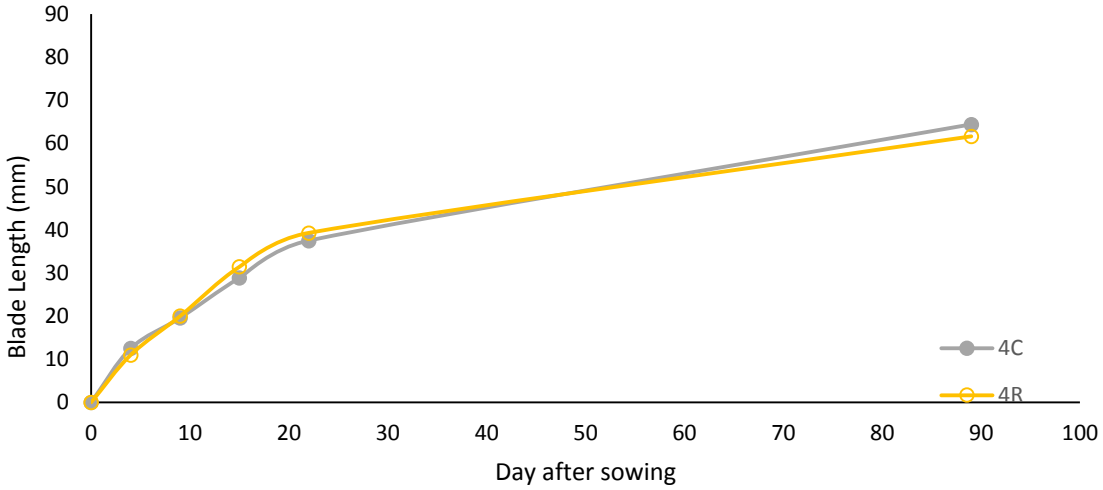

(d)

Fig. 3.43 Average blade length from day 0 to day 89 for: (a) group 1 section comparison; (b) group 2 section comparison; (c) group 3 section comparison; (d) group 4 section comparison; (e) all groups with the average value for each group (continued).

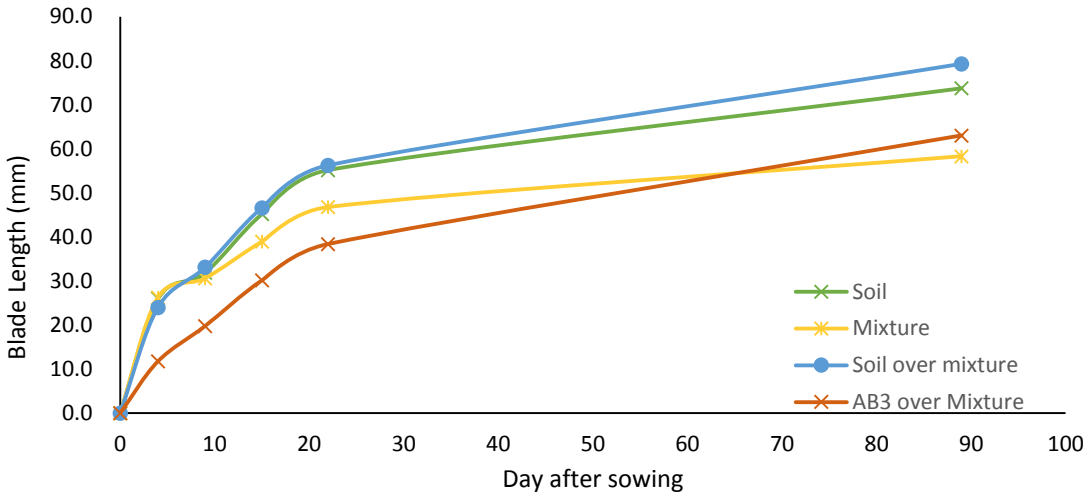

(e)

Fig. 3.43 Average blade length from day 0 to day 89 for: (a) group 1 section comparison; (b) group 2 section comparison; (c) group 3 section comparison; (d) group 4 section comparison; (e) all groups with the average value for each group (continued).

The comparisons of the results between the reinforced and control sections indicate that the geocell reinforcement had a minor or no effect on the vegetation at the establishment stage. For all the test sections, grass grew rapidly in the first 22 days, then the growth rate slowed down from day 22 to day 89. The blade length and the trend of vegetation growth from day 0 to day 22 were almost identical between the control and reinforced sections in all groups. On day 89 the sections in groups 1 and 2 started to show some difference in the blade length. In group 2 the control section out-grew the reinforced section by 15 mm in average while the standard deviation of the samples from both sections were around 14 mm. The

reinforced section in group 1 grew 10 mm longer in average than the control section while the standard deviations of these two sections were 13 mm and 19 mm respectively. Both sections in group 2 and 4 had the similar blade length. Figure 3.43 (e) shows the average blade length of each group from day 0 to day 89. In the first 22 days, group 4 with the AB3 aggregate over the soil-aggregate mixture grew the slowest. On day 22, the average blade length of group 4 was 38 mm. The vegetation in group 2 grew the second slowest with an average blade length of 47 mm on day 22. The vegetation growths in groups 1 and 3 were similar with an average blade length around 55 mm. Such vegetation growth show a correlation with the type of the soil cover. Groups 1 and 3 with a topsoil cover showed the fastest blade growth. Group 2 with a soil cover of soil-aggregate mixture had a medium blade growth rate. Group 4 with an AB3 aggregate cover resulted in the slowest blade growth.

Figure 3.44 presents the blade lengths from day 89 to day 333, which were obtained in the winter of 2013 and the spring and the summer of 2014. The error bar on each data point was constructed with the standard deviation of blade length measurements to represent the distribution of blade length.

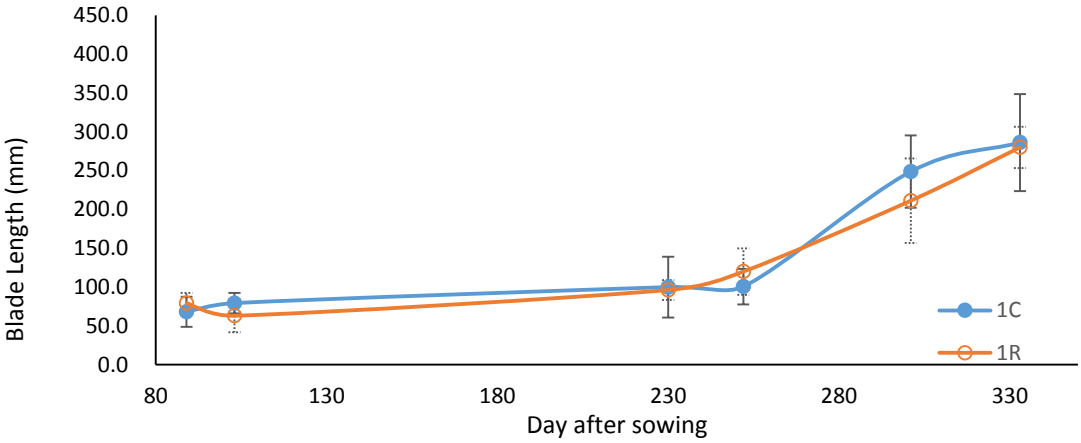
Blade Length (mm)
450.0
400.0
350.0
300.0
250.0
200.0
150.0
100.0
50.0
0.0
80
130
180
230
280
330
Day after sowing
1C
1R

(a)

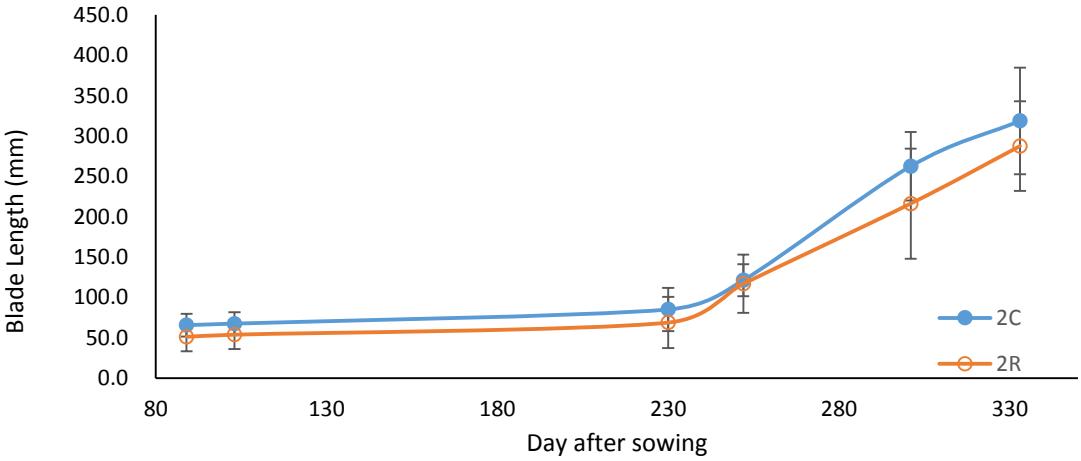
Blade Length (mm)
450.0
400.0
350.0
300.0
250.0
200.0
150.0
100.0
50.0
0.0
80
130
180
230
280
330
Day after sowing
2C
2R

(b)

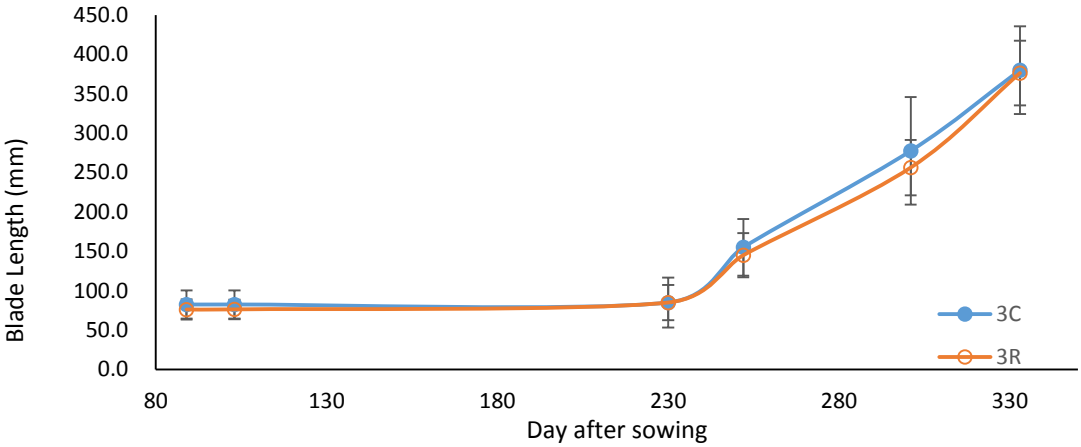
Blade Length (mm)
450.0
400.0
350.0
300.0
250.0
200.0
150.0
100.0
50.0
0.0
80
130
180
230
280
330
Day after sowing
3C
3R

(c)

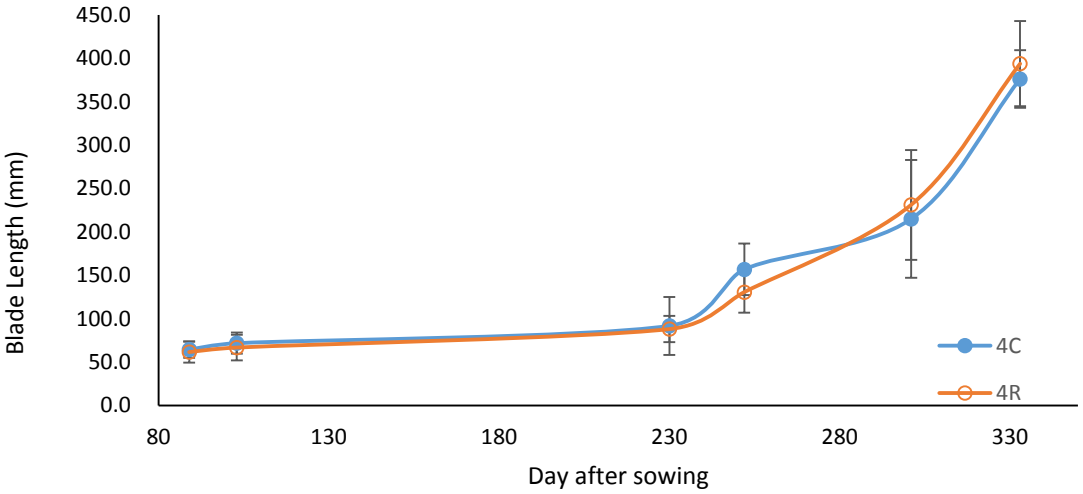

(d)

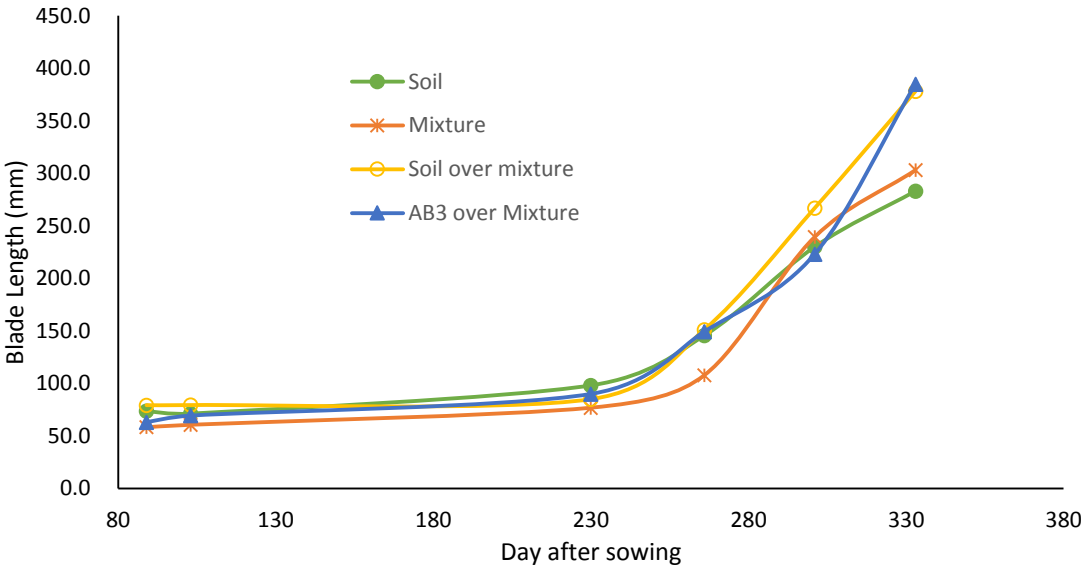

(e)

Figure 3.44 Average blade length from day 89 to day 333 for: (a) group 1 section comparison; (b) group 2 section comparison; (c) group 3 section comparison; (d) group 4 section comparison; (e) all groups with the average value for each group.

Leaf blade length from day 89 to day 230 showed little growth because it was in the winter. The lowest temperature recorded over the winter was -24.4℃ and there were 66 days in this winter with the average temperature lower than 0℃. After Day 230, most sections started to show an increase in the blade length. By day 333, the longest average blade length was 393 mm on section 4R. In groups 3 and 4, the average blade length from the reinforced section showed no significant difference from that of the control section throughout the test period. The greatest length difference between the reinforced and control sections occurred on day 301 in groups 1 and 2. Figures 3.44 (a) and (b) show that the control section in group 1 out-grew the reinforced section by 35 mm while in group 2 the control section grew 45 mm longer than the reinforced section. However, in both cases, the error bars of the reinforced sections had a fair portion overlapped with those of the control sections. This result indicates that although there were differences in the average blade length between the reinforced and control sections in each group, the populations of the blade lengths were similar. The larger error bars on day 301 were related to the vegetation densities, which will be discussed later in this paper.

Figure 3.44 (e) shows the average blade length of each group from day 89 to 333. The blade lengths of all groups were similar on day 230. From day 230 to day 266, groups 1, 3, and 4 had a similar growth rate. From day 266 to day 333, the leaf growth in group 1 slowed down while those in groups 2, 3, and 4 increased.

Over the 3 month period from day 230 to day 333, the leaf growth rate in groups 3 and 4 was averaged at 2.8 mm/day, followed by that in group 2 at 2.2 mm/day. Group 1 yield the slowest growth rate at 1.8 mm/day. These results suggested that the soil mixture allowed the already established vegetation to grow faster in the spring and the early summer. According to the above comparisons, it can be concluded that geocell reinforcement and the type of soil cover had a minor effect on the development of the already established vegetation. The reason for less effect of the type of soil cover in this stage than that in the initial establishment is related to the root lengths, which will be discussed in the following section.

Root Length

To further investigate the effect of the type of soil cover, measurements of root lengths were conducted on day 25 and day 397. Five individual plants were selected randomly and dug out from each section. The average root length of each section is shown in Table 3.4. On day 25, the average root lengths of all sections were shorter than 50 mm, which is the thickness of the cover layer; therefore, within the first 25 days, the soil cover influenced the development of vegetation. Based on the blade length within the first 22 days, the soil cover with a higher fine content allowed the faster leaf growth in the early stage.

Table 3.5 shows that the root lengths in all the sections except the reinforced section in group 2 on day 397 were greater than 200 mm, which is the total thickness

of the base course and the soil cover. In other words, the roots of the plants in almost all the sections reached the subgrade, which is a topsoil. Because of this fact, the type of soil cover did not have much effect on the vegetation at the later stage.

Table 3.4 Average root length on day 25.

Group	1	2	3	4
Control (mm)	22.2	25.4	47.6	22.2
Reinforced (mm)	28.6	46.3	28.6	38.1

Table 3.5 Average root length on day 397.

Group	1	2	3	4
Control (mm)	212	209	223	227
Reinforced (mm)	216	193	218	231

Vegetation Density

To measure the population density of vegetation, a 600 mm × 600 mm frame was placed on each section randomly. The area surrounded by the frame was

considered as the measurement area. The total number of alive individual plants, regardless of species type, in the measurement area was counted and used to compute the grass population density of the measured section. Figure 3.45 displays measuring equipment. The grass densities comparison between sections and groups were plotted in figure 3.46.

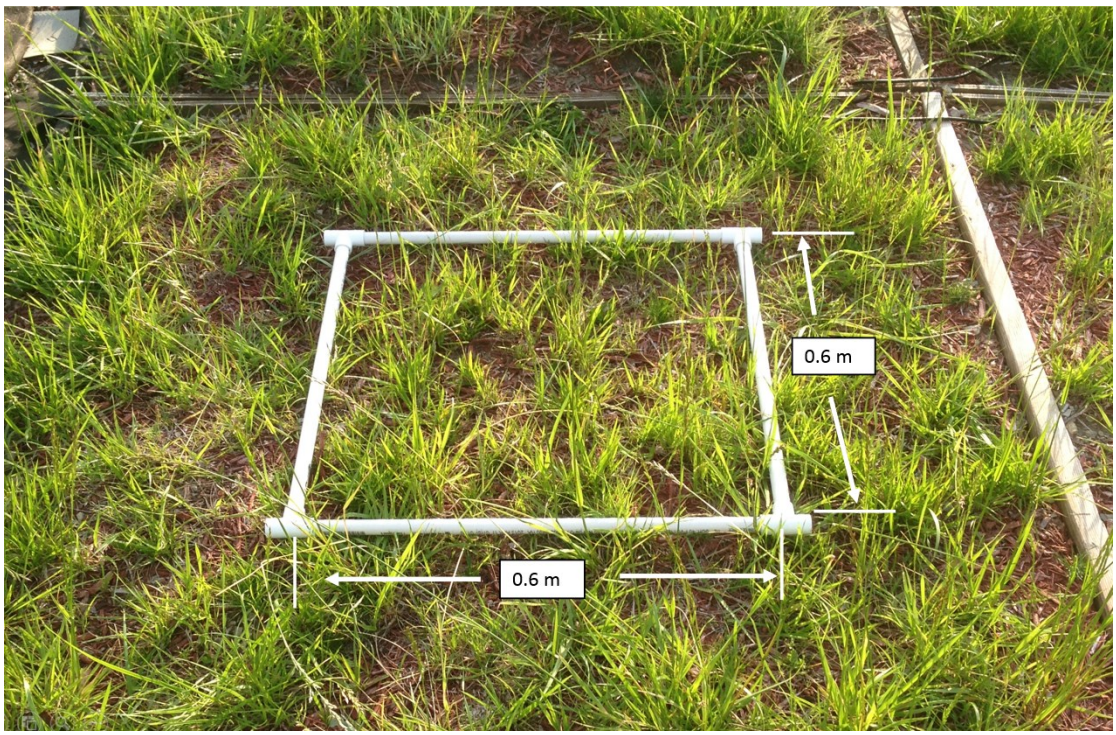

Figure. 3.45 Frame for vegetation density measurement

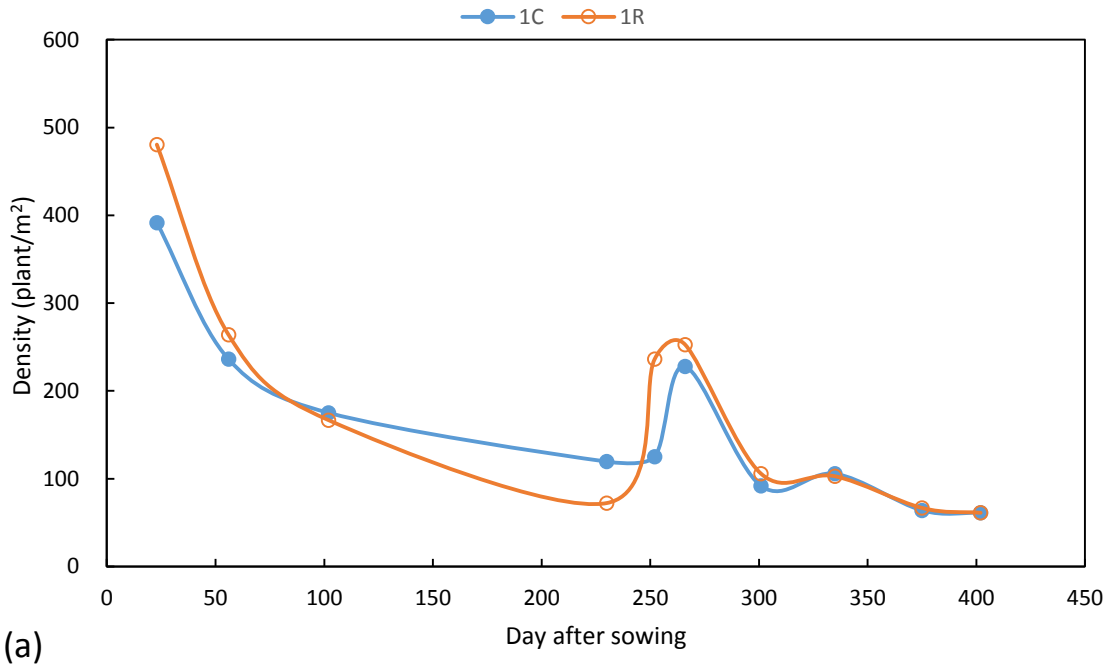
1C
1R
Density (plant/m²)
Day after sowing
0
100
200
300
400
500
600
0
50
100
150
200
250
300
350
400
450

(a)

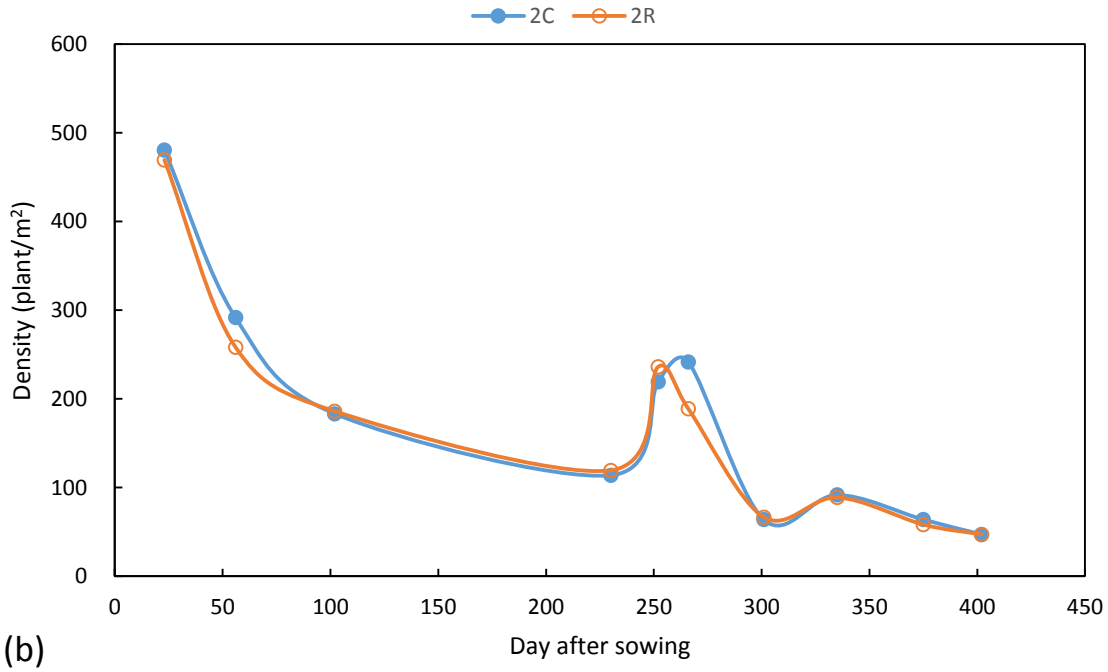
2C
2R
Density (plant/m²)
Day after sowing
0
100
200
300
400
500
600
0
50
100
150
200
250
300
350
400
450

(b)

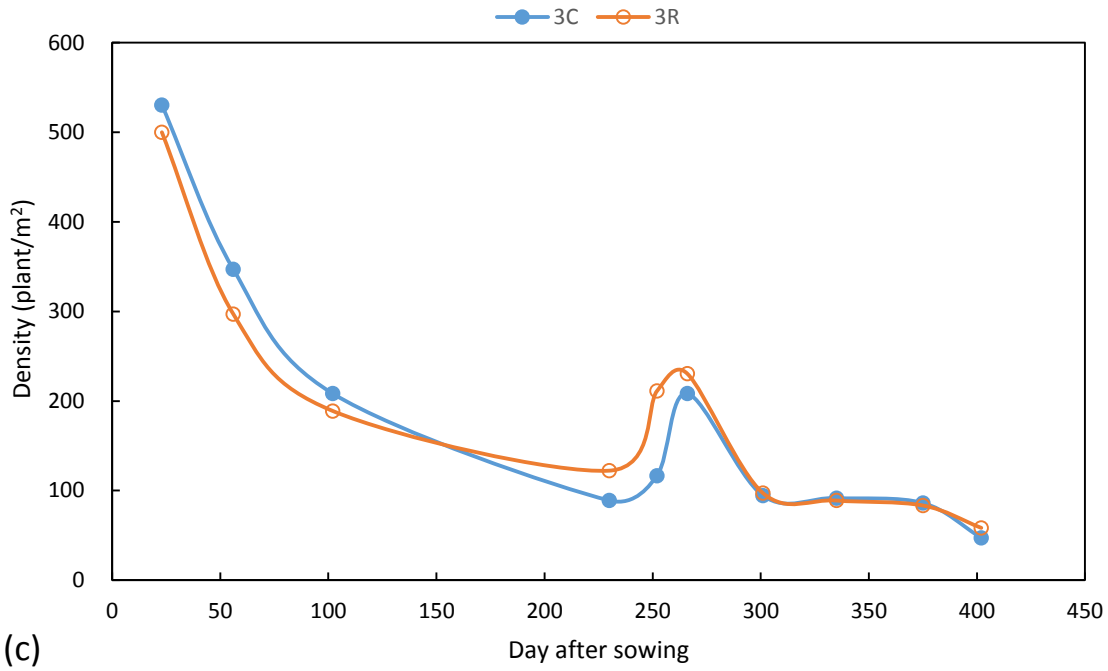
3C
3R
600
500
400
300
200
100
0
Density (plant/m²)
0
50
100
150
200
250
300
350
400
450
Day after sowing

(c)

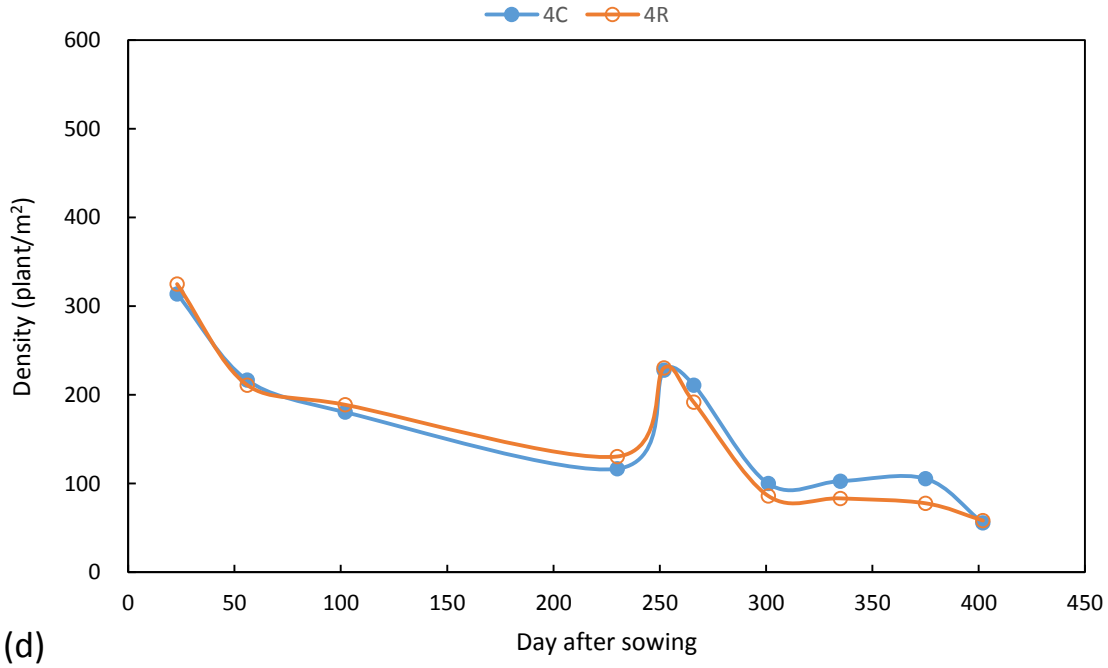
4C
4R
600
500
400
300
200
100
0
Density (plant/m²)
0
50
100
150
200
250
300
350
400
450
Day after sowing

(d)

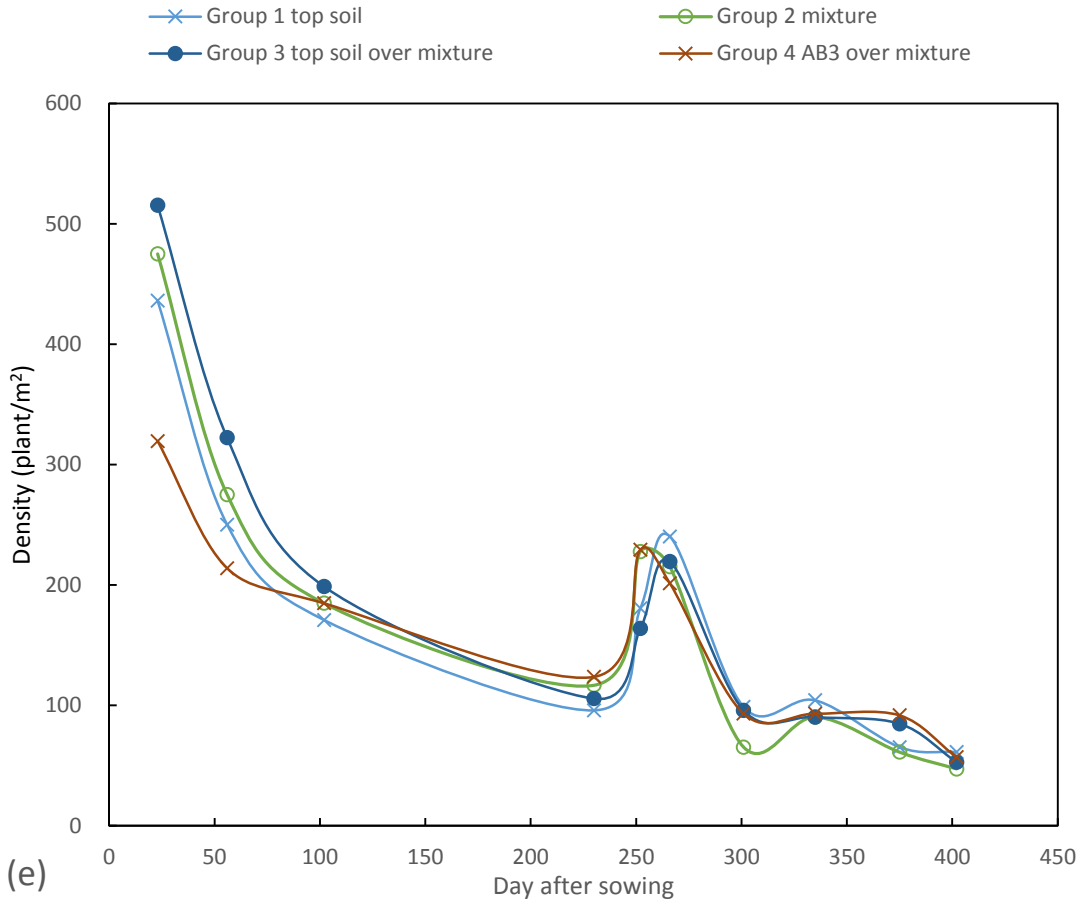

Figure. 3.46 Grass population density for: (a) group 1 section comparison; (b) group 2 section comparison; (c) group 3 section comparison; (d) group 4 section comparison; (e) comparison between groups.

All eight test sections show a similar trend in the population density. The maximum density in all sections was recorded on day 23 (i.e., the first data point in Figure 3.46). The population densities then decreased rapidly from day 23 to day 102 as the season was transited from the fall to the winter. An increase in the

densities was observed from day 230 to day 250 during the spring of 2014. Then the densities decreased again after day 266 during the summer of 2014. The densities stabilized from day 300 to day 400. The peak densities in the spring were contributed by the revival of the already established grass and the newborn grass. The leaves on the revival plants tended to grow faster as their root systems were well established while the newborn grass tended to grow slowly due to the establishment of their roots. Consequently, an increase in the standard deviation of the blade length measurements occurred.

Figure 3.46 (a) shows that group 1 had the greatest difference between the reinforced and control sections in the spring from day 230 to day 266. The control section had almost twice the density as the reinforced section on day 230. Then a rapid increase in the density was observed on the reinforced section between day 230 and day 252. By day 266, the density difference between these two sections was small. Such a phenomenon was also observed on group 3. The density of the reinforced section increased faster than that of the control section. However, the peak densities of these two sections were similar on day 266. The population densities of both the reinforced and control sections in groups 2 and 4 show no significant difference throughout the test period. Based on these comparisons, it can be concluded that geocell reinforcement had minor or no effect on the vegetation population density.

Figure 3.46(e) shows the group average densities of the control and reinforced

sections in all groups. In the initial establishment stage, group 3 had the maximum density at 517 plants per m^2. Groups 1 and 2 had 436 and 475 plants per m^2 respectively. Group 4 with the AB3 aggregate top layer had a significantly lower density of 115 plants per m^2 than other groups. On day 50, the differences between the sections decreased. By the early winter on day 102, the densities of all the groups were between 167 and 194 individual plants per m^2 and small differences among the groups were observed. The vegetation densities in the spring showed some differences. The densities in groups 2 and 4 increased faster than groups 1 and 3 from day 230 to day 252. However, group 1 yielded the maximum density of 242 individual plants per m^2 in the spring period. By day 400, all groups show similar vegetation densities. The significant difference in the vegetation density between group 4 and other groups at the beginning indicates that the AB3 aggregate cover layer was harshest for the initial establishment of grass while the soil-aggregate mixture performed as well as the topsoil. The minor differences in the vegetation densities among all the groups from day 100 to day 400 indicate that the soil-aggregate mixture had the ability to sustain the similar vegetation density as the topsoil and the aggregate cover layer presented minor or no effect on the developed vegetation because the roots reached the subgrade.

Dry biomass

Dry biomass is a more comprehensive measurement to evaluate vegetation. The grass was first trimmed and collected in this study. Then the collected biomass

was then oven dried at 105℃ for a period of 24 hours according to the ASTM standard. Due to the destructive nature, this evaluation was conducted toward the end of the testing period. The grass in each section was first cut off at 150 mm from the ground surface on day 339. Figure 3.47 shows the biomass collecting process on day 339. The wood frame had a height of 150 mm. Then on day 421, the grass was cut off at the ground surface and all the vegetation parts above ground surface were collected. Figure 12 shows the dry biomasses from each section on both day 339 and day 421.

Figure. 3.47 150-mm tall reference frame and biomass collection

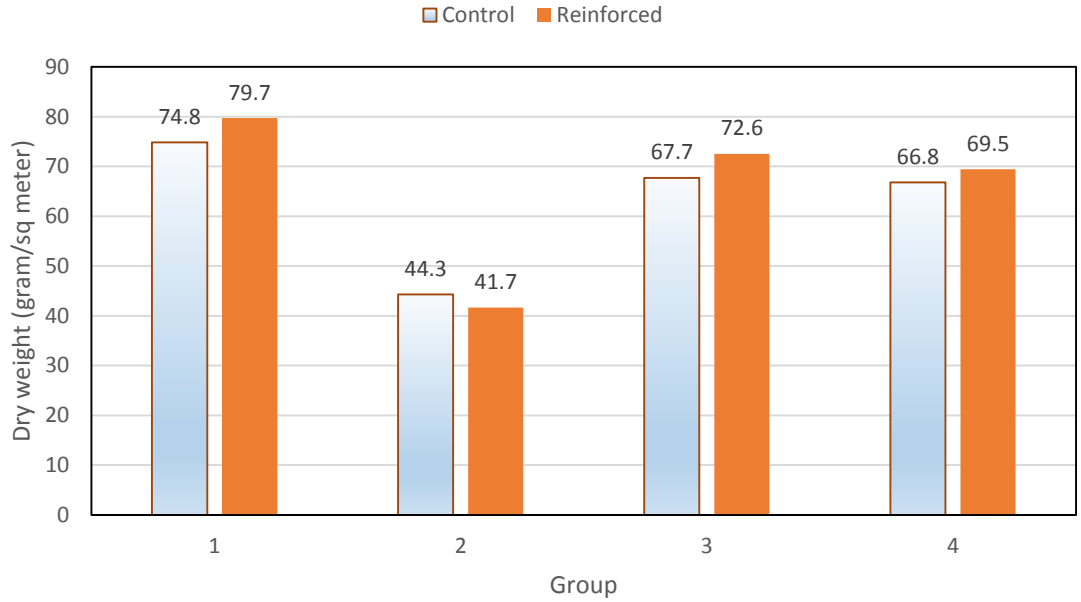

(a)

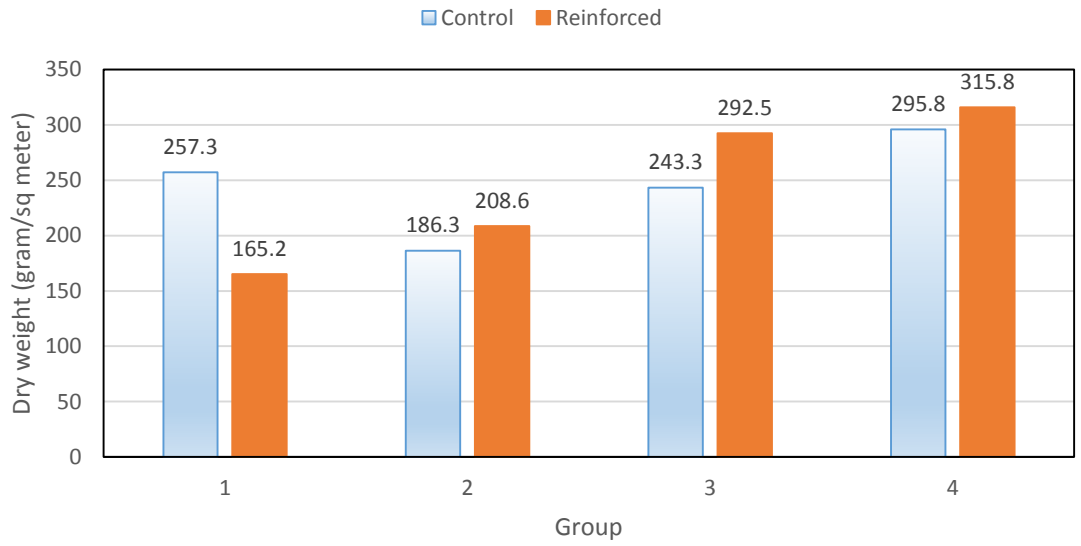

(b)

Figure 3.48 Dry biomass comparison on: (a) day 339 and (b) day 421

The biomass collected on day 339 included seeds, stems, and leaves. The dry

biomass from day 339 indicated the reinforced sections from groups 1, 3, and 4 produced more biomass than the control sections. The control section produced more biomass than the reinforced section in group 2. The biomass production between the control and reinforced sections in all four groups differed within 5 g/m2. The average dry biomass in group 1 was the highest of 77 gram/m2. Productions from groups 3 and 4 (i.e., 70 and 68 gram/m2 respectively) were similar. During the biomass collection, it was noticed that the biomass from group 2, both the control and reinforced sections, contained less seeds and stems than those in other groups. The dry biomass from group 2 was significantly less than those from other groups.

The biomass collected on day 421 included all the vegetation parts above the ground surface. The collection on day 339 trimmed off most of stems and seeds thus little stems and seeds were collected on day 421 and the biomass collected on day 421 contained mainly leaves. Based on Figure 11 (b), only the control section from group 1 produced more biomass than the reinforced section. The reinforced sections in groups 2, 3, and 4 produced 12%, 20%, and 7% more biomass than the control sections respectively. Compared with section 1C, the reinforced section from group 3 and both sections from group 4 produced more biomass; the control section from group 3 produced slightly less biomass. Group 4 produced the greatest amount of biomass among all groups (i.e., average production = 305.8 g/m2). Group 3 had an average production of 267.9 g/m2, which was similar to section 1C (257.3 g/m2 production). Group 2 produced the least amount of biomass.

The above comparisons showed that the dry biomass productions in the control and reinforced sections in groups 2, 3, and 4 differed slightly. The reinforced sections from groups 3 and 4 produced more biomass than the control sections on both day 339 and day 421. Group 3 and 4 produced the similar amount of biomass as group 1 indicated their ability to sustain vegetation was similar and the type of the soil cover layer had little influence on the established vegetation.

3.4.3 Conclusion

To investigate the effect of geocell reinforcement on vegetation, four test section groups with different bass courses and soil cover layers to represent unpaved shoulders were constructed. Each group consisted of a control section and a geocell reinforced section. Two species (tall fescue and ryegrass) were planted on all the test sections. Blade length, root length, grass population density, and biomass were measured for all test sections. Based on the test data, the following conclusions can be drawn from this study:

(1) Throughout the one-year test period, no definite evidence of geocell reinforcement limiting vegetation growth in unpaved shoulders was found.

(2) The type of soil cover had a significant effect on the vegetation growth at the initial establishment stage. The soil cover containing a high percentage of

aggregate retarded the establishment of vegetation while the soil cover containing a high percentage of fines promoted the establishment of vegetation.

(3) In almost all the test sections, the roots of the plants reached the fine-grained subgrade at the later stage. As a result, the type of soil cover had minor influence on the vegetation one year after sowing.

(4) The soil-aggregate mixture showed no significant difference from the native topsoil on the ability to sustain the already established vegetation

.

Chapter Four

Mat Systems for Unpaved Temporary Roads

The literature review shows that subgrade conditions had significant impact on the performance of mat systems. Most mat systems investigated in the past had connection systems between mats but did not have any anchorage system. The anchorage system is expected to better restrain mat movement and improve performance of mat systems. This study focused on one type of polyethylene mat system with specially designed and made earth anchors. The performance of this mat system over soft and intermediate subgrade with CBR values ranging from 1% to 4% was investigated. Six cyclic plate loading tests were conducted using the large-scale geotechnical box available at the University of Kansas to investigate the permanent deformation and the vertical interface stress in the test section under each loading cycle.

4.1 Material

4.1.1 Subgrade and base course

The subgrade material used in this study was an artificial material which consisted of 75% Kansas River sand and 25% Kaolin by dry weight. The base course material used was AB3, a well-graded aggregate commonly used in the state

of Kansas. The properties of these two materials were presented in Chapter 3.

4.1.2 Mat System

The polyethylene mats, trademarked GEOTERRA ®, were provided by Presto Geosystems. The mat system consisted of polyethylene mat units, connectors (PadLoc®), and the optional earth anchors as shown in Figure 4.1. Even though the ground anchors area optional, they were used in this study. The specification and parameters of the mat are provided in Table 4.1.

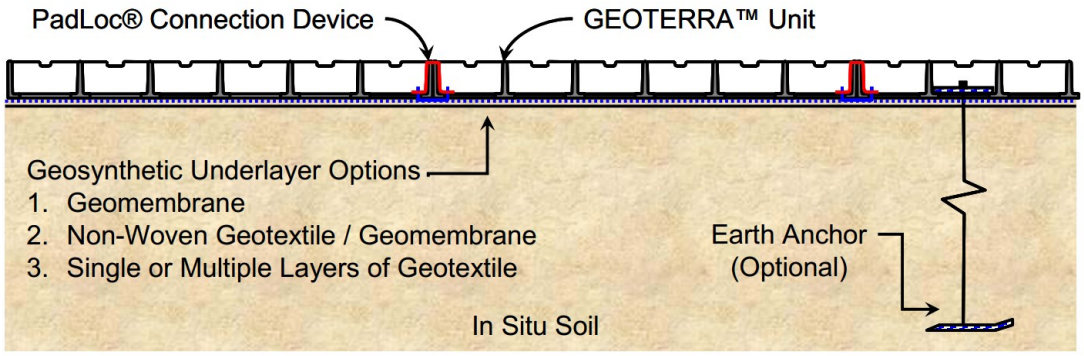

Figure 4.1 Mat system components with options (Presto 2009)

Table 4.1 Specification and parameters of the polyethylene mat system (Presto 2009)

Item	Specifications and parameters
Material	High-performance/High-Modulus Blend of Polyethylene
Nominal Dimensions (width × length)	0.48 m × 0.96 m
Nominal Unit Depth	50 mm
Nominal Unit Weight	4.11 kg
Cell Size	79 mm × 81 mm
Top Open Area per Unit	87%
Bottom Open Area Per Unit	41%
Unit Minimum Crush Strength at 21℃	2.9 MPa
Equivalent Elastic Stiffness, Simply supported at 25mm deflection	140 N-m^2
Material Flexural Modulus at 23℃	240 MPa

4.1.3 Geotextile

A woven geotextile, manufactured by TenCate, was placed between the mat system and soft subgrade as separator. The specifications and parameters of this geotextile are shown in Table 4.2.

Table 4.2 Specifications and parameters of woven geotextile (Tencate 2013)

Item	Specifications and parameters
Material	High-tenacity Polypropylene
Tensile Strength at 2% strain	19.3 kN/m
Tensile Strength at 2% strain	39.4 kN/m
Apparent Opening Size (AOS)	0.6 mm (No. 30 US sieve)
Unit Weight	390 g/m^2
Thickness	1.5 mm

4.2 Test Setup and Sections

The same large-scale geotechnical test box with the same loading pattern used for geocell tests was utilized in this study. The schematics of test sections are presented in Figure 4.2. The subgrade of 0.9 m thick was constructed with the same method as the subgrade construction in the geocell tests. Vane shear tests were conducted after the compaction of each lift (approximately 300 mm thick) to monitor the subgrade quality. DCP tests were conducted prior to the application of cyclic loading.

Four to five earth pressure cells were installed at the interface between the base and the subgrade in the base test section or between the geotextile and the subgrade in the mat system test sections. Pressure cells were placed at distance of 0, 150, 300,

600, and 900 mm form the center of the loading plate as shown in the schematics.

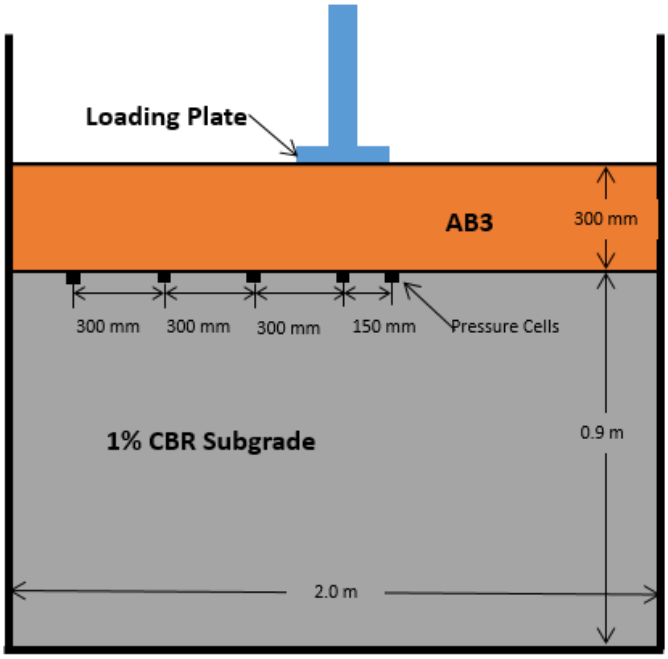

(a)

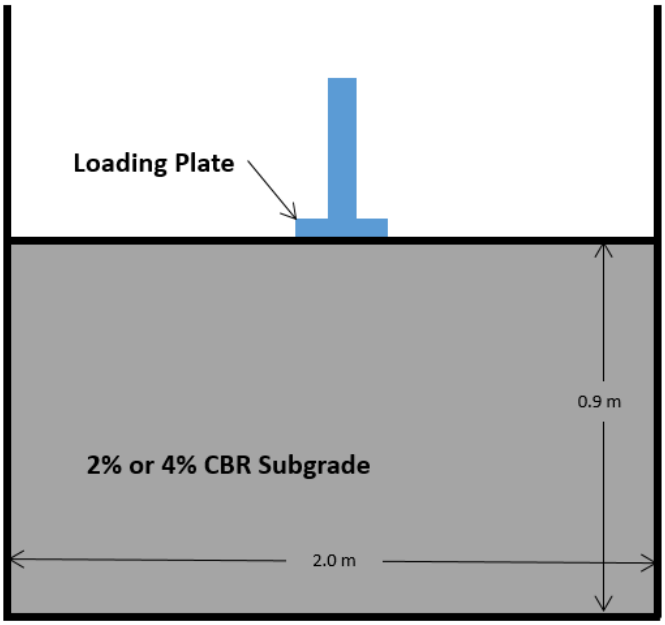

(b)

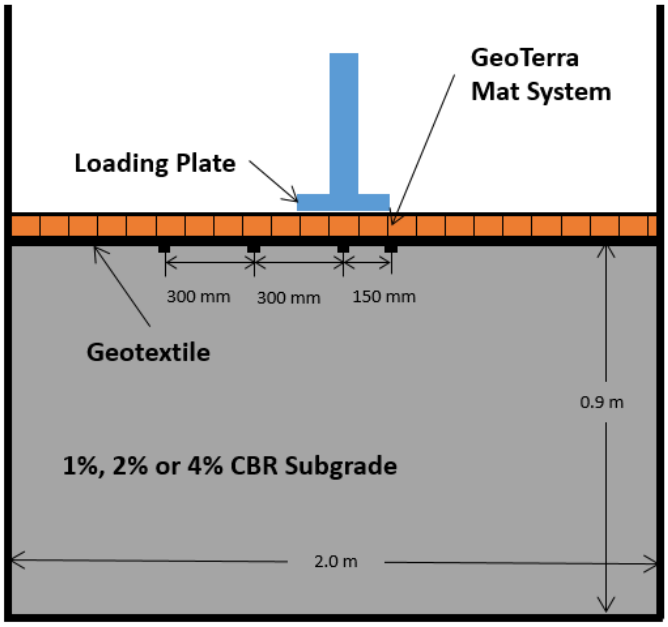

(c)

Figure 4.2 Schematics of test sections: (a) AB3 base over subgrade, (b) subgrade only, and (3) mat system over subgrade

The mat panels were assembled in a bricklayer pattern in this study, as shown in figure 4.3. The crosses represent the locations of earth anchors. The red circle indicates the position of the loading plate.

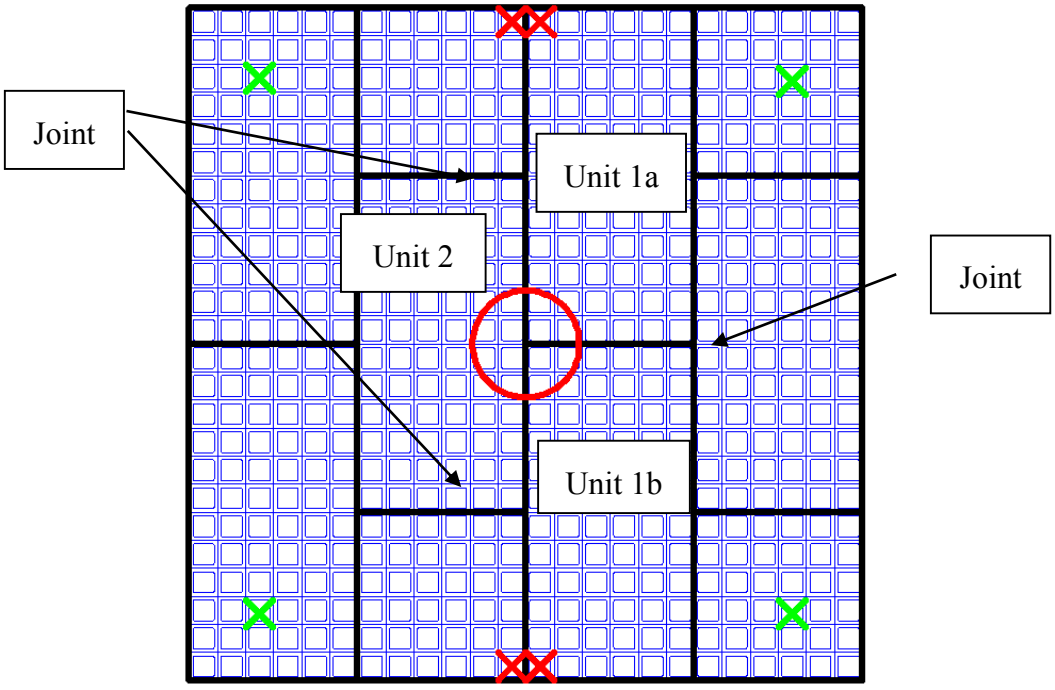

Figure 4.3 Layout of mat system

Individual mat panels were joined together with connectors, which consisted of a clamp and a strap fixed with a torsion tool as shown in Figure 4.4. Figure 4.4 (b) shows the connectors on the left and right before fixed by the torsion tool.

(a)

(b)

Figure 4.4 Connecting panels with (a) torsion tool and (b) connectors.

The earth anchors, shown in Figure 4.5, were installed after the mat system was

joined together. The earth anchors were driven into the soil by a driving rod with a cable, which was pulled until resistance was reached. The washer and cable stoppers were then positioned in the bottom of the panel cell and a crimp tool was used to secure the cable stopper.

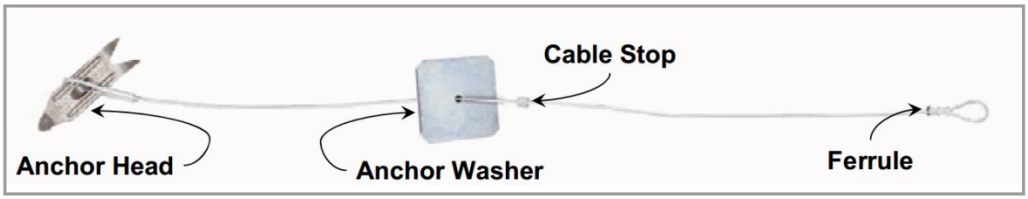

(a)

(b)

(c)

Figure 4.5 Earth anchor: (a) components (Presto 2009), (b) driving rod and earth anchor, and (c) crimp tool.

4.3 Test Results and Discussions

Six large-scale cyclic plate loading tests were conducted. Table 4.3 provides the test sections and CBR values of subgrade and base courses.

Table 4.3 Test section CBR values

Section No.	Surface layer	Base CBR (%)	Subgrade CBR (%)
1	300 mm thick base course (control)	14.7 (DCP)	1.1 (vane shear) and 1.0 (DCP)
2	Mat	NA	1.1 (vane shear)
3	Subgrade (control)	NA	2.4% (vane shear)
4	Mat	NA	2.0 (vane shear) and 1.8 (DCP)
5	Subgrade (control)	NA	4.0% (vane shear) and 4.6% (DCP)
6	Mat	NA	4.1% (vane shear) and 4.5% (DCP)

Permanent deformations

The permanent displacements of the loading plate on six test sections are presented in Figures 4.6 to 4.8. Comparisons can be made between test sections with and without a mat system on the similar subgrade CBR. When the subgrade CBR was 1%, the subgrade was too soft to be subjected to an applied load of 40 kN directly; therefore, a 300 mm thick aggregate base course was placed above the subgrade.

Figure 4.6 shows the permanent displacement versus number of cycles from Tests 1 and 2. The mat system had the higher initial permanent displacement due to

the partial or imperfect contact between the mat and the uneven subgrade surface. After the full contact was established, the rate of increase in the permanent displacement of the plate on the mat system significantly decreased. On the other hand, the increase in the permanent displacement of the plate on the aggregate base was almost linear. The test results show that the test section with a mat system had similar performance and even better performance than that with a 300 mm thick base course on the 1% CBR subgrade at the large displacement. In other words, the mat system is approximately equivalent to the 300 mm thick aggregate base. It should be pointed out that initially, one ground anchor was installed at each corner of the mat system as represented by the green cross in Figure 4.3. In the testing process, the joints between the mat panels in the middle were lifted up. To simulate a field condition where the mat system would be continuous in the longitudinal direction, the test was paused at the end of the sixth load cycle and two more ground anchors were added on each side near the edge in the middle as, represented by the red crosses in Figure 4.3. Then the test was continued. It is also worth pointing out that the same amount of ground anchors were installed at the same locations in the later tests with a mat system (i.e., Tests 4 and 6).

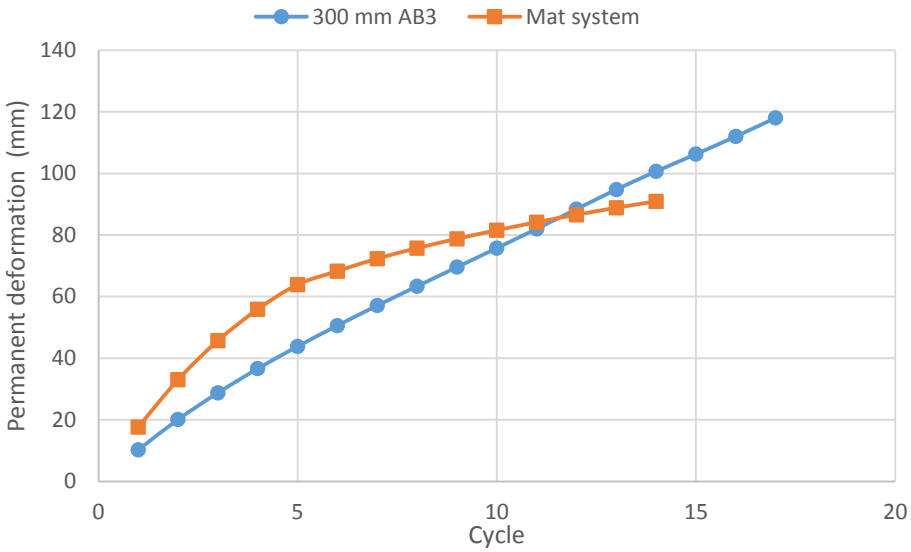

Figure 4.6 Permanent deformation of the loading plate vs. number of cycles from Tests 1 and 2

Figures 4.7 and 4.8 show the comparisons of the permanent displacements of the loading plate with and without the mat system over 2% and 4% CBR subgrade. Both figures show that the subgrade only sections had much faster-growing permanent displacements than the mat system over subgrade sections. When the mat system was used, the rate of increase in the permanent displacement rapidly decreased after the initial number of cycles. The test results demonstrate the benefit of the mat system in reducing the permanent deformation of the subgrade.

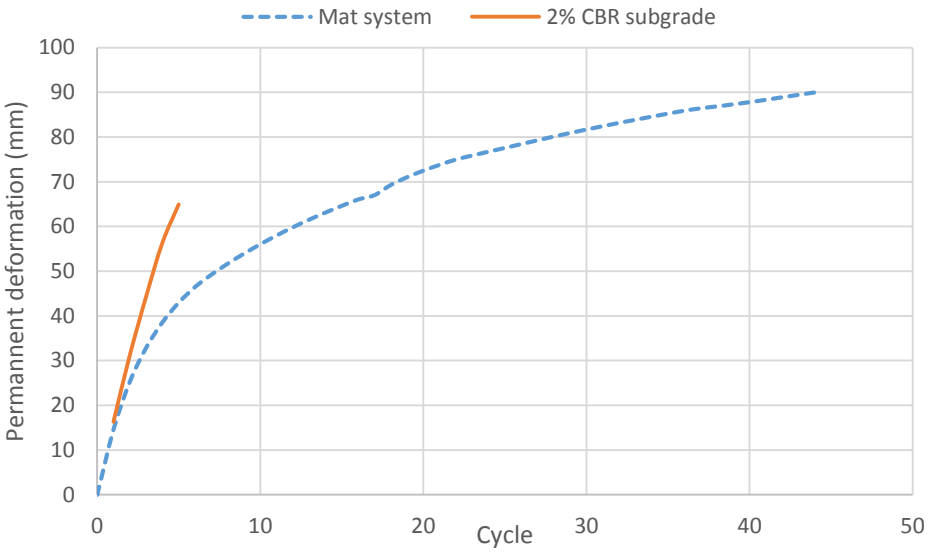

Figure 4.7 Permanent deformation of the loading plate vs. number of cycles from Tests 3 and 4

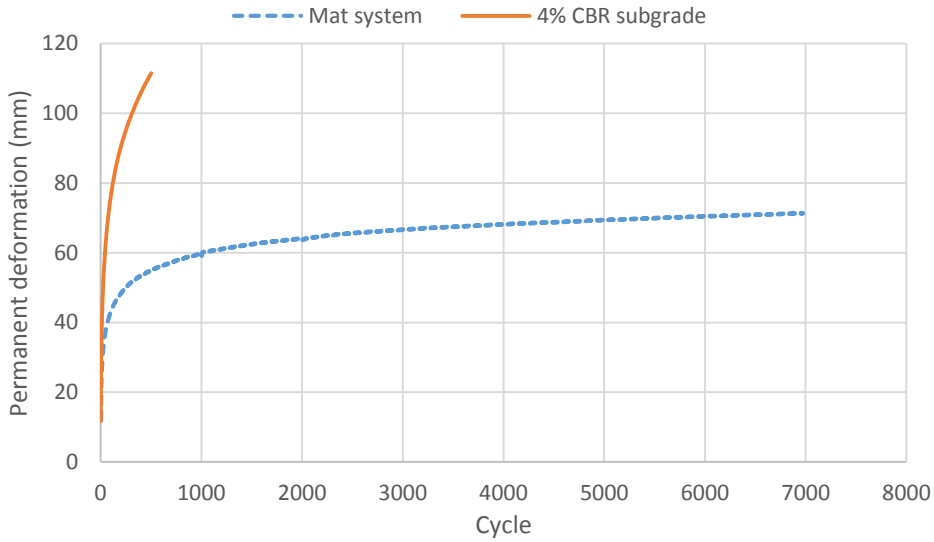

(b)

Figure 4.8 Permanent deformation of the loading plate vs. number of cycles from Tests 5 and 6

A permanent displacement of 75 mm is commonly used as the failure criterion

for unpaved roads *(8)* and was selected as the primary criterion to terminate the cyclic loading tests. However, some tests were conducted beyond the 75 mm permanent displacement to better understand the effectiveness of the tested mat system at a large displacement. On the other hand, some tests were terminated prior to the 75 mm permanent displacement due to some limitation of the test equipment.

To evaluate the benefit of the mat system, the improvement factor is defined here as the ratio of the number of cycles for the test section with a mat system to that without a mat system (i.e., subgrade only) at a specific permanent displacement as follows:

$$\text{Improvement factor} = \frac{N_{mat}}{N_{subgrade}} \qquad \textbf{Equation 4.1}$$

The calculated improvement factors at various permanent deformation are provided in Table 4.4. Since Tests 1 and 2 are incomparable, they are not included in this table. The table shows that the improvement factor increased with the permanent displacement. At the same amount of permanent deformation, the subgrade with a higher CBR resulted in a higher improvement factor.

Table 4.4 Improvement factors at different permanent deformations

Subgrade CBR	Permanent Displacement (mm)	25	50	75	100
2%	$N_{subgrade}$	1	4	6*	8*
	N_{mat}	2	8	25	74*
	Improvement Factor	2	2	4.2	9.3
4%	$N_{subgrade}$	4	25	95	312
	N_{mat}	9	247	11603*	NA
	Improvement Factor	2.3	9.9	122	NA

*: extrapolated data

Vertical interface stresses

Figure 4.9 shows the measured vertical stresses at the interface between the base course and the subgrade or between the mat and the subgrade at different locations with the number of loading cycles.

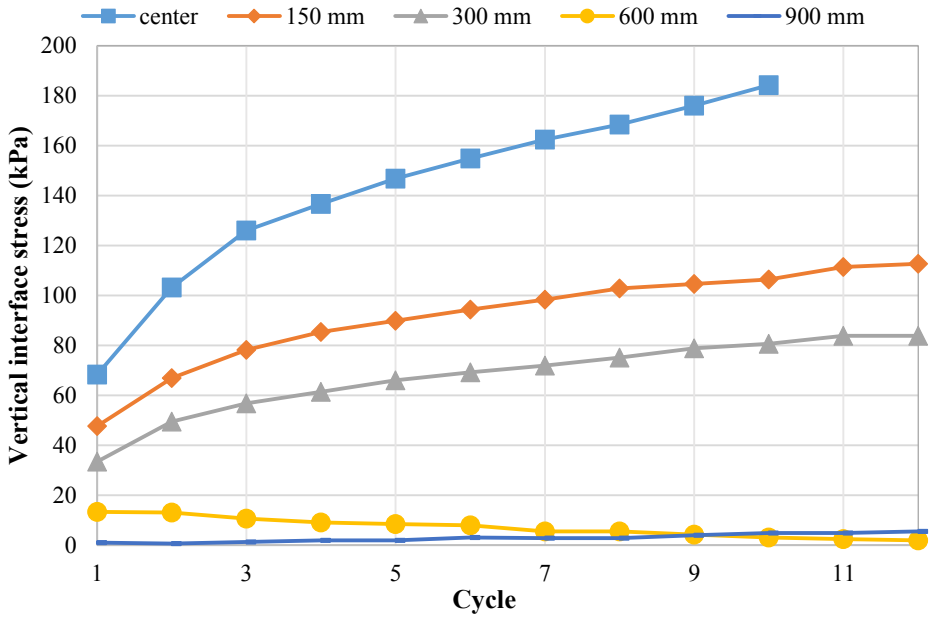
center
150 mm
300 mm
600 mm
900 mm
Vertical interface stress (kPa)
Cycle

(a)

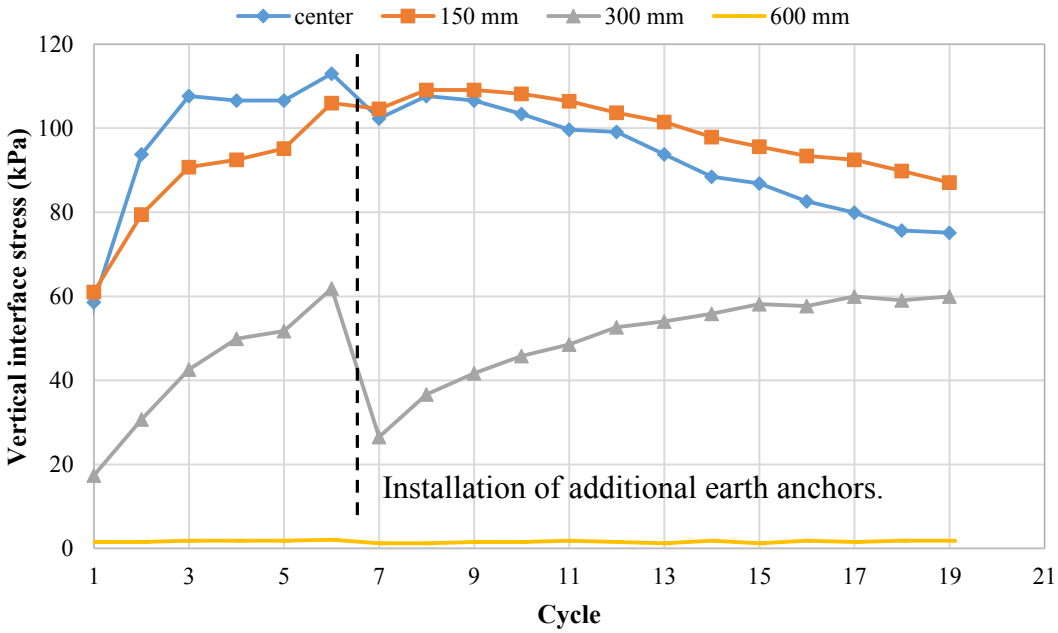
center
150 mm
300 mm
600 mm
Vertical interface stress (kPa)
Installation of additional earth anchors.
Cycle

(b)

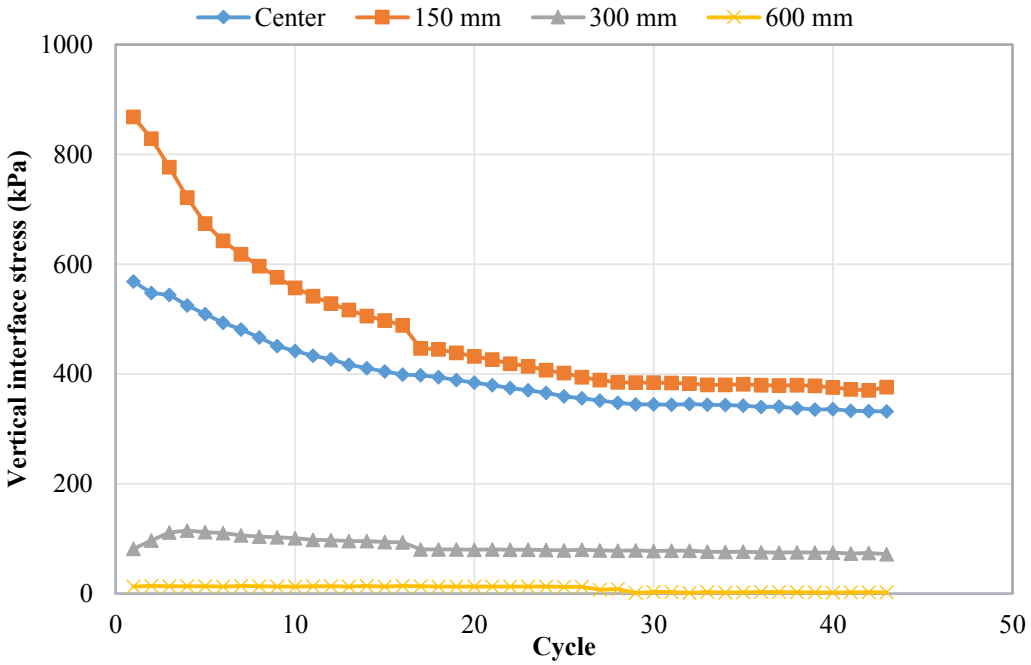

(c)

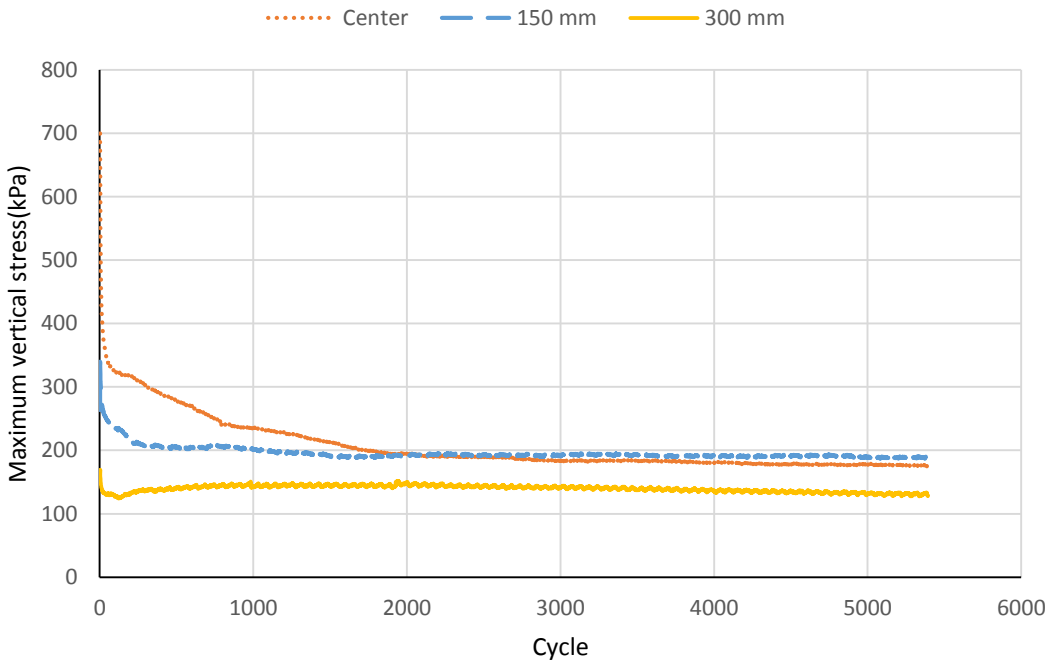

(d)

Figure 4.9 Vertical interface pressure development of: (a) 300-mm thick AB3 base over 1% CBR subgrade, (b) Mat system over 1% CBR subgrade, (c) Mat system over 2% CBR subgrade, and (d) Mat system over 4% CBR subgrade.

In figure 4.9 (a), the vertical interface stresses at the locations from the center to the distance of 300 mm increased with the number of cycles. This result is similar to that reported by Qian (Qian et al. 2013). The explanation was first offered by Giroud and Han (Giroud and Han 2004 a) as the stress distribution angle decreased with the deterioration of the base course under the increased number of cycles. However, in the test sections with a mat system, the measured vertical interface stresses decreased with the increase of the load cycles. The reasons for the stress reduction are: (1) full contact between the mat and the subgrade was established with an increase of the load cycles and (2) the bending plate effect reduced the vertical stress close to the center. As shown in Figure 4.3.2 (b), the installation of additional ground anchors in Test 2 after the sixth load cycle immediately reduced the vertical stresses because the additional anchors provided restraint to the mat and increased the bending plate stiffness. In Tests 4 and 6, the measured vertical interface stresses close to the center were higher than the average applied stress by the plate (i.e., 550 kPa) within the initial few cycles. The reasons for these higher measured stressed are: (1) the earth pressure cells were located at the edge of the mat panel and (2) the earth pressure cells were in contact the mat and the surrounding subgrade might not be in good contact with the mat. As a result, stress concentrated on the earth pressure cells. With an increase of the deformation, the mat became full contact with the subgrade and therefore the vertical stresses decreased.

Chapter Five

Conclusions and Recommendation

In the study of geocells for unpaved shoulders, six large-scale cyclic plate loading tests and a one-year long vegetation test were conducted on different base courses consisting of AB3 aggregate, soil-aggregate mixture, and topsoil to investigate their effects on structural capacities and vegetation. Based on the test results, the following conclusions were drawn:

(1) Geocell reinforcement effectively reduced permanent deformations.

(2) The effectiveness of geocell reinforcement depended on the composition of the base course.

(3) The geocell-reinforced soil-aggregate mixture with a mixture cover or an aggregate cover performed slightly better than the unreinforced aggregate of the same thickness over 6% CBR subgrade.

(4) The high-plasticity topsoil cover could fail rapidly under cyclic loading.

(5) The inclusion of geocell did not affect the vegetation.

(6) The soil-aggregate mixture consisting of 50% topsoil and 50% aggregate showed equal ability as the topsoil to sustain vegetation.

(7) The type of the cover soil had an obvious effect on the early establishment

of vegetation but had a minor effect on the full establishment of vegetation in later stages.

In the study of the mat system, one single mat system with an anchorage system was investigated. Six large-scale cyclic plate loading tests were conducted with and without the mat system installed over soft to intermediate subgrade (i.e., 1%, 2%, and 4%). Based on the test results, the following conclusions were drawn:

(1) The mat system improved the performance of the unreinforced soft subgrade by increasing the number of load cycles to achieve the same amount deformation.

(2) The mat system was more effective over the subgrade with a higher CBR value.

(3) The mat system was more effective with a higher allowable permanent deformation.

(4) The mat system was able to transfer the load to a wider area.

(5) The anchorage system changed the load distribution of the mat system.

Based on the plate loading tests and the vegetation test, the two geocell-reinforced sections, (1) 200-mm thick geocell-reinforced soil-aggregate mixture and (2) 50-mm thick AB3 aggregate over 150-mm geocell-reinforced soil-aggregate mixture, showed the best ability to support traffic loads and sustain vegetation. They should be further investigated with different base course thicknesses and subgrade conditions.

However, moisture apparently had a significant influence on the strength and stiffness of the soil-aggregate mixture. This effect should be further investigated.

Based on the plate loading tests, the mat system is more applicable for intermediate subgrade with a CBR greater than 4%. The tests indicated that the anchor system changed the load distribution under the mat system. A further study should investigate the effect of the anchor system on the mat system performance. The observation during the tests also identified the connection between panels as the weak link in the panel system; therefore, modifications may be made for the connection to improve the performance of the mat system.

References

AASHTO (1993). AASHTO Guide for Design of Pavement Structures, Vol. 1.

Anderton, G., and Gartrell, C. (2005). Rapid maximum-on-ground (MOG) enhancement technologies. *ERDC/GSL TR-05*, 2.

Bathurst, R., and Karpurapu, R. (1993). Large-scale triaxial compression testing of geocell-reinforced granular soils. *ASTM geotechnical testing journal*, 16(3), 296-303.

Chow, J. C., Watson, J. G., Lowenthal, D. H., Solomon, P. A., Magliano, K. L., Ziman, S. D., and Willard Richards, L. (1992). PM10 source apportionment in California's San Joaquin valley. *Atmospheric Environment. Part A. General Topics*, 26(18), 3335-3354.

Doyle, J. D., Howard, I. L., Gartrell, C. A., Anderton, G. L., Newman, J. K., and Berney IV, E. S. (2012). Full-Scale Instrumented Testing and Three-Dimensional Modeling of Airfield Matting Systems. *International Journal of Geomechanics*, 14(2), 161-170.

Dunnett, N. P., Willis, A. J., Hunt, R., & Grime, J. P. (1998). A 38-year study of relations between weather and vegetation dynamics in road verges near Bibury, Gloucestershire. *Journal of Ecology*, *86*(4), 610-623.

Foster, C. R., and Burns, C. D. (1952). *Development of Tentative CBR Design Curves for Landing Mats*. Waterways Expreiment Station

Gantenbein, B. (2006). Unique application – Greendale resurfacing job includes green shoulder. *Western Builder*, April 6, 8-9.

Gartrell, C. A. (2007). *Full-scale instrumented testing and analysis of matting systems for airfield parking ramps and taxiways*. Defense Technical Information Center.

Gartrell, C. A., Newman, J. K., and Anderton, G. L. (2009). Performance measurements of pavement matting systems by full-scale testing over differing soil strengths. *Journal of Materials in Civil Engineering*, 21(10), 561-568.

Giroud, J.-P., and Noiray, L. (1981). Geotextile-reinforced unpaved road design. *Journal of the Geotechnical Engineering Division*, 107(9), 1233-1254.

Giroud, J. P., and Han, J. (2004 a). Design Method for Geogrid-Reinforced Unpaved Roads. I. Development of Design Method. *Journal of Geotechnical and Geoenvironmental Engineering, ASCE*, 130, 775-786.

Giroud, J. P., and Han, J. (2004 b). Design Method for Geogrid-Reinforced Unpaved Roads. II. Calibration and Applications. *Journal of Geotechnical and Geoenvironmental Engineering, ASCE*, 130, 787-797.

Gonzalez, C. R., and Rushing, T. W. (2010). Development of a New Design

Methodology for Structural Airfield Mats. *International Journal of Pavement Research and Technology*, 3(3), 102-109.

Google Map. Retrived Octobor, 2013 from: https://www.google.com/maps/@38.9514565,-95.2731543,191m/data=!3m1!1e3>. (2013).

Henson, J. F. (2001). *Plant Guide: Tall Fescue*. USDA NRCS National Plant Data Center.

Jitendra K. Thakur, J. H., and Robert L. Parsons (2013). Creep Behavior of Geocell-Reinforced Recycled Asphalt Pavement Bases. *Journal of Materials in Civil Eingeering © ASCE*, 25, 1533-1542.

Kansas Department Of Transportation (2013). *Permanent Seed Mixes.*

Leenders, J. K., Boxel, J. H. v., and Sterk, G. (2007). The effect of single vegetation elements on wind speed and sediment transport in the Sahelian zone of Burkina Faso. *Earth Surface Processes and Landforms*, 32(10), 1454-1474.

Madhavi Latha, G., Rajagopal, K., and Krishnaswamy, N. (2006). Experimental and theoretical investigations on geocell-supported embankments. *International Journal of Geomechanics*, 6(1), 30-35.

Mak, A. T. L. (2013). *Modular Road Plate System*. M.S. Thesis in Civil Engineering, the University of Waterloo, Ontario, Canada.

Mason, L. E., and Greenfield, P. H. (1995). Portable crossings for weak soil areas and streams. *Transportation research record*, 1504, 118-124.

Mekkawy, M. M., White, D. J., Jahren, C. T., and Suleiman, M. T. (2010). Performance Problems and Stabilization Techniques for Granular Shoulders. *Journal of Performance of Constructed Facilities ASCE*, 24, 159-169.

Mitchell, J. K., Kao, T., and Kavazanjian Jr, E. (1979). *Analysis of Grid Cell Reinforced Pavement Bases*. Defense Technical Information Center.

Moosmüller, H., Gillies, J. A., Rogers, C. F., DuBois, D. W., Chow, J. C., Watson, J. G., and Langston, R. (1998). Particulate Emission Rates for Unpaved Shoulders along a Paved Road. *Journal of the Air & Waste Management Association*, 48(5), 398-407.

Munson, S. M., Belnap, J., Okin, G. S., and Schlesinger, W. H. (2011). Responses of wind erosion to climate-induced vegetation changes on the Colorado Plateau. *Proceedings of the National Academy of Sciences of the United States of America*, 108(10), 3854-3859.

Newman, D. J. G. a. J. A. (2001). Festuca arundinacea Schreber (F. elatior L. ssp. arundinacea (Schreber) Hackel). *Journal of Ecology*, 89(2), 304-324.

Pokharel, S. K., Han, J., Leshchinsky, D., Parsons, R. L., and Halahmi, I. (2010). Investigation of factors influencing behavior of single geocell-reinforced bases

under static loading. *Geotextiles and Geomembranes*, 28(6), 570-578.

Pokharel, S. K. (2010). *Experimental Study on Geocell-Reinforced Bases under Static and Dynamic Loading.* Doctoral Dissertation in Civil Engineering, the University of Kansas, Kansas, USA.

Pokharel, S. K., Han, J., Manandhar, C., Yang, X., Leshchinsky, D., Halahmi, I., and Parsons, R. L. (2011). Accelerated Pavement Testing of Geocell-Reinforced Unpaved Roads over Weak Subgrade. *Transportation Research Record: Journal of the Transportation Research Board*, 2204(-1), 67-75.

Qian, Y., Han, J., Pokharel, S., and Parsons, R. (2013). Performance of Triangular Aperture Geogrid-Reinforced Base Courses over Weak Subgrade under Cyclic Loading. *Journal of Materials in Civil Engineering*, 25(8), 1013-1021.

Presto Geosystem (2011). *Geoweb - GS30V Spec Summary*. Retrieved from: http://www.prestogeo.com/downloads/YNjJj6EykMeI87iE9Sx4FxrNzFrvYrwx6W7fRBT3NxBLukPt3D/Geoweb%20GW30v6_summary.pdf

Presto Geosystem (2009). *Geoterra Specification Summary*. Retrieved from: http://www.prestogeo.com/downloads/5d2eF5tVoSthZ7S2FTHJYktElB46cxYUp3ZuxIGbz01vRs2k1A/GEOTERRA%20Specification%20Summary.pdf

Presto Geosystem (2009). *Geoterra Specification and Installation Guideline.* Retrieved from:

http://www.prestogeo.com/downloads/BqEa3J4VQhW59e3bvwoA5sECWXdrensKrJC2DYHkuCjthbLTOz/GEOTERRA%20Specification%20and%20Installation%20Guideline-eng.pdf

Rea, C., and Mitchell, J. K. Sand reinforcement using paper grid cells. *Proc., Symposium on Earth Reinforcement*, ASCE, 644-663.

Raeside, M. C., Friend, M. A., Behrendt, R., Lawson, A. R., and Clark, S. G. (2012). A review of summer-active tall fescue use and management in Australia's high-rainfall zone. *New Zealand Journal of Agricultural Research*, 55(4), 393-411.

Rushing, T. W., and Howard, I. L. (2011). Matting Solutions for Low-Volume Roads. *Transportation Research Record: Journal of the Transportation Research Board*, 2204(1), 92-101.

Rushing, T. W., Tingle, J. S., McCaffrey, T. J., Rushing, T. S., Command, U. S. M. C. S., Engineers, U. S. A. C. o., Research, E., Center, D., Geotechnical, and Laboratory, S. (2009). *Evaluation of Supa-Trac Matting for Expeditionary Roads*, [US Army Corps of Engineers, Engineer Research and Development Center], Geotechnical and Structures Laboratory.

Santoni, R. L. (2003). *Enhanced Coastal Trafficability: Road Construction Over Sandy Soils.* Defense Technical Information Center.

Santoni, R. L., Smith, C. J., Tingle, J. S., and Webster, S. L. (2001). *Expedient Road*

Construction Over Soft Soils. Defense Technical Information Center.

State of California Department of Transportation, D. o. E. A., Stormwater Program. Sacramento, CA. (2006). Cellular Confinement System Research.

Thakur, J. K., Han, J., Pokharel, S. K., and Parsons, R. L. (2012). Performance of geocell-reinforced recycled asphalt pavement (RAP) bases over weak subgrade under cyclic plate loading. *Geotextiles and Geomembranes*, 35, 14-24.

Udo, K., and Takewaka, S. (2007). Experimental Study of Blown Sand in a Vegetated Area. *Journal of Coastal Research*, 23(5), 1175-1182.

United State Department of Agreculture Natrual Resources Conservation Service (2002). *Plant Fact Sheet Perennial Ryegrass*. Retrived from: http://plants.usda.gov/factsheet/pdf/fs_lope.pdf

Tencate (2013). *Mirafi HP570 Reinforced Properties*. Retrived from: http://www.tencate.com/amer/Images/TDS_HP570A1_tcm29-17221.pdf

United State Department of Agreculture Natrual Resources Conservation Service (2002). *Plant Fact Sheet: Tall Fescue,* Plant Materials Program.

Van de Ven, T., Fryrear, D., and Spaan, W. (1989). Vegetation characteristics and soil loss by wind. *Journal of Soil and Water Conservation*, 44(4), 347-349.

Webster, S. L. (1979). *Investigation of Beach Sand Trafficability Enhancement Using*

Sand-Grid Confinement and Membrane Reinforcement Concepts. Report 1. Sand Test Sections 1 and 2 (No. WES/TR/GL-79-20). Aarmy Engineer Waterways Expreiment Station.

Webster, S. L. (1981). *Investigation of beach sand trafficability enhancement using sand-grid confinement and membrane reinforcement concepts -report 2*. Aarmy Engineer Waterways Expreiment Station.

Webster, S. L., and Tingle, J. S. (1998). *Expedient road construction over sands using lightweight mats.* Defense Technical Information Center.

Webster, S. L., and Watkins, J. E. (1977). *Investigation of construction techniques for tactical bridge approach roads across soft ground : final report.* (No. Tech Rpt. S-77-1). United States. Army. Corps of Engineers.; Soils and Pavements Laboratory (U.S.).

Yang, X., Han, J., Leshchinsky, D., and Parsons, R. L. (2008). Behavior of Geocell-Reinforced Sand Under a Vertical Load. *Transportation Research Record: Journal of the Transportation Research Board*, 2045(-1), 95-101.

Yang, X., Han, J., Pokharel, S. K., Manandhar, C., Parsons, R. L., Leshchinsky, D., and Halahmi, I. (2012). Accelerated pavement testing of unpaved roads with geocell-reinforced sand bases. *Geotextiles and Geomembranes*, 32, 95-103.

Yuu, J., Han, J., Rosen, A., Parsons, R., and Leshchinsky, D. Technical review of

geocell-reinforced base courses over weak subgrade. *Proc., First Pan American geosynthetics conference, Cancun, Mexico*, 2-5.